NASA TECHNICAL REPORT

NASA TR R-371

NASA TR R-371

SUBSYSTEM RADIATION SUSCEPTIBILITY
ANALYSIS FOR DEEP-SPACE MISSIONS

by Wm. S. West, W. Poch, A. Holmes-Siedle,
H. W. Bilsky, and D. Carroll
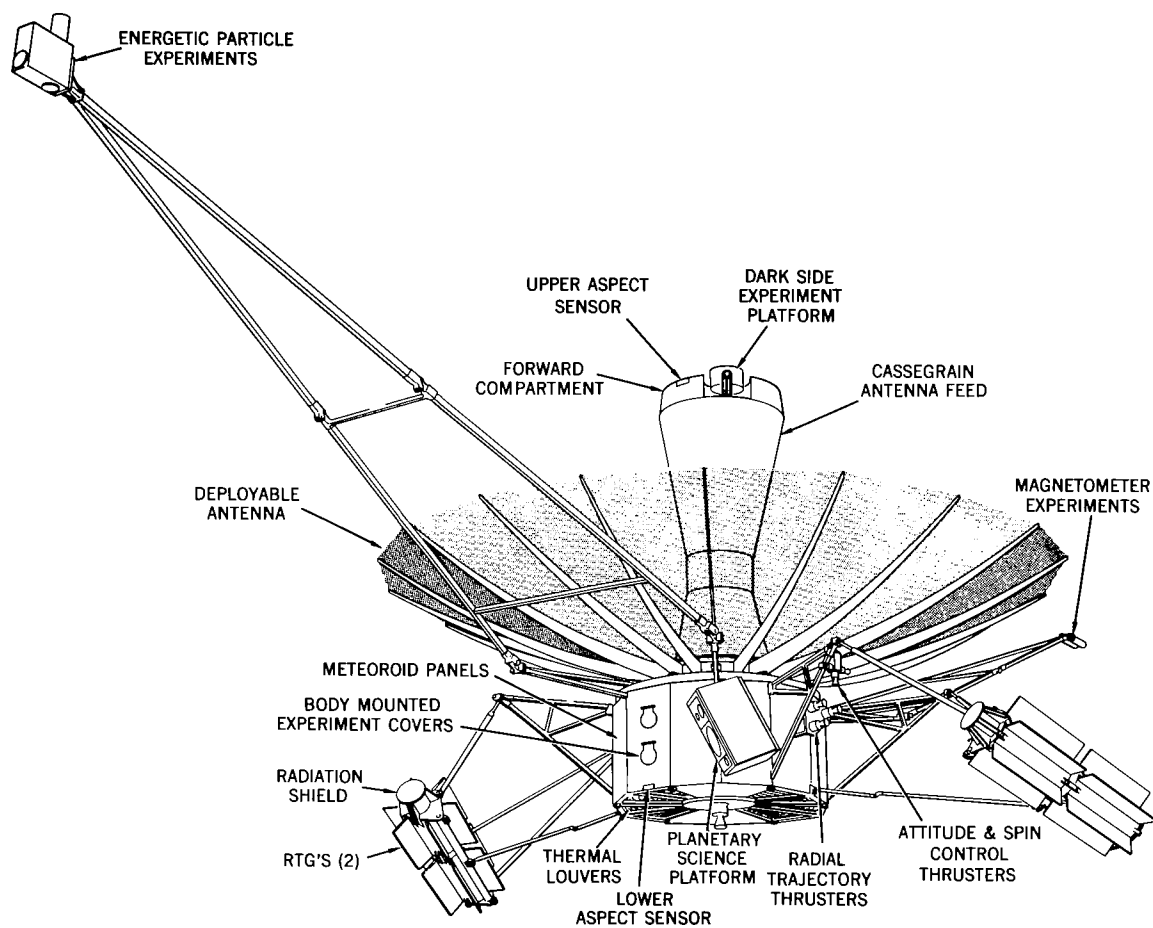
Goddard Space Flight Center
Greenbelt, Md.   20771

1. Report No. NASA TR R-371	2. Government Accession No.	3. Recipient's Catalog No.	
4. Title and Subtitle Subsystem Radiation Susceptibility Analysis for Deep-Space Missions		5. Report Date November 1971	
		6. Performing Organization Code	
7. Author(s) Wm. S. West, W. Poch, A. Holmes-Siedle, H. W. Bilsky, and D. Carroll		8. Performing Organization Report No. G-1029	
9. Performing Organization Name and Address Goddard Space Flight Center Greenbelt, Maryland 20771		10. Work Unit No.	
		11. Contract or Grant No.	
		13. Type of Report and Period Covered	
12. Sponsoring Agency Name and Address National Aeronautics and Space Administration Washington, D.C. 20546		Technical Report	
		14. Sponsoring Agency Code	

15. Supplementary Notes

16. Abstract

Scientific, unmanned spacecraft on missions to Jupiter and beyond will be subjected to nuclear radiation from the natural environment and onboard nuclear power sources which may be harmful to subsystems. This report postulates these environments and discusses practical considerations to ensure confidence that the spacecraft's materials and subsystems will withstand the effects of anticipated radiation. Degradation mechanisms are discussed.

17. Key Words Suggested by Author Radiation, Radiation Hardening Deep Space, Sector Analysis Planetary/Interplanetary Environment Annealing, Spacecraft Design		18. Distribution Statement Unclassified-Unlimited		
19. Security Classif. (of this report) Unclassified	20. Security Classif. (of this page) Unclassified		21. No. of Pages 167	22. Price 3.00
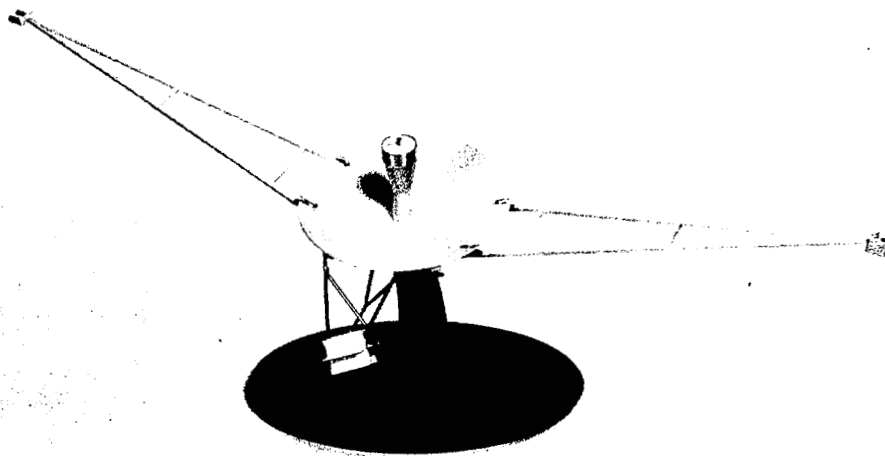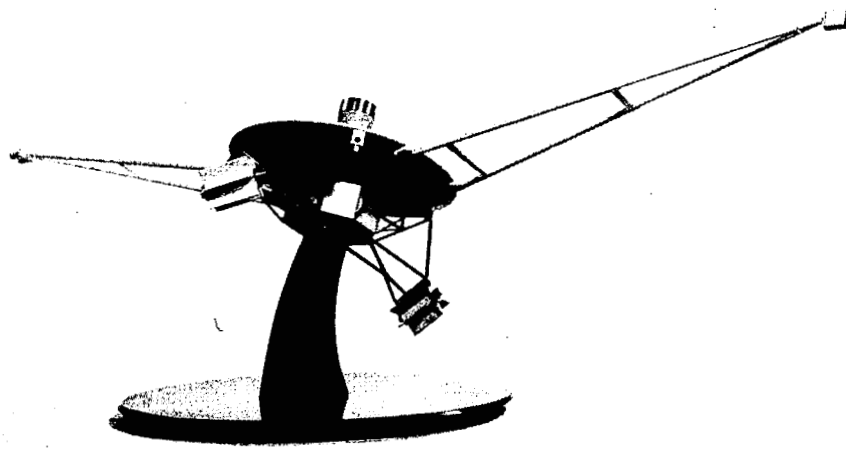
Frontispiece A—Two Views of a Model of the Galactic Jupiter Probe which served as the "Reference Design" for this Task

ENERGETIC PARTICLE
EXPERIMENTS

UPPER ASPECT
SENSOR

DARK SIDE
EXPERIMENT
PLATFORM

FORWARD
COMPARTMENT

CASSEGRAIN
ANTENNA FEED

DEPLOYABLE
ANTENNA

MAGNETOMETER
EXPERIMENTS

METEOROID PANELS

BODY MOUNTED
EXPERIMENT COVERS

RADIATION
SHIELD

RTG'S (2)

THERMAL
LOUVERS

PLANETARY
SCIENCE
PLATFORM

RADIAL
TRAJECTORY
THRUSTERS

ATTITUDE & SPIN
CONTROL
THRUSTERS

LOWER
ASPECT SENSOR

Frontispiece B—Outer Planets Explorer

CONTENTS

LIST OF ILLUSTRATIONS

LIST OF TABLES

SUBSYSTEM RADIATION SUSCEPTIBILITY ANALYSIS
FOR DEEP-SPACE MISSIONS

by

Wm. S. West
Goddard Space Flight Center

and

W. Poch, A. Holmes-Siedle, H. W. Bilsky, and D. Carroll
RCA Astro-Electronics Division

SECTION I

BACKGROUND, INTRODUCTION, AND SUMMARY

A. Background

Since the early 1960's, personnel of the Goddard Space Flight Center (GSFC) have been interested in deep-space missions to obtain information concerning the planets, Jupiter, Saturn, Uranus, Neptune, and Pluto, as well as information concerning the interplanetary medium. Studies have been performed to establish the feasibility of such missions and various reports were written by GSFC personnel and by others.

For almost as long as these missions have been considered, the engineers, scientists, and managers at GSFC have realized the necessity for systems, independent of the Sun's energy, to meet the spacecraft electric power requirement. In general, GSFC studies have indicated that there is a weight advantage in using small nuclear power systems such as radioisotope fueled thermoelectric generators (RTG's) instead of presently available solar cells when missions go beyond 2.5 or 3 AU. Further, there are technological and practical uncertainties

in projecting use of solar arrays in a range starting beyond 3 to 5 AU*, whereas the use of small nuclear power supplies is technically and practically feasible. However, the use of small nuclear systems, while feasible, nevertheless presents technical questions. An in-house GSFC study identified pertinent technological areas requiring study prior to the use of these nuclear generators on spacecraft designed for scientific deep-space missions. These areas were divided into the following numbered Tasks:

Task Number	Task Description — Title	Reference Document
I	Analysis of Selected Deep-Space Missions	NASA TR R-372
IIA	Subsystem Radiation Susceptibility Analysis for Deep-Space Missions	NASA TR P 371
IIB	Spacecraft Charge Buildup Analysis	NASA SP 276
III	Techniques for Achieving Magnetic Cleanliness	NASA TR R-373
IV	Weight Minimization Analysis	X-701-69-174*
V	Spacecraft Analysis and Design	X-701-69-175*
VI	Spacecraft Test Documentation	X-701-69-176*
VIIA	Planar RTG-Component Feasibility Study	X-701-69-177*
VIIB	Planar RTG-Spacecraft Feasibility Study	X-701-69-178*
VIII	RTG Interface Specification	TM X63617
	Summary Report of NEW MOONS	X-701-69-190*

*Goddard Space Flight Center unpublished report.

---

*Technical uncertainties involve practical design questions arising from the use of very large solar array areas, their survival through meteroid belts, and their system performance when operating at the low temperature and low illumination levels anticipated.

A contract* was established for further study of these areas. This study was entitled NASA Evaluation With Models Of Optimized Nuclear Spacecraft (NEW MOONS). During the execution of the NEW MOONS technology study, GSFC was assigned the task of conducting a Phase A study covering a Galactic Jupiter Probe. These two study efforts, Galactic Jupiter Probe and NEW MOONS, were directed to provide the maximum practical benefit to each other. In general, the Galactic Jupiter Probe was considered as a "baseline spacecraft and mission" or a "reference design" during the NEW MOONS technology study. On the other hand, the Galactic Jupiter Probe Study team made use of the technology and data as developed by the NEW MOONS Study in areas of missions analysis, shielding, aerospace nuclear safety, thermal and structural analysis, and other related areas.

As the NEW MOONS contract was being concluded, the scope of Galactic Jupiter Probe project was broadened and adopted the name Outer Planets Explorer (OPE). The Outer Planet Explorer is considered for a generally more ambitious program than the original Galactic Jupiter Probe (GJP) in that the OPE is intended for a family of single- and multiple-planet missions. †

The OPE, as presently visualized, encompasses spacecraft in the 750- to 950-pound class and also in the 1100- to 1400-pound class whereas the GJP "reference-design spacecraft" for the NEW MOONS Study was 500 to 600 pounds. This is a significant practical difference from a flight project viewpoint; however, the technology and techniques of NEW MOONS are generally applicable. Specific numeric values will be different when solutions are developed, but the techniques and rationale indicated in the NEW MOONS reports are applicable to the general problem of integrating and using small nuclear power systems on a scientific spacecraft designed for deep-space missions.

The NEW MOONS technology and techniques reported may have applicability or some relevancy to additional space missions that may in the future use nuclear systems such as planetary landers and rovers as well as applications spacecraft.

B. Introduction

Scientific spacecraft on missions into deep space will be exposed to naturally occurring radiation and radiation from onboard nuclear sources. This

---

*NASA Evaluation With Models Of Optimized Nuclear Spacecraft (NEW MOONS), Contract NAS 5-10441, performed by RCA Astro-Electronics Division, Defense Electronic Products, Princeton, New Jersey.

†Also, see Frontispieces A and B.

radiation may affect adversely various electronic subsystems and materials such as electrical insulation, thermal coatings, optical devices, and electronic elements unless suitable precautions are taken. This report discusses the problem generally.

1. Statement of the Problem—Subsystems Radiation Susceptibility Analysis

Spacecraft subsystem performance deterioration caused by nuclear radiation can be classified arbitrarily and rather broadly according to the subsystem which is affected. One category or class consists of spacecraft electronic subsystems which degrade as a result of damage to sensitive components, primarily bipolar and MOS transistors and diodes, both discrete and integrated devices. Component damage manifests itself in the form of electrical parameter changes. The net effect of these parameter changes throughout a circuit, e.g., the reduction of transistor gain below (or the rise of junction leakages above) a certain value may result in subsystem performance below acceptable limits or even catastrophic failure.

A second class of subsystem degradation may occur in sensor subsystems. Among the scientific objectives of the NEW MOONS mission, as described in Task I, are the measurements of magnetic fields and particle radiation during the cruise phase of the mission and during planetary encounter. These measurements would involve the use of onboard magnetometers and particle detectors. The composition, pressure, and temperature of Jupiter's atmosphere may also be measured using spacecraft-borne IR, UV, and microwave instruments capable of measuring the intensity of radiation. All of these instruments are operated by electronic components, which are susceptible to the same parameter changes as the electronic subsystems. It should be noted, however, that a degree of degradation tolerable in general functional electronics (e.g., power regulators) may not be tolerable in the carefully calibrated linear amplifier circuits used for photometric and other scientific measurements. Optical systems (lenses, light-sensitive surfaces, etc.) may also degrade and hence go out of calibration. A unique problem in this subsystem class is presented by the particle detectors. The purpose of these devices is to measure high-energy space radiation at the same time the spacecraft power supply (two RTG's)* is emitting such radiation, thereby presenting a possible interference that must be reconciled if accurate measurements of the environment are to be made.

---

*In general, this report does not cover the effects of onboard RTG's on scientific data. Task IV concentrates on this facet of the problem. In this task, IIA, emphasis is placed on damaging effects of radiation on various spacecraft elements.

The third class of radiation damage pertains to materials other than semi-conductors. This category spans all subsystems and covers thermal-control coatings, conformal coatings, seals, lubricants, bearing material, wire coatings, insulators, etc. The degradation of bulk materials, particularly of highly stressed materials, is an important consideration because every subsystem contains some of them and precision in prediction of all conceivable failure modes is less feasible than with electronic and optical materials. In addition many structural and coating materials may be directly exposed to the full impact of the space environment including solar UV radiation and the very-low-energy protons and electrons which, because of their limited penetration capabilities, only affect the properties of outer surfaces, particularly the reflectance. A typical example is the discoloration of certain types of white paint.

2. Task Objectives and Technical Approach

The objectives of Task IIA are as follows:

1. Estimate the magnitude of the combined radiation environment (Section II) and its effect on the performance of sensitive spacecraft subsystems (Section III).

2. Provide system engineers and subsystem designers with information on critical constraints (Section I).

3. Define a radiation hardening program (Section IV).

4. Provide a preliminary assessment of the magnitude of the programmatic considerations to be encountered (Section V).

The approach to meeting these objectives consisted of four parts. The first of these was to determine the anticipated types and levels of space and RTG radiation that will arrive at the surface of the spacecraft over the prescribed mission period. This analysis, as described in Section II of this report, was followed by the preparation of internal dose level estimates, based on the calculated environment and radiation shielding provided by the spacecraft structure. ("Internal" includes the internal effects even within thin coatings on the surface of the spacecraft.)

The second part, described in Section III, consisted of assessing the magnitude of the radiation hardening problem to be encountered by spacecraft design engineers. In this connection, the various types of critical components and materials anticipated for use in the spacecraft were discussed; failure mechanisms were examined, and based on experience and a large quantity of existing test data, predictions were made with respect to the level of component degradation

that can reasonably be expected for the dose levels estimated in Section II, and the resulting effects on subsystem performance.

Throughout this report, a spacecraft configuration has been postulated that is in substantial accordance with the Galactic Jupiter Probe. A photograph of a 1/18 scale model of this spacecraft is shown in the Frontispiece. Other spacecraft configurations could be used and the analysis techniques presented in this report would remain applicable.

The postulated spacecraft employs two RTG's, each rated at 1725 W(t) using $Pu^{238} O_2$ as the fuel.

In the third part, described in Section IV, radiation hardening concepts were developed in detail. The goal of radiation hardening is to achieve the condition whereby spacecraft subsystems, when exposed to the damaging effects of irradiation, will not experience performance degradation below acceptable levels. There are various alternative approaches to achieve this goal. The techniques employed for the ideal radiation hardening program are tailored to the specific needs of the spacecraft configuration and the intended mission. In the NEW MOONS mission the seriousness of the radiation problem may vary considerably, depending on the precise spacecraft configuration and device packaging method chosen; on the final trajectory and mission duration; and on the actual intensity of the Jupiter radiation belts and solar flares which future scientific investigations reveal. Thus, the treatment of damage possibilities has been extended considerably beyond the "nominal" environment models used for quantitative calculations. Therefore, two programs, producing different degrees of radiation tolerance, by somewhat different methods, were developed. These programs incorporate sufficient flexibility to serve the needs of the spacecraft, within the range of the missions postulated in Task I and the generally postulated spacecraft configuration.

The final part of the Task IIA effort consisted of estimating the approximate impact of radiation hardening on the NEW MOONS program with respect to time and cost. Various levels of effort have been evaluated and labor estimates are given. In addition this section also includes a development plan to take advantage of improvements which are desirable in the state of the art in device, material, and system technology before the spacecraft is built, so that the benefits from such improvements can be realized and potential problems eliminated.

C. Summary

The Subsystem Radiation Susceptibility Analysis was prepared in four parts. The work performed on each of these four parts will be described briefly and the results and/or conclusions summarized.

6

1. Analysis of the Radiation Environment

Both the space and RTG radiation environments were evaluated, first separately, then in combination. The following regions were considered: pre-launch, near-Earth, interplanetary space (Earth to Jupiter), near-Jupiter, and interplanetary space (Jupiter and beyond). It was concluded that, in the near-Earth and near-Jupiter regions the particles of concern are high-energy electrons and protons. In interplanetary space, the only radiation likely to damage the spacecraft will be the protons ejected from the Sun in the solar wind and solar flares. Radiation from the RTG's will consist, primarily, of fast neutrons and gamma ray photons. Spacecraft surfaces may also be affected by ultraviolet radiation from the Sun. Of the space regions considered, the near-Jupiter is very significant. This conclusion would still hold even if future studies reveal that the Jupiter environment is of a less severe order than was assumed here. It is emphasized that there is, indeed, considerable uncertainty as to the intensity and form of the trapped radiation belts of Jupiter.

The two effects caused by the energy dissipation of bombarding particles were discussed: The first effect concerns single-crystal semiconductor components; it occurs when a high-energy bombarding particle collides with the nucleus of an atom, dislodging the atom from its position in the crystal lattice. The resulting defect affects the electrical properties of the crystal. The degree of bulk displacement can be conveniently expressed as the equivalent fluence of the 1-MeV electrons which cause the damage. The resulting unit of damage capability is called the "DENI"*. The second effect occurs when a bombarding particle interacts with the electron cloud surrounding the atom, causing the ejection of some of the electrons surrounding the atom. The result is ionization damage, which is due to the subsequent rearrangement of the atoms or charges and can produce changes in the characteristics of the material. The dose from ionization damage is usually expressed in rads.† Bulk damage has serious deleterious effects on semiconductors, and ionization damage adversely affects all spacecraft materials as well as "planar" semiconductor devices (these include MOS devices, many bipolar transistors, and integrated circuits).

The estimate of radiation damage due to the near-Earth environment, the flight path being postulated as part of the Task I effort, "Analysis of Selected Deep-Space Missions," was based on data on the Van Allen belt, available in NASA documents (Ref. 1). The anticipated levels for interplanetary radiation

---

*Damage-Equivalent Normally-Incident, 1-MeV Electrons/cm^2.

†One rad is the dose resulting from radiation incident on a material when the energy deposited in the material is 100 ergs per gram.

were also derived from published data (Refs. 2 and 3). The near-Jupiter environment was based on particle flux data included in the Galactic Jupiter Probe Study and an assumed similarity of the Jupiter radiation belt to the Earth's Van Allen belt. The estimate prepared for each of these three environments was summed in terms of estimated total bulk damage and total ionization dose.

An estimate of radiation damage stemming from the two RTG's was also prepared for three RTG-spacecraft separation distances, calculated on the basis of the essentially inverse-square relationship between radiation flux and distance from the RTG. The total radiation environment external to the spacecraft was then obtained by summing total bulk damage and ionization dose as a function of RTG-spacecraft separation distance.

Internal radiation levels were estimated for exposed and protected levels within the spacecraft. The range of difference in internal dose levels is based on the amount of "equivalent" shielding surrounding any component as a result of spacecraft configuration and internal packaging.

Table 1 summarizes the worst-case damage levels from the combination of all radiation sources. More detailed data of this kind are presented in Tables 4 and 5 in Section II.

Notes for Table 1

1. For the 5-year mission the regions considered were near-Earth, Earth to Jupiter, near-Jupiter, and Jupiter and beyond. However, for worst-case presentation a 9-month pre-launch period is assumed during which time the RTG's, fueled with PuO$_2$, are assumed to be located 18 inches from electronic subsystems. This period of time is occupied with the integration of the spacecraft and pre-launch check-out of the spacecraft at the launch site.

2. The energy spectrum for the RTG's is given in Appendix II. The flux and fluence are discussed in Section IID.

3. The proton and electron flux near Earth and near Jupiter are dependent upon the distance from the planets. These data are given in Section IIC-2 for near-Earth and Section IIC-4 for near-Jupiter. The solar wind as well as the solar flare proton flux varies inversely as the square of the distance from the Sun (see Section IIC-3). The solar flare flux is highly sporadic, but an average flux was used based on measurements for the period of 1956 to 1961.

4. For an estimate of damage to electronic subsystems only the naturally occurring electrons and protons noted were used.

5. The tabulated particle data are in terms of integrated fluence ($\phi > E$).

6. Exposed internal location is equivalent to a spherical shield of 100 mils of aluminum around a component.

7. Typical internal location is equivalent to a spherical shield of 270 mils of aluminum around a component.

8. Two RTG's are used, each containing 1725 watts (t) of 5-year-aged PuO$_2$ fuel with naturally occurring oxygen.

9. A detailed explanation of the units DENI and rads are found in Section II, B.

Table 1

Summary of Worst-Case Estimates of Radiation Damage Levels for 5-Year NEW MOONS Mission

Regions	Duration	Natural Environment — Protons: Energy Spectrum, MeV	Flux,[3] Particles/cm²-sec	Fluence[5] Particles/cm²	Electrons: Energy Spectrum, MeV	Flux,[3] Particles/cm²-sec	Fluence,[5] Particles/cm²	Exposed[6] Internal Location Bulk,[9] Deni	Ionization, Rads[9]	Typical[7] Internal Location Bulk, Deni	Ionization, Rads	RTG Env.[8] Sep. Dist. Flux,[7] Particles/cm²-sec	Fluence[7] Particles/cm²	Bulk, Deni	Ionization, Rads	Combined Exposed[6] Bulk, Deni	Ionization, Rads	Combined Typical[7] Bulk, Deni	Ionization, Rads
Pre-Launch	9 months[1]	—	—	—	—	—	—	—	—	—	—	—	—	$.153 \times 10^{14}$	$.063 \times 10^{4}$	$.153 \times 10^{14}$	$.063 \times 10^{4}$	$.153 \times 10^{14}$	$.063 \times 10^{4}$
Near-Earth	1 Hour	Trapped Particles: 0.1, 0.4, 1.0, 4.0, 10, 15, 30	9.7×10^{10}, 4.0, 0.12, 0.050, 0.0080, 0.0028, 0.00068		Trapped Particles: 0.001, 0.5, 1, 2, 3, 4, 5, 6, 7		2.7×10^{11}, 0.38, 0.092, 0.011, 0.0026, 0.00078, 0.00024, 0.000075, 0.000025	8.5×10^{9}	55	1.4×10^{9}	2.3	—	—			Negligible	$.006 \times 10^{4}$	Negligible	Negligible
Interplanetary Earth-Jupiter (1-5 AU)	550 Days (1.5 Yrs.)	Solar Wind: 0.001-0.05; Solar Flares: 1.0, 4.0, 10, 15, 30	2.5×10^{15}; 0.080×10^{12}, 0.0085, 0.00215, 0.00117, 0.00043		Not Applicable	Not Applicable	Not Applicable	2.9×10^{11}	215	1.38×10^{11}	95			$.306 \times 10^{14}$	$.126 \times 10^{4}$	$.309 \times 10^{14}$	$.148 \times 10^{4}$	$.307 \times 10^{14}$	$.136 \times 10^{4}$
Near-Jupiter	15 Hours	Trapped Particles: 0.1, 0.4, 1.0, 4.0, 10, 15, 30	44.2×10^{12}, 23.0, 6.7, 0.050, 0.00118, 0.00027, 0.000015		Trapped Particles: 0.001, 0.5, 1, 2, 3, 4, 5, 6, 7		6.91×10^{13}, 1.02, 0.306, 0.0613, 0.0143, 0.00368, 0.000956, 0.000253, 0.000068	1.35×10^{12}	3.2×10^{4}	2.0×10^{10}	550	—	—			$.014 \times 10^{14}$	3.2×10^{4}	Negligible	$.055 \times 10^{4}$
Interplanetary Jupiter to Beyond (5-16 AU)	1280 Days (3.5 Yrs.)	Solar Wind: 0.001-0.05; Solar Flares: 1.0, 4.0, 10, 15, 30	0.4×10^{15}; 0.013×10^{12}, 0.0014, 0.00033, 0.00019, 0.00007		Not Applicable	Not Applicable	Not Applicable	4.0×10^{10}	35	2.2×10^{10}	15			$.714 \times 10^{14}$	$.294 \times 10^{4}$	$.714 \times 10^{14}$	$.298 \times 10^{4}$	$.714 \times 10^{14}$	$.296 \times 10^{4}$
TOTALS								0.017×10^{14}	3.231×10^{4}	0.002×10^{14}	$.066 \times 10^{4}$			1.173×10^{14}	$.483 \times 10^{4}$	1.19×10^{14}	3.71×10^{4}	1.18×10^{14}	0.55×10^{4}

2. The Accommodation of Radiation Damage Effects in Spacecraft Subsystems

Whether or not a spacecraft subsystem can survive a particular radiation environment depends primarily on the effect of the environment on those components whose parameters will be significantly altered at the anticipated dose levels. Subsystem performance degradation can usually be held within tolerable limits by providing adequate allowances in the design of the subsystems for the anticipated component parameter changes. Such changes can usually be accommodated by the application of various circuit design techniques such as feedback, for example, to maintain amplifier gain in spite of significant transistor Beta reduction. If such measures unduly complicate a circuit design then consideration can be given to other possible approaches to the problem such as the addition of shielding to reduce the dose levels affecting the more sensitive components. Measures of this kind form part of the subsystem design procedure called "radiation hardening" which is outlined later in this report and described in detail in Section IV.

A difficulty arises, however, if the design cycle of already available spacecraft subsystems did not include a radiation hardening procedure. In situations of this kind, a detailed worst-case analysis of all the circuits using radiation-sensitive components must be made to determine the dose levels corresponding to the threshold of just acceptable subsystem performance. If these threshold dose levels are below those predicted by an analysis of the anticipated environment, then suitable preventive measures must be taken. If component substitutions or circuit modifications to reduce sensitivity to radiation are impractical, then the only remaining solution to the problem may be to add the shielding needed to keep component degradation to within acceptable limits. Radiation hardening by this "after-the-fact" method is usually much more involved and costly than is needed if radiation hardening forms part of the normal design procedure as recommended in the present project. Radiation testing of complete subsystems has also been considered as a possible method for determining the overall radiation susceptibility of particular subsystem designs. Unfortunately, unlike vacuum or thermal testing, radiation is frequently destructive. In cases where damage is reversible, high annealing temperatures are required. Restoring complete subsystems to their original condition by such an annealing process does not appear feasible at this time. Conceivably, it would be possible to irradiate a sufficient number of subsystems so that the behavior of similar unirradiated units could be predicted on a statistical basis. In most instances, however, the cost of following a test procedure of this kind would probably be prohibitive. This would not exclude a "proof-of-principle" test or a test to destruction of a single engineering test model or a breadboard of an electronic package during the design phase of a program.

It is assumed, therefore, that the design of subsystems for the NEW MOONS program will include a radiation hardening procedure based primarily on conservative predictions of the effect of the anticipated environment on individual radiation-sensitive components obtained by careful testing of piece parts. Any radiation tests or preconditioning of components for flight units would be done on only a few selected types and would be carried out before assembly into electronic packages.

Based on estimates of the NEW MOONS environment, the prediction of damage effects includes analyses of radiation susceptibility in three important areas: (1) electronic subsystems which degrade in performance as a result of component damage; (2) detector subsystems which are subject to the same effects as electronic subsystems, and are, in addition, subject to inaccurate measurements if flooded by excessive local radiation emanating from the RTG's; and (3) bulk materials, such as thermal coatings, optical windows, etc., which are also subject to deterioration primarily from particle bombardment and consequently may not adequately serve the purpose for which they were intended.

In accommodating the probable effect of the NEW MOONS environment on spacecraft subsystems, it is necessary to consider only those components that will be affected at the anticipated dose levels as generally indicated in Figure 1. This Figure shows the dose level ranges that can be expected to produce significant changes in the characteristics of various devices and materials. The data presented in Figure 1 are based on the results of extensive tests, compiled principally by the Lockheed Aircraft Co., The Battelle Memorial Institute, and RCA (Refs. 4 and 5). At the worst-case dose levels estimated for the NEW MOONS environment as summarized in Table 1, the components of interest are transistors, integrated circuits and germanium devices, MOS devices, diodes, and thyristors. Each of these devices was treated first in terms of the physics of radiation-induced failure, then in terms of sensitivity to the dose levels anticipated for the NEW MOONS mission. The evaluation of the radiation sensitivity of these devices is empirical to the extent that the predictions are based on past experience and experiments made on earlier projects. (Devices in use at the time of the mission may incur a different set of damage problems.) They will serve only as guidelines to indicate where performance deterioration due to radiation damage can be clearly anticipated.

3. Recommended Radiation Hardening Program

Radiation hardening is a comprehensive program involved in every phase of spacecraft planning and design functions. Activities of radiation specialists and
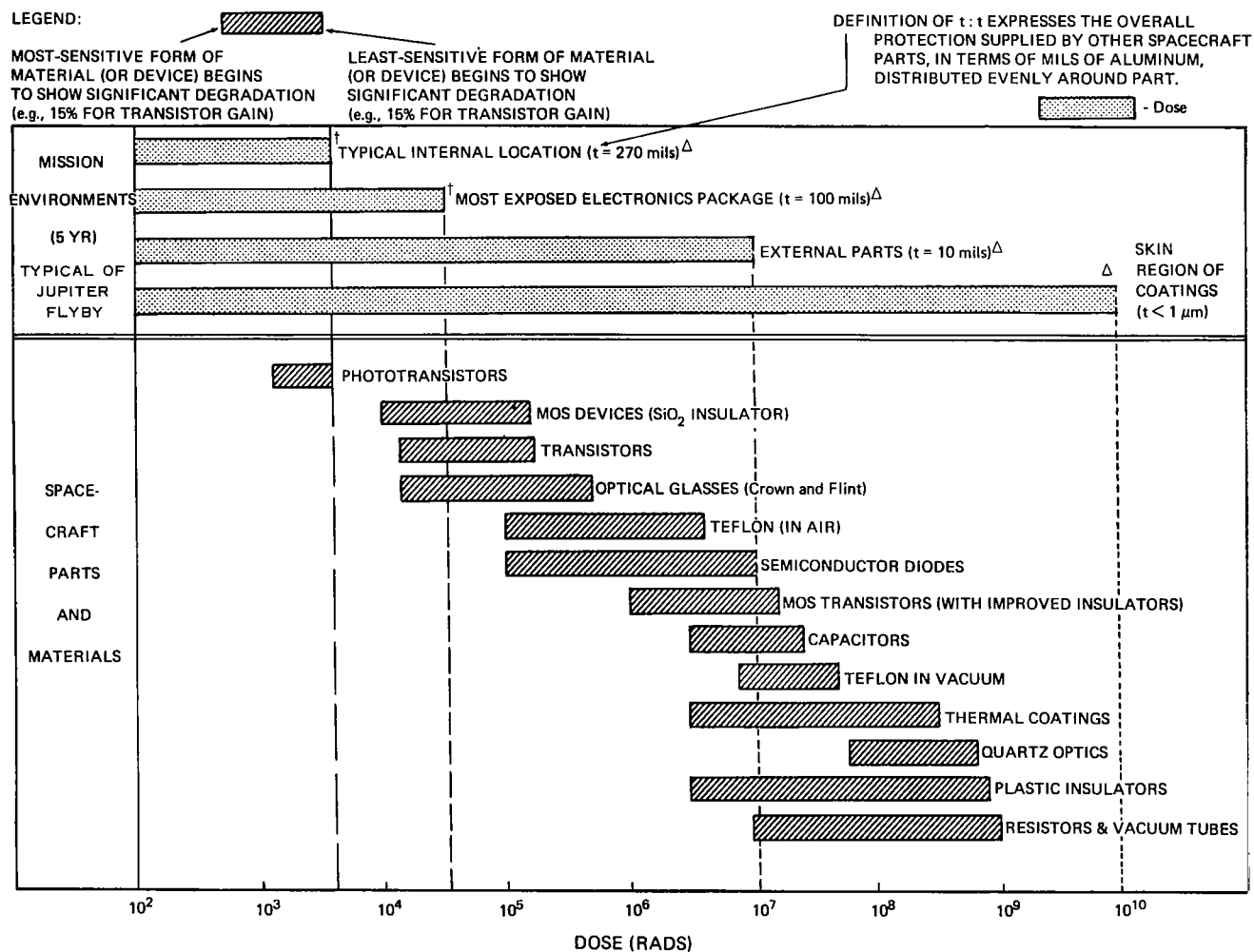
Figure 1(A). Illustrative Example — Sensitivity of Various Spacecraft Components to the Ionization Effects of Radiation, Correlated With Ionization Levels in Various Zones of the NEW MOONS Spacecraft
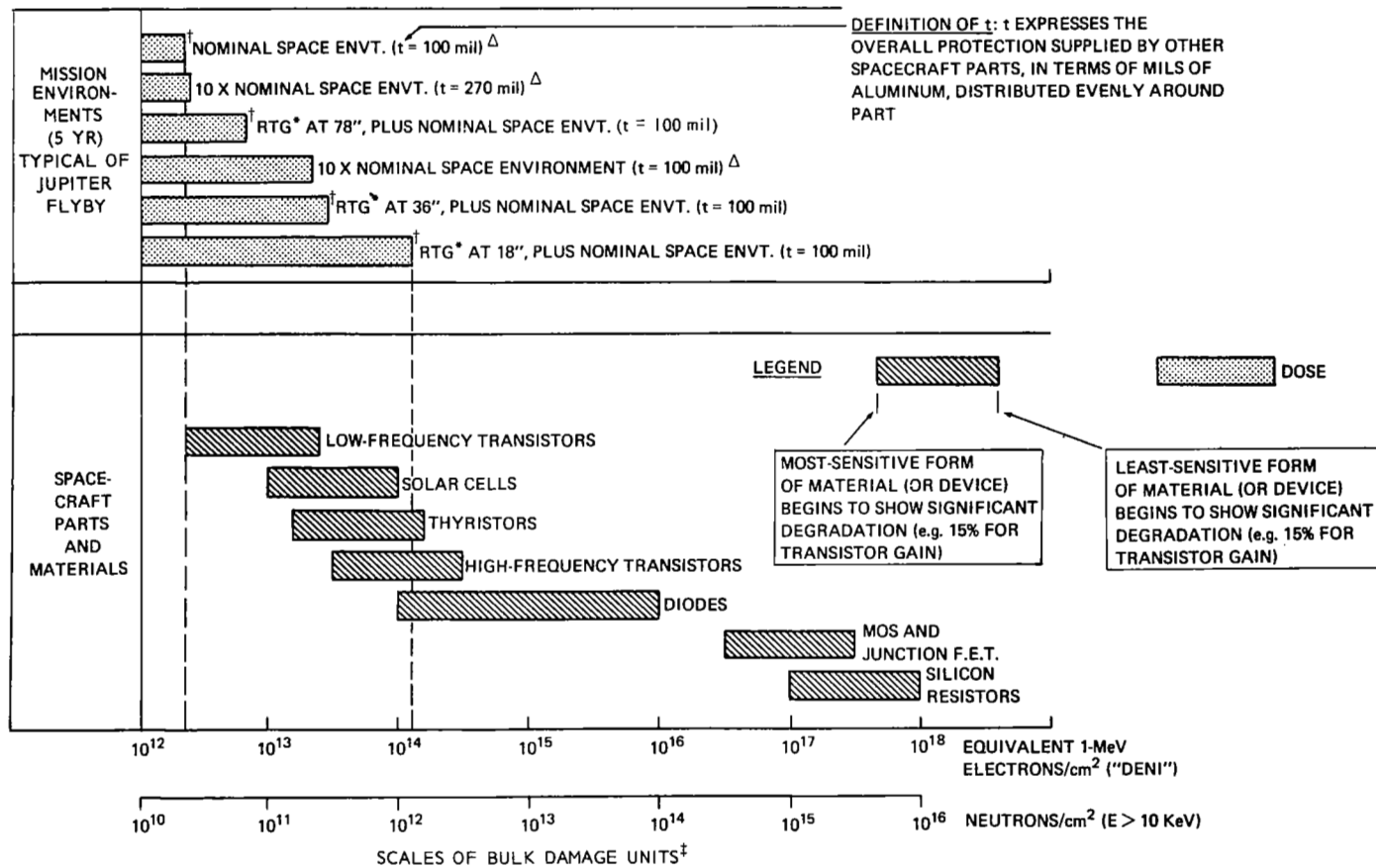
Figure 1(B). Illustrative Example — Sensitivity of Various Spacecraft Components to the Bulk Damage Effects of Radiation, Correlated With Bulk Damage Levels in Various Zones of the NEW MOONS Spacecraft

design engineers will need coordination throughout an overall program such as the development of a spacecraft to perform the NEW MOONS missions. During the various program phases the major anticipated corresponding project and radiation hardening activities are listed below.

I. DEFINITION PHASE

General Project Activity	Radiation Hardening Activity
Mission Description	Analysis of the Space Environment and RTG Radiation Environment
Spacecraft Concept	
	Estimates of Dose Levels Affecting Components
Subsystem Performance Specifications	
	Determination of Critical Parts and Materials
Spacecraft Subsystems Layout	
	Estimates of Spacecraft Radiation Zones and Degradation of Parts and Materials as Laid Out
	Recommendations for Radiation Testing

II. DESIGN AND DEVELOPMENT PHASE

General Project Activity	Radiation Hardening Activity
Spacecraft Structural Design	Refinement of Environmental and Dose Level Data
Subsystems Design	
	Map Breadboard Spacecraft to Verify Shielding Estimates
Build Subsystems Breadboard	
Design Reviews	Radiation Testing of Critical Components and Materials
Build Breadboard Radiation Spacecraft	Analysis of Problem Areas Caused by Device or Material Degradation
	Recommendations for Shielding or Alternate Radiation Problem Solutions, including special onboard dosimetry*

*Such dosimetric experiments would be complementary to the scientific experiments and would monitor dose levels within the spacecraft at various locations to confirm hazard estimates.

III. HARDWARE PHASE

General Project Activity	Radiation Hardening Activity

a. Prototype

      Build Prototype Subsystems   Proof-of-Principle Radiation
                                          Exposure Tests on Selected
      Subsystems and Systems   Subsystems
          Testing

      Build Prototype Spacecraft

b. Flight

      Build Flight Units   Life Tests on Selected Subsystems

As indicated previously, a suitable radiation hardening procedure should be included as an essential part of the NEW MOONS program to ensure the survival of all subsystems without performance deterioration beyond acceptable limits. Both the project definition phase and the hardware phase will involve a cooperative effort between design engineers and radiation specialists. This cooperation is an essential part of the radiation hardening procedure even during the early part of the program because tradeoffs at this stage will probably involve such questions, for example, as the optimum placement of subsystems on the spacecraft structure. Those subsystems particularly sensitive to radiation from the RTG's should, other factors permitting, be placed at the maximum possible distance from these radiation sources.

Two alternative programs for radiation hardening NEW MOONS components are described in this report. Both are predicated on the results of previous tests and the need for supplementary radiation testing of critical components and materials. Although a large quantity of component radiation test data is available as a result of extensive tests by RCA and other organizations, there is a continuing need for updating information on older component types and thoroughly evaluating new ones. Differences in the effect of radiation on semiconductor devices even of the same type are not uncommon. The reasons for this variability are not always clear. Variability can arise from changes in manufacturing process techniques, from some inherent difference in materials from batch to batch, or from inadequate control of manufacturing processes with regard to reproducibility.

The two radiation hardening programs under consideration represent different approaches to the same end, each with its particular advantages and disadvantages. The first of these programs, based on worst-case prediction data, appears to have the advantage of economy in both program time and cost if the damage hazard is not, after analysis, found to be too serious. For this type of test program, small statistical samples of each device are irradiated and subsequently measured for change in electrical performance. These measurements form the basis for predicting the worst-case level of radiation degradation expected for a particular device from a specific manufacturer. The design engineer then applies the prediction data to his circuit and determines what measures may be taken to avoid failure. If the device degrades within tolerable limits, no major circuit changes is needed. If the device is not within tolerable limits, he has an array of alternatives, e.g., choose another device (and test it), redesign his circuit to accept reduced performance, find a more protected spacecraft location for the circuit, provide additional shielding, or seek other possible alternatives.

The second radiation hardening program under consideration is based on the promising experimental results from recent RCA tests of a radiation preconditioning procedure. The object of this procedure is to determine in advance with high accuracy the anticipated effect of space radiation on particularly critical transistors. Test samples in this case would be 100 percent of the quantity needed for a particular device plus a percentage of extras. The subsystem design engineer would submit performance criteria to the radiation evaluation project in terms of allowable degradation. The total batch would then be irradiated and subsequently measured to determine percent of degradation. All those devices that were found to be within tolerance would be baked; the baking procedure produces an annealing effect which serves to restore the device to near its original (pre-irradiation) performance level. For any subsequent irradiation (to the same dose level used for testing), the component is expected to degrade to approximately the same level measured after the initial irradiation. By way of this irradiate-measure-anneal cycle then, the designer is supplied with space-qualified devices, suitable for spacecraft integration, whose performance is within tolerance and whose subsequent degradation during flight is known.

This screening process not only makes possible much greater uniformity of radiation resistance in semiconductor devices used but also, most significantly, obviates the possibility of inadvertently incorporating a "maverick" into a critical circuit. A device is called a "maverick" if its parameter changes are greatly in excess of the amount that would normally be expected on a statistical basis from radiation testing a batch of devices of the same type. While the incidence of "mavericks" is exceedingly infrequent, their occasional occurrence represents a small but definite possibility of a catastrophic failure even at relatively low dose levels. For very long spacecraft missions in particular, it is extremely important to avoid the possibility of incorporating such anomalously sensitive devices in critical circuits.

Although the worst-case prediction program incorporates, by comparison, a small test effort, it still retains an element of reliability risk in that the design engineer receives only statistical estimates of worst-case degradation which involve inherent uncertainties. In addition, since he must design for worst-case performance he may have to penalize his system unduly to anticipate such changes. This can lead to redundancy (added weight and added power drain) or consideration of a possible reduction in subsystem performance requirements. Obviously, such a design change in one circuit can often affect all subsequent circuits in the electronic chain and lead, in the end, to a much larger and longer design or redesign effort.

The recommended choice of radiation hardening programs will be strongly influenced by the final estimate of the somewhat uncertain space hazard and the final spacecraft RTG configuration, since dose levels will depend on the placement of the RTG's on the spacecraft structure. It is also reasonable to consider a combination of the two proposed programs, where worst-case testing would be suitable for devices in less critical circuits or, where due to location, dose levels would be low. In the opposite instance, however, in unprotected locations or where dose levels may be high, preselection seems to be the best approach to ascertain that subsystem performance will not degrade below tolerable levels due to radiation damage of components.

Onboard flight dosimetry data telemetered from early flybys would provide an important contribution to post-launch analysis. Feedback or guidance is thereby provided for later phases of the program. Furthermore, decisions on the real-time management of each spacecraft in flight could be influenced by a knowledge of the true degree of radiation damage existing in a payload at a given stage. In the same sense as temperature telemetry assists such decisions, radiation-damage telemetry would be a factor in assessing the practical life-expectancy of the system of unexpected failure modes threatened to curtail the mission.

4. Impact of Radiation Effects on the NEW MOONS Program (Time and Cost)

Radiation hardening as a design parameter inevitably has some time and cost implications. A well-planned radiation analysis effort need not add greatly to the time required to bring a spacecraft from concept to launch phase, since the work involved can be dovetailed with the routine design process. However, the services of "radiation effects" specialists grounded to some degree in radiation physics, test procedures, and design engineering are required.

SECTION II

ANALYSIS OF THE RADIATION ENVIRONMENT

A. General

The flight path of the NEW MOONS spacecraft, for the purposes of this discussion, is based on data taken from the Task I report. Over a 5-year period, the spacecraft is expected to follow a trajectory essentially in the plane of the ecliptic from a near-Earth parking orbit to a near-encounter with Jupiter and then continuing on well beyond Jupiter. The distance from the center of Jupiter to the spacecraft at its closest point to the planet is taken as 8.4 Jupiter radii (R_j). From a 200 mi (nautical) parking orbit near the Earth the elapsed time to reach Jupiter at about 5 AU will take about 549.5 days. The remaining part of the 5-year mission period will take the spacecraft to nearly 16 AU.

A substantial part of the radiation dose accumulated by spacecraft components during the mission is expected to come from exposure to relatively intense radiation during passage through the Earth's Van Allen belt and the presumed equivalent belt surrounding Jupiter even though the exposure times will be relatively short, about 1 hour near the Earth, and about 15 hours near Jupiter. * In interplanetary space, although the radiation intensity in this region is much lower than it is in the belts, the long exposure time will allow a significant buildup in dose levels. Radiation from the RTG's will, of course, contribute continuously to the dose received by the spacecraft.

Radiation from the RTG's consists primarily of fast neutrons and gamma rays. In contrast, the source of space radiation encountered during the 5-year mission consists mainly of high-energy electrons and protons. In addition, bombarding electrons, interacting with the material of the spacecraft, will also generate X-rays of the same general nature as the gamma rays from the RTG's. Intensity of radiation in the near-Earth region reaches a maximum at about 1500 mi (nautical) above the equator because of the high-energy electrons and protons trapped in the Earth's magnetic field. In the region between the planets, the only radiation likely to affect the spacecraft will be the protons ejected from the Sun in the solar wind and solar flares. In addition, ultraviolet radiation from the Sun can affect the outer surfaces of the spacecraft. Present evidence suggests that a radiation belt of the same general characteristics as that of the Earth's Van Allen belt, but of considerably greater intensity, exists within the presumed strong magnetic field surrounding Jupiter.

---

*See Appendix I for variations of fluence with variations in radius of closest approach.

Estimating the combined effect of subsystem exposure to the space and RTG radiation environments is a complex procedure. It is first necessary to determine the anticipated types and levels of space and RTG radiation that will arrive at the surface of the spacecraft over the prescribed mission period. This determination is then followed by the preparation of internal dose level estimates, based on the calculated external environment and the radiation shielding provided by the spacecraft structure and the protection provided a particular device by surrounding components and enclosures. Estimates of the impact of these dose levels on individual devices and circuits form the basis for determining the overall effect on subsystem performance and the measures that must be taken, such as added shielding, to prevent performance deterioration beyond acceptable limits.

The approach used to arrive at a final estimate of the internal radiation environment and its effect is outlined briefly in Section III. The remainder of this section, then, describes each step of the analysis in detail, providing estimated results and conclusions.

B. Technical Approach

1. General

In predicting the combined effect of various types of radiation on materials, particularly semiconductors, it is necessary to distinguish between two types of radiation damage: bulk damage and ionization damage.

a. <u>Bulk Damage.</u> Bulk damage is the effect produced by particle bombardment described as the displacement of atoms from the crystal lattice of a semiconductor as a consequence of collisions. The resulting defects affect the electrical properties of the crystal; in the range of interest, the principal effect is normally a reduction in the lifetime of the minority carriers.

The bulk-damage-producing capability of bombarding particles is strongly dependent on their energy, charge, and mass. Electrons in the 8-MeV range, for example, produce about 15 times more damage in silicon than 1-MeV electrons. 1-MeV neutrons produce more damage than 1-MeV electrons. To facilitate comparisons of bulk-damage-producing capabilities, a method was evolved by Bell Telephone Laboratories (BTL) and RCA for converting a mixed-particle energy spectrum into units which express the damage this spectrum could cause (Ref. 6).

As described in Section IC-1, the degree of bulk displacement can be conveniently expressed as the equivalent fluence of 1-MeV electrons which cause

20

the damage, and the resulting unit of damage capability is called the DENI. Several investigators (Refs. 1 and 7) have determined efficiency factors experimentally for different energy ranges which, when multiplied by the particle population in that energy range, give the damage-producing potential in DENI's.

These damage efficiency factors depend strongly on the nature of the bombarding particles, their energy, and the type of semiconductor device subjected to bombardment. Also of importance is the injection level at which the device is to operate as well as the type of doping impurity and its concentration in the silicon. However, so long as these factors are remembered*, a similar bulk-damage-summing procedure for mixed fluxes of particles is practical for the purpose of making a worst-case engineering estimate of device degradation during a mission. Some definitive RCA work in this field is given in Reference 7.

b. Ionization Damage. Ionization damage is the effect produced in a material by the passage of high-energy particles or photons which eject some of the electrons bound to atoms. Subsequent rearrangement of the atoms or charges may produce changes in the characteristics of the material. This is the type of damage which most affects all common spacecraft materials (e.g., plastics, optics) and is a primary cause of degradation in "planar" semiconductor devices. Ionization damage will, for example, turn glass brown throughout its thickness, whereas, in the case of bipolar transistors, only the surface of the transistor chip is sensitive. This circumstance has lead to the description of ionization damage, as it pertains to transistors, as "surface damage."

---

*Limitations to the Use of Bulk Damage Efficiency Factors

The term, "Bulk Damage Efficiency Factors," as used in this footnote concerns the conversion from "Equivalent 1-MeV Electrons/cm^2 (DENI)" to "Bulk Damage Units − Neutrons/cm^2 (E > 10 KeV)".

The fluence of 1-MeV electrons which produce a given amount of damage in a solar cell is about 10^3 times higher than the fluence of reactor neutrons required to do the same damage (Ref. 7); on the other hand, with bipolar transistors, the factor is about 10^2. The reason for this is the difference in "injection level" in the two situations. In earlier explanatory sections (see e.g., Fig. 1B) the latter factor, 10^2, is taken as a working ratio to deal with the normal silicon junction devices used internally in the spacecraft (e.g., transistors, SCR's, diodes, integrated circuits, etc.) in which the electrical degradation is controlled by the degradation of minority-carrier lifetime and the injection levels are high.

The case of the MOS device is different; here, the only important effects of neutrons on the silicon is to reduce majority-carrier conduction (Ref. 20); the ratio of damage efficiencies for neutrons and electrons will be different again here, although the ratio of damage efficiencies of the two particle types is still in the region of 10^2 (see, for example, H. Stein and R. Gereth, J. Appl. Phys. 39 (6), 28701968). Note also, however, that in most common radiation situations, and with state-of-the-art MOS devices, it is not the bulk damage effect, produced by neutrons, which dominates the electrical changes in the device. Long before this effect is significant, the ionization effect has produced very extensive changes in the device.

In a similar manner as that described for bulk damage, the ionization-damage-producing capability of a mixed radiation environment can be summed and expressed in rads. By definition, 100 ergs of ionization energy deposited in a gram of material constitutes a dose of 1 rad. The amount of energy absorbed per gram of material per particle or photon depends on the energy and type of the incident radiation. For electrons, this variation in absorbed energy vs particle energy in the range from 0 to 8 MeV is relatively small. For the protons in the range from 0 to 1000 MeV, however, it may be several orders of magnitude. Thus, it will be seen that calculation of the ionizing dose will, as for the bulk damage calculations, be complicated by the need for using energy-dependence factors for electrons, protons, neutrons, and gamma photons.

The advantage of using the DENI and rad system in estimating the radiation dose affecting a subsystem is that contributions from various sources can be converted into the same units and added arithmetically.

2. Procedure for Estimating Total Radiation Dose from the Space Environment

To estimate the combined effect of the various types of space radiation on particular spacecraft subsystems, four different kinds of information are needed:

(1) The number and directionality of the particles which the spacecraft will encounter during the mission, classified according to their energy content for each of the radiation regions (near-Earth, Interplanetary-Earth to Jupiter, near-Jupiter, and Interplanetary-Jupiter and Beyond).

(2) The relationship between the energy content of the particles and their damage-producing capability.

(3) The relationship between the energy content of the particles and their ability to penetrate materials, such as aluminum, used in the construction of the spacecraft.

(4) The radiation shielding provided by adjacent devices and enclosures surrounding individual components.

The relationship between the damage-producing capability of the incoming particles and the shielding effect of the intervening materials and structures protecting sensitive components is then expressed as a "damage profile" for each of the two types of damage, bulk and ionization.

3. Procedure for Estimating Total Radiation Dose from Two RTG's

Major differences in the nature and source of the radiation from the RTG's compared with space radiation dictate a somewhat different approach to the

evaluation of damage effects from this source. The fast neutrons and gamma rays emanating from the RTG's are highly penetrating compared with most of the electron and proton population in space. Protecting sensitive components from RTG radiation by providing sufficient shielding could impose a severe weight penalty on the spacecraft. However, the essentially inverse-square relationship between radiation flux and distance from the RTG can be used to determine radiation levels at various distances from the RTG, and a safe distance for the placement of sensitive components can then be determined. By using isoflux maps, which indicate the contours of equal radiation flux in the region surrounding an RTG, the relationship between dose level and distance may again be plotted in terms of rads and DENI's.

NOTE: Radiation effects on spacecraft subsystems can be reduced by shielding techniques and by separation techniques and combinations of these. The weight considerations associated with reducing the radiation background at the scientific experiments is covered in Task IV.

4. Calculation of Internal Environment

In estimating the radiation dose affecting a particular component, the contributions from various sources expressed in compatible damage units can be added arithmetically. Dose-vs-distance curves will provide the information necessary to estimate the dose from the RTG's, assuming that no special shielding is added to attenuate neutron and gamma flux.

In estimating the dose contribution from space radiation, the necessary data are taken from damage profiles, which show how the anticipated dose from the space environment affecting a component will vary as a function of the thickness of a hypothetical uniform spherical shell of aluminum surrounding the component. The data from the damage profiles are then applied to a Sector Analysis* of the spacecraft structure, which is, in effect, a technique for calculating the amount of shielding surrounding any component, based on the spacecraft configuration and packaging. The values of equivalent shield thicknesses for various particle paths through the spacecraft are determined, and through the use of the damage profiles, the net level of internal radiation to which a component will be exposed can be estimated. In addition to analytical techniques for determining spacecraft shielding exposure of a breadboard radiation spacecraft to a suitable radiation source with appropriate detectors at various locations within the spacecraft a more precise estimate of the thickness of an idealized aluminum shield can be obtained. An idea of the large variety of radiation exposure conditions produced within the structure of a spacecraft is shown in Figure 2.

---

*Discussed in Sections IIE and IVB of this report.

IONIZING DOSE DUE TO
EXTERNAL FLUX (IN RADS)

10^7 TO 10^{10}

10^6 TO 10^7

10^5 TO 10^6

10^4 TO 10^5

10^3 TO 10^4

METAL OR PLASTIC SKIN

②ACTIVE ELEMENT OF
EXTERNAL PIECE PARTS

①SURFACE
COATINGS

ZONE NO. ① ② ③ ④ ⑤ 500 200 100 10 0.1

EXTERNAL FLUXES,
(ENERGY IN MeV), ARE
COMPOSED OF:

ELECTRONS (BELT): 0.1 – 10

PROTONS (BELT): 0.1–100

PROTONS (FLARE): 1–100

ALPHAS (FLARE): 1–100

PROTONS (SOLAR WIND):
10^{-4} TO 10^{-2}

RTG NEUTRONS: 0.1–10

RTG GAMMA RAYS: ~ 1

THICKNESS, t, OF ALUMINUM
STRUCTURE AND OTHER
SPACECRAFT MATERIALS
(IN MILS)

BOXED COMPONENTS ⑤

BOXED COMPONENTS ④

OUTSIDE SURFACE ③
OF BOXES

*EXPOSED LOCATION
100 MIL

*TYPICAL LOCATION
270 MIL

MISSION:

5-YR INTERPLANETARY WITH
18-INCH RTG/SPACECRAFT
SEPARATION DISTANCE AND
JUPITER FLYBY

*LOCATIONS USED AS EXAMPLES IN THE TEXT.

Figure 2. The Various Radiation Zones on a Spacecraft

The final summing of the combined dose levels from space and RTG radiation in two categories of ionization and bulk damage is then achieved by adding the damage values for space radiation to that for RTG radiation for various distances of the RTG from the spacecraft structure. The procedure described above is shown in block diagram form in Figure 3.

C. Detailed Analysis of External Radiation Flux From Space Environment*

In estimating the anticipated radiation dose from the space environment that will affect sensitive components within the spacecraft, the result of exposure to each of the different radiation regions has been evaluated. Damage vs shield-thickness profiles for the combined effect of the various types and energies of space radiation particle were then plotted.

In general, a review of Table 1, Summary of Worst-Case Estimates of Radiation Damage Levels for a 5-Year NEW MOONS Mission, indicates the relative orders of magnitude of radiation dose attributable to various regions of the mission. Assuming that the total "mission dose" for components in a typical and exposed spacecraft location is 100 percent, then, for ionization damage, the percent distribution among the various regions, including the RTG contribution in the region, could be thought of in the following terms:

Region	Dose (percent)	
	Typical Location	Exposed Location
1 Integration and Pre-Launch	11	2
2 Near-Earth	Neg.	Neg.
3 Earth to Jupiter	25	4
4 Near-Jupiter	10	86
5 Jupiter and Beyond	54	8

While this is not a complete presentation, it does serve to illustrate the relative area of concern. Each of these areas is discussed in the following sections:

1. Integration and Pre-Launch

Radiation to the spacecraft during the integration and pre-launch period is due to the RTG environment and not space environment but it is noted here be-

*References are given at appropriate points in the text to the principal sources from which the basic space environment data were taken. See References 1, 2, 3, 9, and 13.

SPACE RADIATION
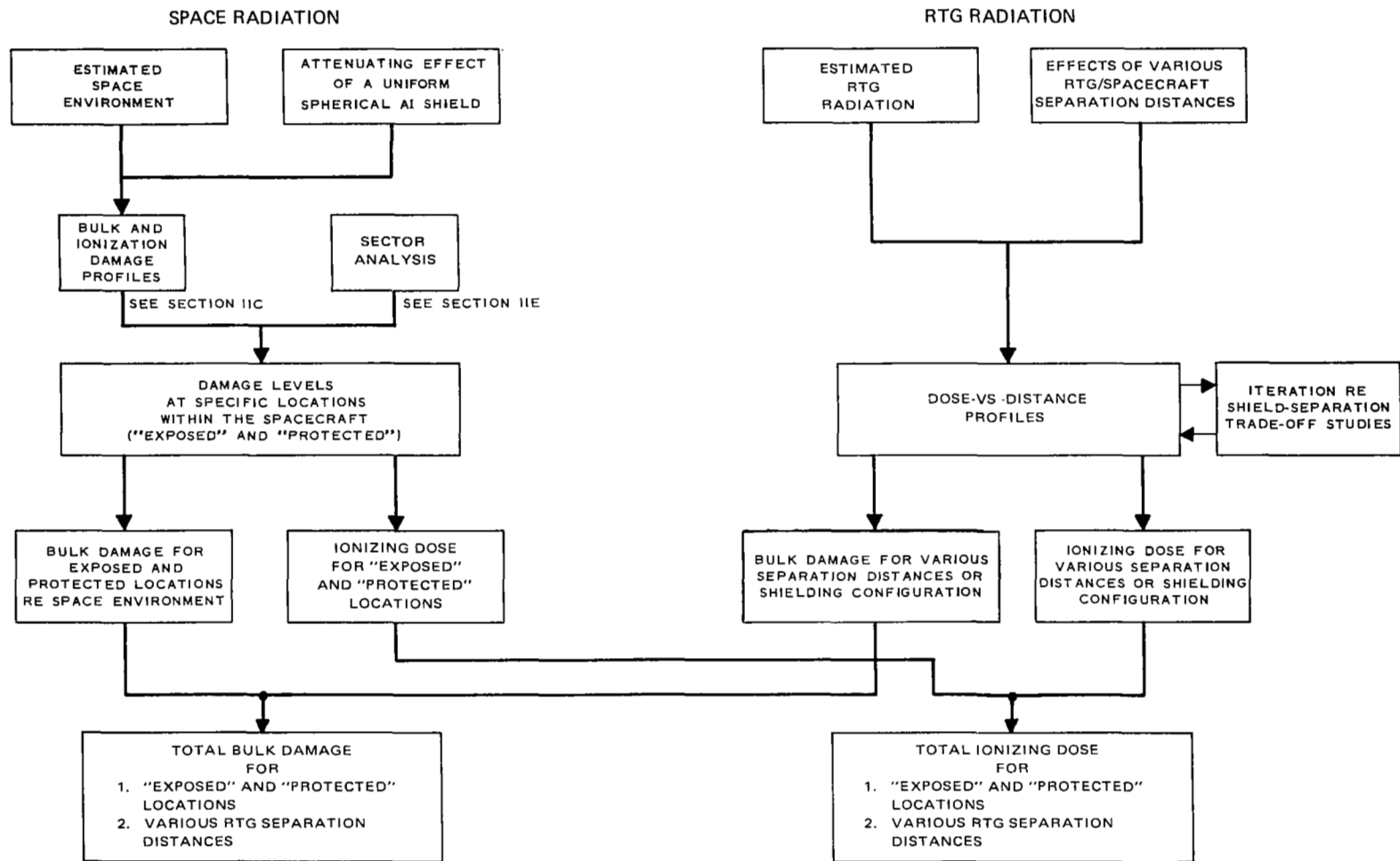
RTG RADIATION

Figure 3. Procedure for Estimating Combined Radiation Damage Levels Within Spacecraft Structure

cause it represents the first region, ground, of exposure of the spacecraft to a radiation field. Ground testing can add greatly to the radiation dose level depending on the exposure period and the proximity of the RTG's to sensitive spacecraft components. A worst-case estimate has been made based on a 9-month exposure and an 18-inch RTG-spacecraft separation distance. The magnitude of the dose level accumulated under these conditions is given in Table 1. A thorough discussion of RTG-produced radiation is given in Section IID, "Radiation Dose from RTG's." Although the ground region is of concern, this report deals primarily with the flight portion of the mission, and subsequent discussions do not include the integration and pre-launch dose level.

2. The Near-Earth Region

The electrons and protons trapped in the Earth's magnetic field occur principally in a region referred to as the Van Allen belt. This is a region of intense high-energy-particle radiation that surrounds Earth outside the atmosphere. Trapped electrons have energies from a few hundred electron volts to over 8 MeV, protons from a few kilovolts to over 1000 MeV. However, the population of both particle types is concentrated toward the low energy region.

Passage through the Earth's Van Allen belt will subject the spacecraft to relatively intense radiation for a short period of time. Information needed to estimate the magnitude of the effect includes the trajectory through the belt and the variation of radiation intensity with altitude. Curve A in Figure 4 shows the variation in spacecraft altitude above Earth from the time it leaves a parking orbit* 100 mi (nautical) until it is well beyond the most intense region of the radiation belt. The altitude curve is based on a computer run, prepared for Task I, determining the flight path during the initial phase of the trip to Jupiter.

Figure 5 is a typical map showing the distribution of electron flux with energies > 0.5 MeV in the Van Allen belt, averaged over a 24-hour period. Estimates of the particle flux affecting the spacecraft during this part of the journey are based on data available in NASA publications. One of these publications lists the anticipated electron and proton environment in late 1968; these data were used unchanged (Ref. 1). The error in using the same data for launch dates in 1974 is not expected to exceed a factor of two since the particle population in the Van Allen belt is apparently reaching a relatively stable level after being greatly disturbed by the "Starfish" explosions in 1962. This situation could be drastically altered if nuclear experiments in space are resumed.

Curve B in Figure 4 shows the variation in electron flux with time corresponding to the altitude variation of Curve A. The area under Curve B is, there-

---

*Since the particle flux at the parking orbit altitude is only a small fraction of the flux at altitudes above about 300 mi (nautical), the dose contribution from exposure to radiation in the parking orbit can be neglected.
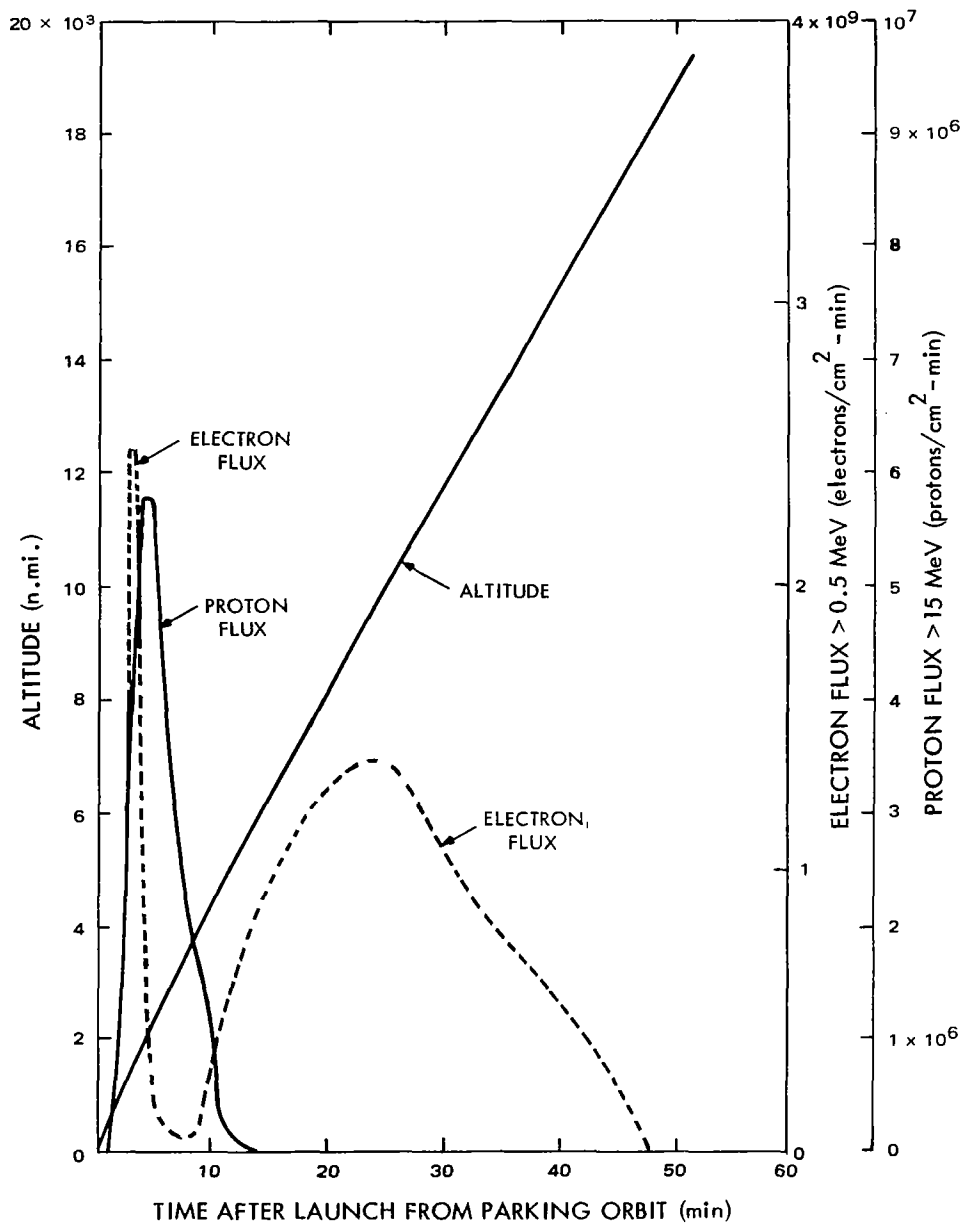
Figure 4. Irradiation in the Van Allen Belt (Based on 1968 Epoch)
Adapted From Vette (Ref. 1)
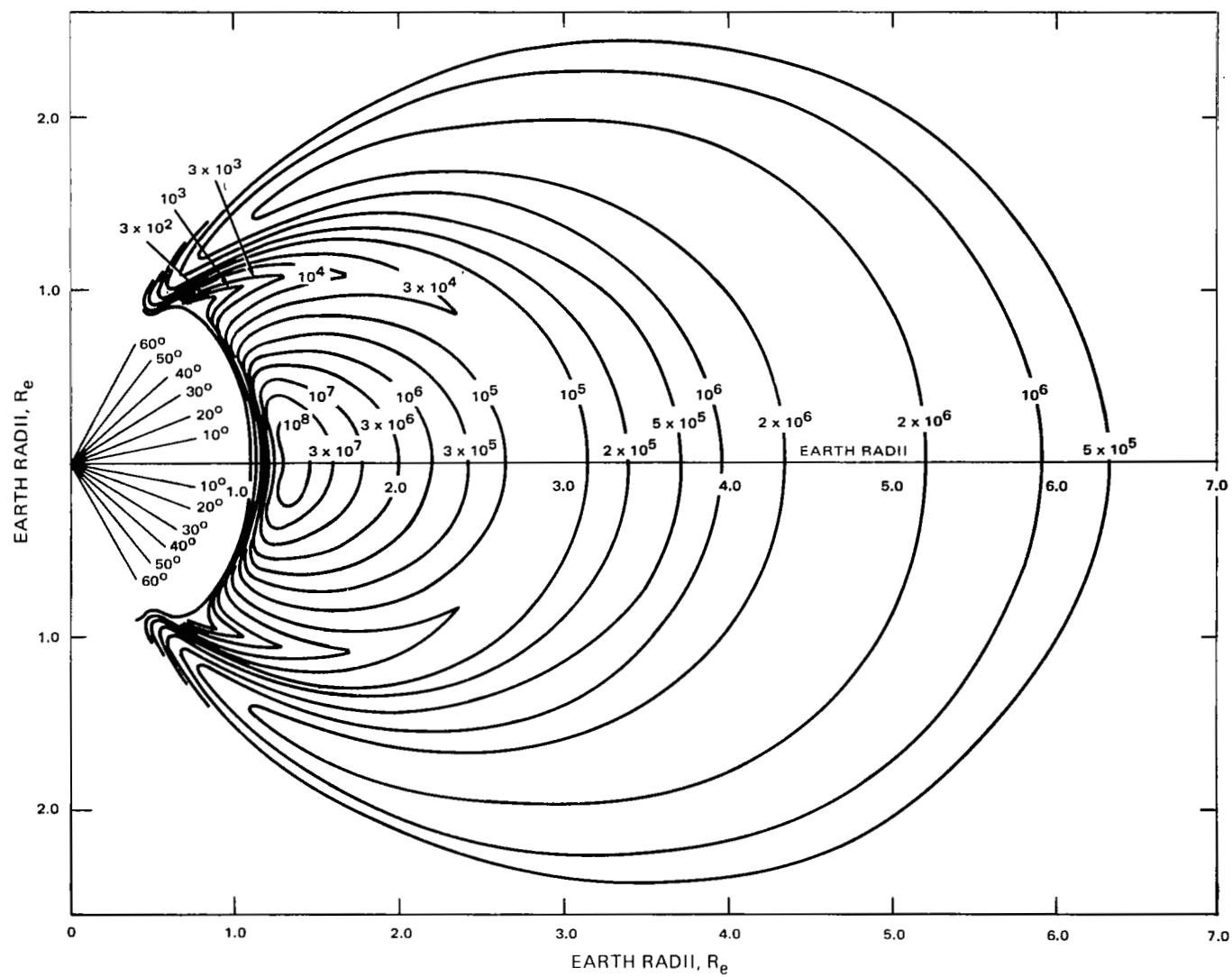
Figure 5. Electron Map AE-2, August 1964, Omnidirectional Flux (electrons/cm²-sec), Energy > 0.5 MeV, From Vette (Ref. 1)

fore, a measure of the total flux of electrons having energies above 0.5 MeV that strike the surface of the spacecraft during passage through the Van Allen belt. The result of graphical integration is an electron fluence of 3.8×10^{10} electron/cm^2 of energy greater than 0.5 MeV. In obtaining Curve B from the NASA data, it was assumed that the flight path would not be inclined more than about 20 degrees from Earth's geomagnetic equator. It was also assumed that the variation in flux with longitude could be ignored without causing serious errors. Since the NASA tables are based on 24-hour averages, using the data for shorter exposures will be somewhat in error, particularly at low altitudes.

Curve C in Figure 4 showing the variation in proton flux with time, was obtained in the same manner as Curve B. A graphical determination of the area under Curve C gives a proton fluence of 2.8×10^7 protons/cm^2 of energy greater than 15 MeV.

The procedure, illustrated by Figure 4, was repeated a number of times, each time using a different value for the minimum particle energy and different from those forming the basis for the curves in Figure 4. The results of such calculations are summarized in Table 2, Column A. Data of this kind, combined with similar data from exposure to radiation over other segments of the flight path, form the basis for calculations of the anticipated total radiation damage or dose levels from exposure to the combination of the space and RTG environments.

3. Interplanetary Space (Earth to Jupiter)

a. <u>Solar Flares</u>. The solar disturbances called flares occasionally eject into space short but extremely intense clouds of high-energy protons. The major proton flares occur at highly irregular time intervals, and there are rarely more than five per year. Predictions of the frequency and intensity of these bursts are based largely on the history of such events and are, therefore, subject to considerable error. Observations of these phenomena since the early 1800's indicate that solar disturbances of this kind follow an 11-year cycle of increasing and decreasing intensity. A launch date in 1974 would coincide approximately with a minimum in solar activity. To determine the approximate average effect of this radiation, an estimate was prepared of the possible total integrated solar proton flux on the following basis: It was assumed that the solar proton flux in the region near the Earth but outside its magnetic field would be constant and equal to the average measured over the period from 1956 to 1961. This average, determined from data included in reports by Dr. W. Webber (Ref. 2) is shown in Table 3. It was also assumed that this flux will vary inversely as the square of the distance from the Sun.

The technique used previously in estimating the total flux from trapped protons and electrons was also found useful in calculating the total integrated flux

30

Table 2

Summary of Estimates of Particle Fluence
From Space Environment — 5-Year Mission*

		A	B	C	D
Particles	Energy (MeV)	Trapped Particles Near-Earth $(\phi > E)$[‡]	Interplanetary Space[†] $(\phi > E)$	Trapped Particles Near-Jupiter[§] $(\phi > E)$	Total $(\phi > E)$
Electrons per sq. cm.	0.001	2.7×10^{11}	Not Applicable	6.91×10^{13}	6.94×10^{13}
	0.5	0.38		1.02	1.02
	1	0.092		0.306	0.307
	2	0.011		0.0613	0.0614
	3	0.0026		0.0143	0.0143
	4	0.00078		0.00368	0.00369
	5	0.00024		0.000956	0.000958
	6	0.000075		0.000253	0.000254
	7	0.000025		0.000068	0.000068
Protons per sq. cm.	Solar Wind 0.001 to 0.050	Not Applicable	$\sim 2.9 \times 10^{15}$	Not Applicable	$\sim 2.9 \times 10^{15}$
			Solar Flare		
	>0.1	9.7×10^{10}	—	44.2×10^{12}	44.3×10^{12}
	0.4	4.0	—	23.0	23.0
	1.0	0.12	0.093×10^{12}	6.7	6.79
	4.0	0.050	0.0099	0.050	0.0604
	10	0.0080	0.00248	0.00118	0.00374
	15	0.0028	0.00136	0.00027	0.00163
	30	0.00068	0.00050	0.000015	0.00052

*For a more detailed breakdown see Table 1.

† A large uncertainty exists as to the flux and energy content of the solar wind protons. It is thought that the peak is in the region of 1 to 50 keV. At this energy level no semiconductor device would be adversely affected, since this energy component would be absorbed in the first few microns of the spacecraft exterior surface. The effects on Thermal Coatings are described in Section III. The proton fluence from solar flares is taken as the average over the period 1956-1961 inclusive.

‡ Fluence, ϕ, is given above specific energy values, E.

§ See text for discussion on the uncertainties of the Jupiter radiation belt.

31
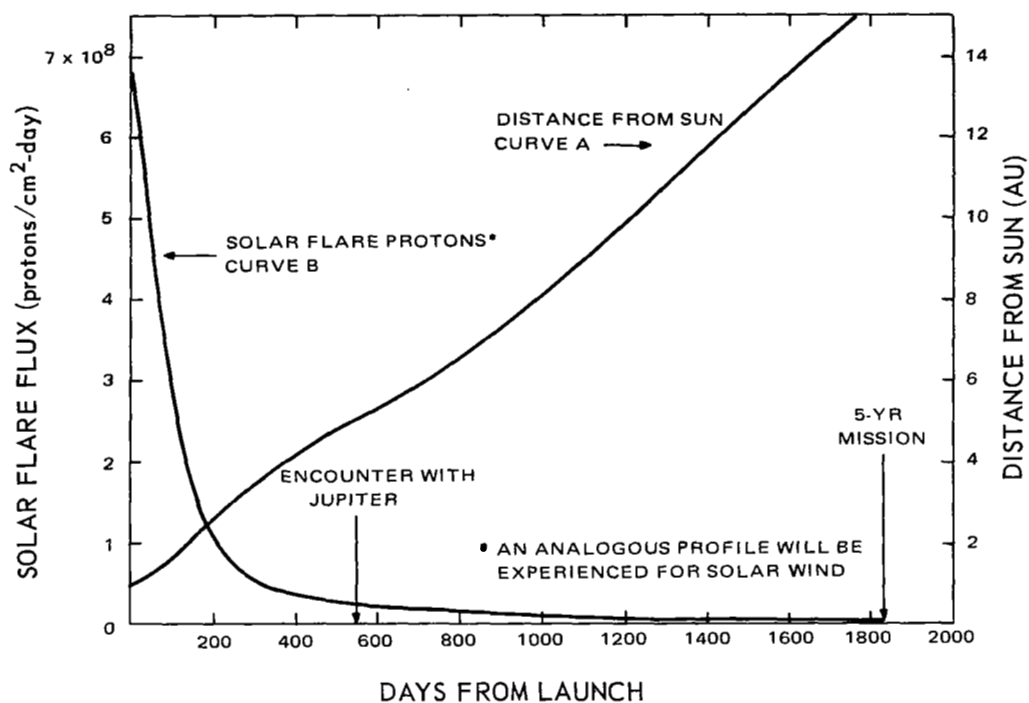
Figure 6. Solar Proton Flux and Distance Variations With Time

Table 3

Six-Year Total — Solar Flare Protons in the Region Near the Earth
(From Data by W. R. Webber)

E (MeV)	$\phi > E$
	protons/cm^2
1	1.5×10^{12}
4	0.16
10	0.04
15	0.022
30	0.008

from solar flare protons. Trajectory information taken from the Task I report provided the basis for Curve A on Figure 6, showing how distance of the spacecraft from the Sun varies with time in days from launch. Curve B shows the resulting variation in proton flux of energy above 1 MeV as a function of time. Based on the area underneath Curve B, from the beginning of the interplanetary portion of the mission to Jupiter encounter, the integrated flux at the end of this period will be 8.0×10^{10} protons/cm^2.

b. Solar Wind. Particle-measuring devices on such satellites as IMP 1 have shown that a relatively constant stream of low-energy protons is continuously emitted from the Sun. A recent article by N. F. Ness (Ref. 3) describes the general characteristics of this type of space radiation. The average flux in the region near the Earth but outside the influence of its magnetic field is in the neighborhood of 2.5×10^8 particles/cm^2-sec. The average energy of these particles is approximately 1 keV with a maximum of the order of 50 keV.

In this energy range, protons will only penetrate a few microns of the outer surface and will, therefore, have no effect on such components as transistors and diodes. However, thermal-control coatings applied to the skin of the spacecraft may be appreciably affected by prolonged exposure to the solar wind. The same would apply to any solar-cell or sensor cover glasses (Ref. 8).

The integrated flux from the solar wind at the spacecraft surface can be estimated in the same manner used previously in evaluating the effect of solar flare protons. This estimate is again based on an assumed inverse-square relationship between proton flux and distance from the Sun. Integrating the flux over the Earth to Jupiter part of the mission period gives an average total dose of 2.5×10^{15} protons/cm^2 with energies between 0.1 to 50 keV. A dose of this magnitude will substantially alter the reflectance properties of certain types of paints. This subject is treated in greater detail in Section III of this report including an evaluation of enhanced damage from the effect of ultraviolet radiation.

4. The Near-Jupiter Region

Particles trapped in the Jovian magnetic field will only affect the spacecraft during the relatively short flyby maneuver. However, present estimates of the number of trapped particles indicate that the dose accumulated during only a few hours will be one of the dominant elements in the radiation environment and sufficient to cause significant damage effects in sensitive components. The radiation dose from this source will, of course, be strongly dependent on the spacecraft trajectory in the near-Jupiter region. The trajectory used in the calculations, as shown in Figure 7, was taken from the Task I report. Curve A in Figure 8 derived from Figure 7 indicates the time variation in altitude of the spacecraft expressed in terms of the distance from the center of Jupiter in
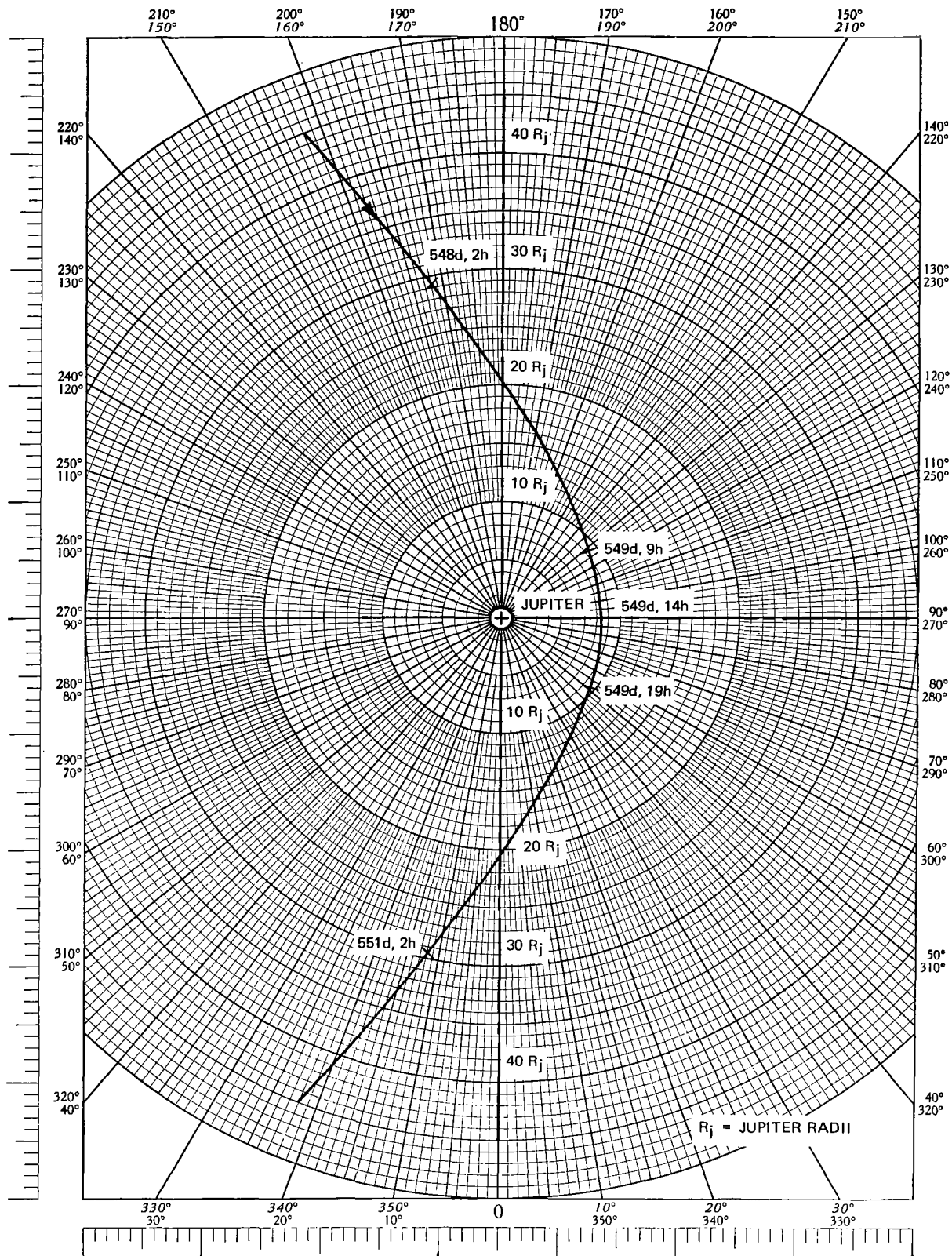
Figure 7. Jupiter Probe Trajectory
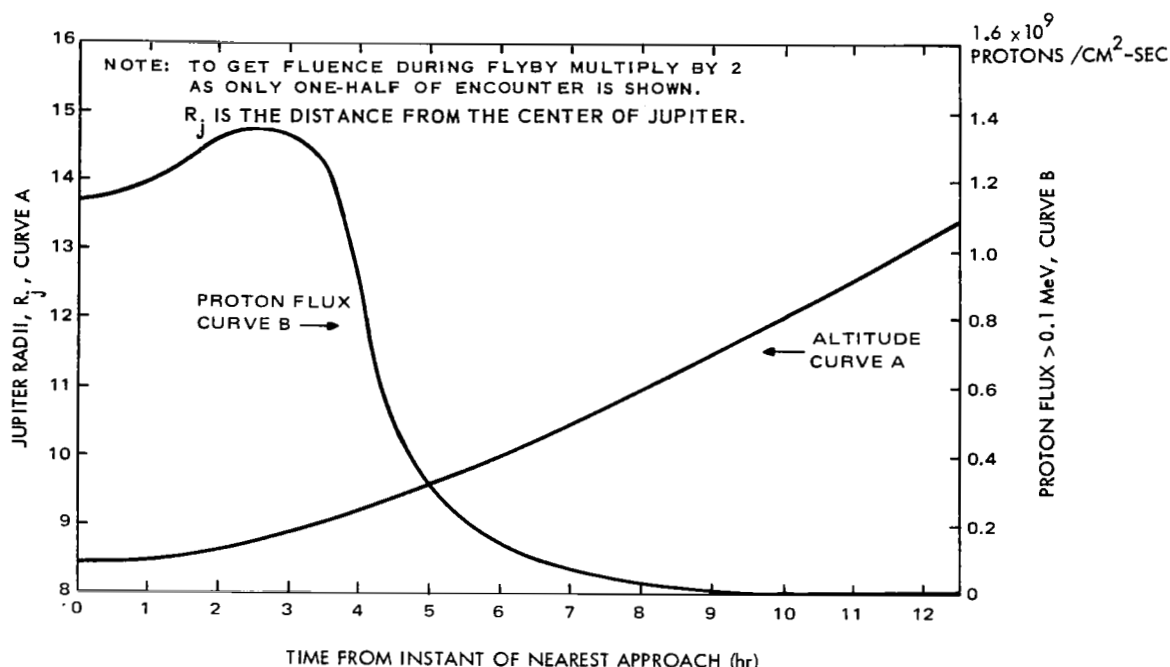
Figure 8. Variation With Time of Altitude and Proton Flux in the Near-Jupiter Region

Jupiter radii. It is assumed that the trajectory is symmetrical about the vertical axis at t = 0. The effect of trajectories that will bring the spacecraft closer to the surface of Jupiter will be considered later in this section and in Appendix II.

The information provided by the GJP study team relating the near-Jupiter particle flux to the altitude above Jupiter formed the principal basis for calculations of estimated dose levels resulting from the Jupiter flyby maneuver. These data, however, are limited to the electron flux in the range from 5 to 100 MeV and the proton flux in the range from 0.1 to 4 MeV. Since, in the Earth's Van Allen belt the electron flux extends to the region below 5 MeV as far as 40 keV and the proton flux extends above 4 MeV to at least 1000 MeV, it was assumed that electrons and protons in these energy ranges would also be trapped in the radiation belt that presumably surrounds Jupiter. The particle flux data from the Phase A report was therefore extrapolated to include electrons in the energy range below 5 MeV and protons in the energy range above 4 MeV. It was also assumed that the energy distribution of the particles in these energy ranges would be similar to that in the Van Allen belt.

In addition it was assumed that—

(1) The angle of inclination of the trajectory with the Jovian geomagnetic equatorial plane is sufficiently small so that Van Allen belt data taken for a zero angle of inclination (equatorial orbit) will be applicable.

(2) Longitudinal and temporal variations of the Jovian particle flux can be neglected.

a. __Calculation of the Trapped Proton Environment.__ The two curves of
Figure 9 allow a comparison of the assumed variation in proton flux as a func-
tion of distance from the center of Jupiter with the equivalent data for Earth.
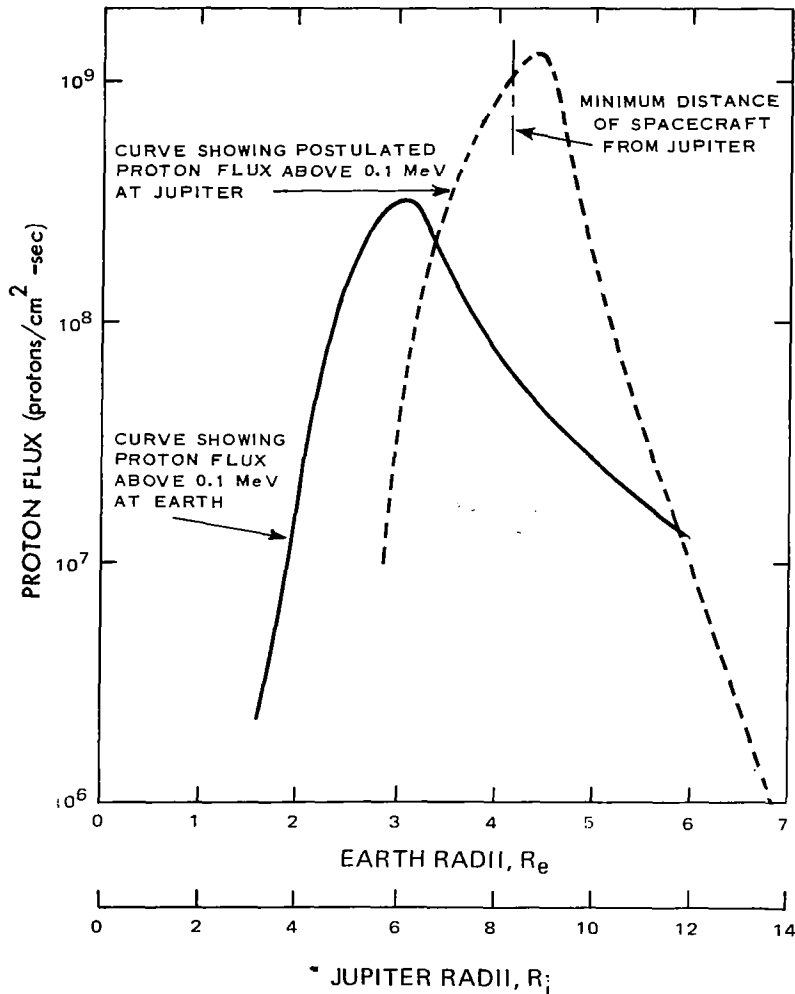
Figure 9. Comparison of Jupiter and Earth Proton Flux Above 0.1 MeV

Proton flux models AP1 through AP5 prepared by Dr. Vette (Ref. 1) and co-
authors formed the basis for the curve designated "Earth." This curve shows
the total flux above 0.1 MeV while the curve marked "Jupiter" shows only the
flux between E = 0.1 to 4 MeV. However, if the assumption regarding the simi-
larity of the energy spectra is correct, the curve for total flux above 0.1 MeV
for Jupiter will not be significantly different from the one shown, since the flux
of E > 4 MeV is such a small fraction of the total.

36

It will be seen that the trajectory as shown in Figures 7 and 8 will bring the spacecraft into the region of maximum proton flux, as shown in Figure 9. Exposure to proton bombardment will be confined largely to the region traversed from a distance of about 12 Jupiter radii to the minimum distance at 8.4 radii and again to the outer part of the belt at 12 radii. The relationship in Figure 9 of proton flux of E > 0.1 MeV to Jupiter radii was used to construct Curve B in Figure 8, showing the variation with time of the proton flux affecting the spacecraft. The area underneath Curve B is, therefore, a measure of the total integrated proton flux of E > 0.1 MeV encountered during the Jupiter flyby. Converting the hours to seconds, integrating graphically, and multiplying by 2 (because of symmetry around the vertical axis at t = 0) results in a total of 4.42×10^{13} protons/cm^2 of E > 0.1 MeV.

The energy distribution of the proton flux in the Van Allen belt near its peak at about 3 Earth radii, as shown in Figure 9, was taken as the model for the energy distribution in the region traversed during the Jupiter flyby also near its proton flux peak. Other assumptions could be made but the assumption that the proton energy distribution remains constant in this region probably provides a substantial margin of safety since in the Van Allen belt the proton spectrum becomes markedly softer beyond the peak at 3 Earth radii. However, the total proton population decreases more slowly with altitude in the Van Allen belt than the data indicate is the case for Jupiter, according to the curves shown in Figure 9. This condition, however, was also recognized as noted in a NASA study on the Galactic Jupiter Probe. Column C of Table 2 shows the resulting estimate of the total integrated proton flux and its energy distribution, based on the model just discussed.

b. Calculation of the Trapped Electron Environment. The technique just described was also used as the basis for an estimate of the total integrated electron flux and its energy distribution. Figure 10 shows the electron flux variation with altitude in the near-Earth and near-Jupiter radiation belts. Dr. Vette's reports (Ref. 1) provide the data for the Van Allen belt; the equivalent data for Jupiter were taken from the NASA Galactic Jupiter Probe Study. Of particular interest is the "valley" in the curves, which is not in evidence in the proton curves of Figure 9.

The various factors that cause the valley in the Van Allen belt could be altogether different in the belt surrounding Jupiter. If, indeed, the electron contours proceeded smoothly upwards with decreasing altitude, then the fluences accumulated near the point of nearest approach would be larger by a factor of 2 to 3. The valley in Earth's belt arises because electron trapping on certain magnetic shells is inefficient and particles are "dumped" from these shells, probably into the polar atmosphere.
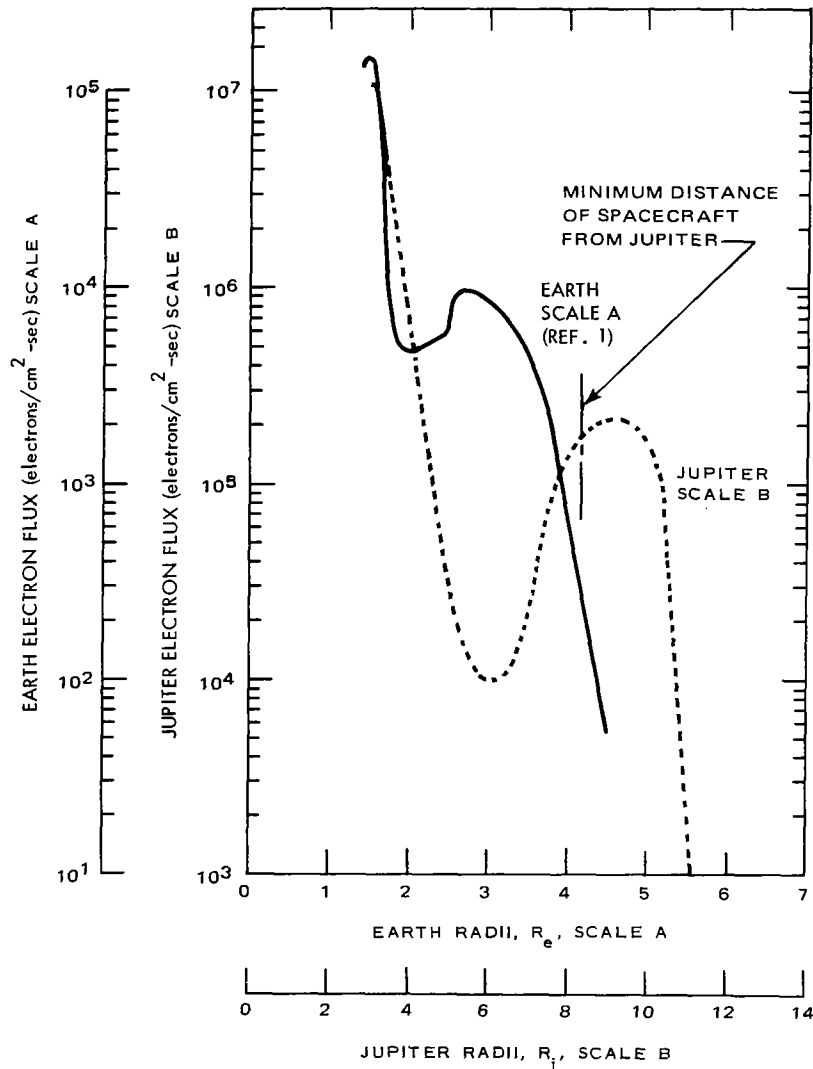
Figure 10. Comparison of Jupiter and Earth Electron Flux Above 5 MeV

The estimated total integrated electron flux of E > 5 MeV to be encountered by the spacecraft was determined by the same graphical integration method described previously. On the basis of the area under Curve B of Figure 11, the total flux is 9.56×10^9 electrons/cm^2 (E > 5 MeV). The energy distribution of electrons at the second "peak" in Earth's Van Allen belt served as the model for the equivalent energy distribution in the region around the second peak of the Jupiter belt from about 8 to 11 Jupiter radii, as shown in Figure 10. Column C of Table 2 shows the resulting estimate of the total integrated electron flux above given values of minimum particle energy.
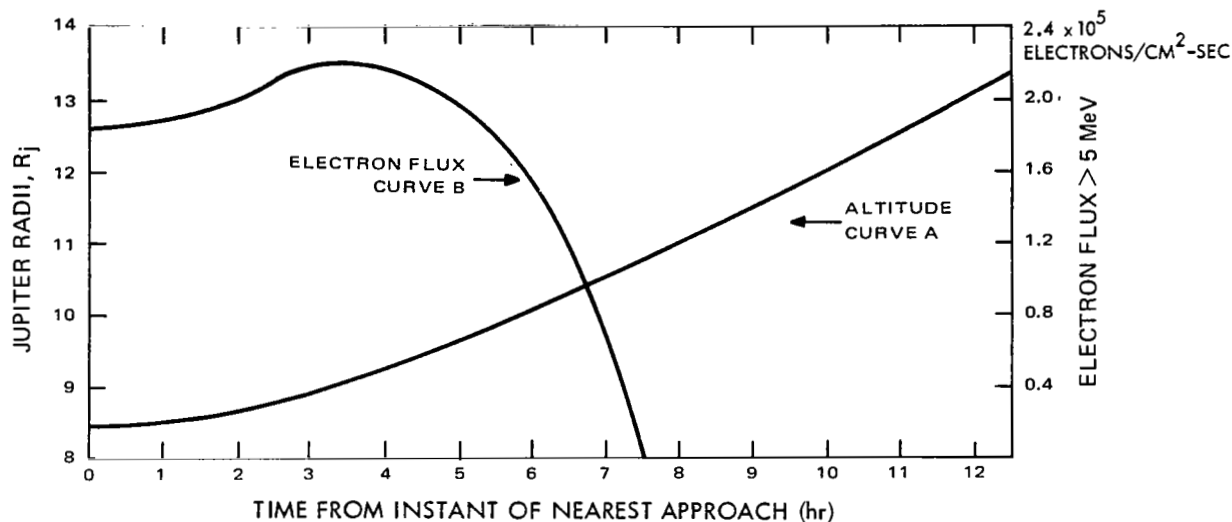
Figure 11. Variation With Time of Altitude and Electron Flux in the Near-Jupiter Region

The highly speculative nature of the assumptions regarding the presumed radiation belt around Jupiter should again be emphasized. Data of this kind taken from the Phase A study represent a compromise in the estimates prepared by a number of different investigators. These estimates are based primarily on observations of radio emission from the near-Jupiter region. The motion of high-energy electrons trapped in a magnetic field around Jupiter can presumably account for the observed radio signals. The intensity of the radio signals and their frequency spectrum provide a basis for estimating the strength of the magnetic field around Jupiter and the trapped electron population. Estimates of trapped protons are even more speculative since there is no direct evidence of their presence in the near-Jupiter region. An assumed similarity of the radiation belt around Jupiter to the Van Allen belt provides the only available basis for estimating the near-Jupiter proton flux and its energy distribution.

As may be expected, published estimates of the near-Jupiter electron and proton flux vary over several orders of magnitude. The estimates from the Phase A report are apparently above the average but less than the maximum and, therefore, appear to be reasonably conservative. The remote possibility that the actual particle flux values may be above the estimates by perhaps an order of magnitude should not be overlooked. The problem of providing an adequate factor of safety in this respect will be treated later in the text.

A substantial increase in the radiation dose affecting spacecraft components would also result if the trajectory were altered to bring the spacecraft closer to

39

the surface of Jupiter. Figures 9 and 10 show that as the spacecraft approaches closer to Jupiter than 8.4 R_j both the electron and proton flux encountered fall substantially below the peak values at around 9 R_j. The electron flux, however, (Figure 10) reaches a valley at about 6 R_j and then rises to a much higher peak at 3 R_j.

These variations are of particular importance since the following discussion shows that the electron flux will probably be the principal source of radiation damage from the Jupiter flyby maneuver. The increase in the velocity of the spacecraft in trajectories closer to Jupiter will tend to reduce the dose rate in the region of minimum distance to Jupiter. However, the total exposure time will increase, and therefore the total dose from exposure in the Jupiter radiation belt will also increase. Preliminary estimates indicate that if the minimum distance from Jupiter were decreased from 8.4 R_j to 5 R_j the radiation dose levels would increase by a factor of about 3 and if the distance were reduced to 3 R_j the factor would be about 10. The probability of such increases will also need consideration in determining what factor of safety should be applied to the environmental data to take care of any contingencies.*

5. Interplanetary Space—Jupiter and Beyond

The assumptions and techniques used for estimating the solar flare fluence and the solar wind fluence described in paragraph 3 of this Section, Interplanetary Space—Earth to Jupiter, are equally appropriate for estimating the fluence for Jupiter and beyond. Integrating the area under Curve B of Figure 6 from Jupiter encounter to the end of the 5-year mission gives an integrated flux, above 1 MeV, of 1.3×10^{10} protons/cm^2. The addition of this value, 1.3×10^{10} protons/cm^2, to that accumulated during the Earth to Jupiter portion of the mission, 8.0×10^{10} protons/cm^2, gives the accumulated fluence 9.3×10^{10} protons/cm^2 for the 5-year mission from interplanetary space. Column B of Table 2 shows the energy distribution of these protons assuming that variations of the distribution with distance from the Sun are negligible.

The solar wind fluence for the Jupiter and beyond portion of the mission is 0.4×10^{15} protons/cm^2 and is a total of 2.9×10^{15} protons/cm^2 for the 5-year mission as shown in Column B of Table 2. The damage effects to the outer surfaces of the spacecraft due to solar wind are treated in Section III.

6. Radiation Damage Profile From Space Environment

The relationship between damage-producing capability of the incoming particles and the shielding effect of intervening materials and structures protecting

---

*Also see Appendix I concerning radiation environment of the Jupiter flyby for various near-Jupiter trajectories.

sensitive components can be shown graphically in a particularly useful form called the "damage profile." The method for preparing such profiles from the environmental data of the type shown in Table 2 is described in detail in the TOS Radiation Program Report (Ref. 9), dated September 1965. Two profiles are needed to indicate the separate ionization-damage and bulk-damage effects. These profiles show the dose level dependence on the amount of shielding surrounding a component in terms of the convenient concept of a component at the center of a uniform spherical shell of aluminum, exposed to a specified omnidirectional particle environment. Figures 12 and 13 show the damage profiles derived from the information provided by Table 2. Curves are plotted in these
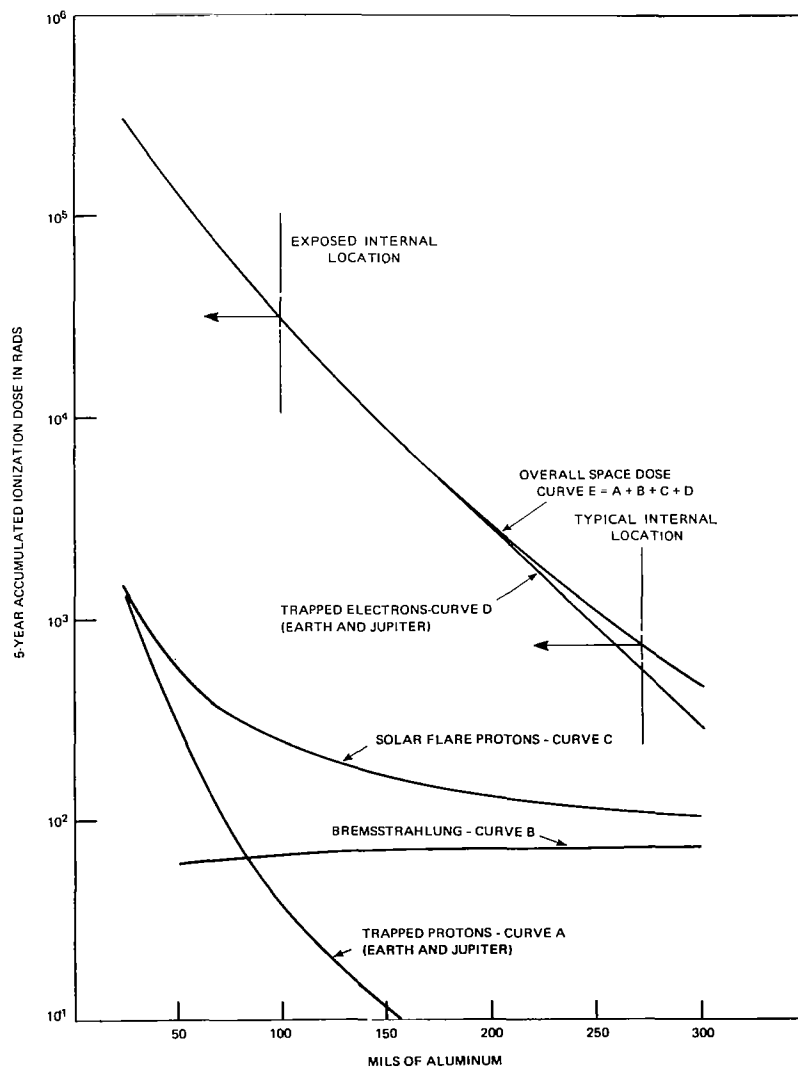
Figure 12. NEW MOONS Spacecraft and 5-Year Mission Ionization Damage Profile From Space Radiation
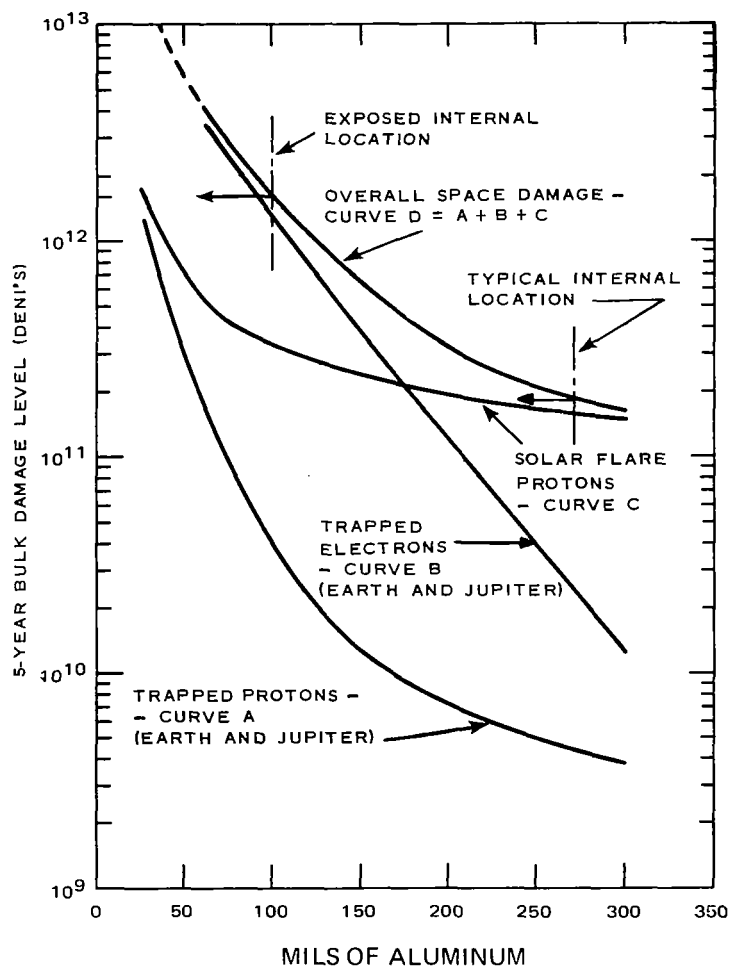
Figure 13. NEW MOONS Spacecraft and 5-Year Mission Bulk Damage Profile
From Space Radiation

figures to indicate the contributions to the total dose from various sources. The overall curves represent the combined effect of exposure in all regions of the flight path over a 5-year mission and indicate how a uniform distribution of packaging material will reduce the space radiation effects incurred on the mission. To these, of course, must be added the level of damage incurred from the RTG sources, dependent upon their location. This will be a sensitive function of distance but will be almost unaffected by the spacecraft structure* and hence would act simply as a "pedestal" for these curves.

---

*The gamma rays and neutrons from the RTG will interact with spacecraft materials and produce secondary emissions. In general, these have not been considered in this study because of their relatively insignificant contribution to total integrated dose.

In addition to the types of particle radiation described thus far, it will be noted that in Figuré 12, there is a curve for bremsstrahlung (brake radiation). Electrons (but not protons), when slowed down in any way, emit some of their energy as X-ray-type electromagnetic radiation. In the artificial electron belt, the bremsstrahlung includes photons in the range of energies characteristic of gamma rays, which will penetrate 300 mils of aluminum with only a 10-percent loss of intensity. The intensity of bremsstrahlung generated is proportional to the atomic weight of the target material. It is fortunate, therefore, that aluminum and magnesium, which are the main structural materials, are moderately inefficient in generating gamma rays.

The principal source of possible damage to the exterior spacecraft surfaces is their bombardment by the extremely large number of low-energy particles, including solar flare and solar wind protons, trapped protons, and trapped electrons. Table 2 provides an estimate of the total number of these particles, but their energy distribution in the range from 10^{-3} to 10^{-1} MeV is poorly defined for lack of accurate data on the interplanetary medium. For this reason it is difficult to make estimates of the dose profile in the external parts of the spacecraft (e.g., within the front surfaces of lenses, active regions of thermal coatings, solar-cell cover glasses, etc.). However, rough calculations of the energy flux values indicate that materials directly exposed to the space environment incur very-high-energy deposition levels at the surface. For example, solar-wind protons will be stopped within a few micrometers of the surface (of the order of 10^{-4} cm). A solar-wind flux, as shown in Table 2, of 2.9×10^{15} proton/cm^2-5 years, with an average energy of the order of 10^3 eV, is thus an energy flux of 2.9×10^{18} eV/cm^2-5 years. This is equivalent to 4×10^6 erg/cm^2-5 years and given the above stopping distance, is equivalent to a total deposition of 4×10^{10} erg/cm^3-5 years in a thin skin. In material of density = 1 g/cm^2 this corresponds to a total dose of 4×10^8 rads in 5 years.

In a similar manner, electrons in the energy range below about 0.5 MeV will deposit most of their energy in the first few thousanths of an inch of the spacecraft surface. However, the available data from energy distribution measurements of these particles is insufficient to define the detailed shape of the dose-vs-depth profiles in the region near to and including the outer skin of the spacecraft. The development of measurement techniques for this purpose and their implementation on a suitable spacecraft system is recommended. The possible contribution to such surface damage effects from ultraviolet radiation also needs further evaluation (Ref. 10).

D. Radiation Dose From RTG's

As stated earlier in this section, the dose from RTG's is different in nature from that of space radiation, necessitating a somewhat different approach to the evaluation of damage effects from this source. The fast neutrons and gamma rays emanating from the RTG's are highly penetrating compared with most of the electron and proton population in space. Protecting sensitive components from RTG radiation by additional shielding involves a weight penalty that can be justified only under particularly compelling circumstances. However, the essentially inverse-square relationship between radiation flux and distance from the RTG's can be used to advantage in the placing of particularly sensitive components.

Estimates of the anticipated neutron and gamma flux that the RTG's will generate are based on the assumption that PuO^2 will be used as the fuel.* The characteristics of this fuel from the radiation viewpoint are discussed in detail in Appendix II. Two possible methods for incorporating the fuel elements into a complete RTG unit are under considerations: (1) a planar assembly that resembles a flat disk and (2) a cylindrical assembly.

Details of the planar generator design were studied in Task VIIA, Planar RTG-Spacecraft Feasibility Study, and the cylindrical design is discussed in studies by Epstein, West, and Harris.

The radiation patterns presented here are for the planar RTG's. For RTG's of the same power in a cylindrical configuration, the neutron contours are essentially the same. Different types of fuel would, in all probability, produce different radiation patterns.

In Appendix II the physical, chemical, and nuclear properties of PuO_2 are presented on the basis of the latest available experimental and theoretical data. A discussion of the relative biological hazards of PuO_2 microspheres and PuO_2 cermets fuel form is also given. In addition, an evaluation is made of the feasibility of O^{18} depletion from PuO_2 and the associated reduction in neutron emission rates. However, for this report, in estimation radiation damage effects from the RTG's, the calculations were based on neutron emission rates associated with naturally occurring oxygen.

The RTG gamma and neutron radiation fields are presented graphically in the form of isoflux contour maps. A separate map was constructed for each of

---

*NASA SP 7031, "Properties of Selected Radioisotopes," by Dale Harris and Joseph Epstein, presents a selection of annotated references to technical papers, journal articles, and books covering radioactivity of Pu and selected other radioisotopes of interest.

44

the three selected RTG electrical power levels, i.e., 50 watts(e), 75 watts(e), and 100 watts(e). The effect of O^{18} depletion is discussed in conjunction with the isoflux data. A description of the nuclear fuel data and the method of analysis is also included.

Conclusions and recommendations with respect to PuO_2 cermets, O^{18} depletion, and the accuracy of the RTG radiation field analysis are also presented.

The isoflux maps of Figures 14 and 15 were taken from Appendix II for a 1725-watt (t) planar RTG, using 5-year-aged PuO_2 fuel with naturally occurring oxygen. The isoflux maps indicate contours of equal radiation flux in the region immediately surrounding a single RTG. These maps are similiar to those for a 1520-watt (t) cylindrical RTG, included in the Phase A study,
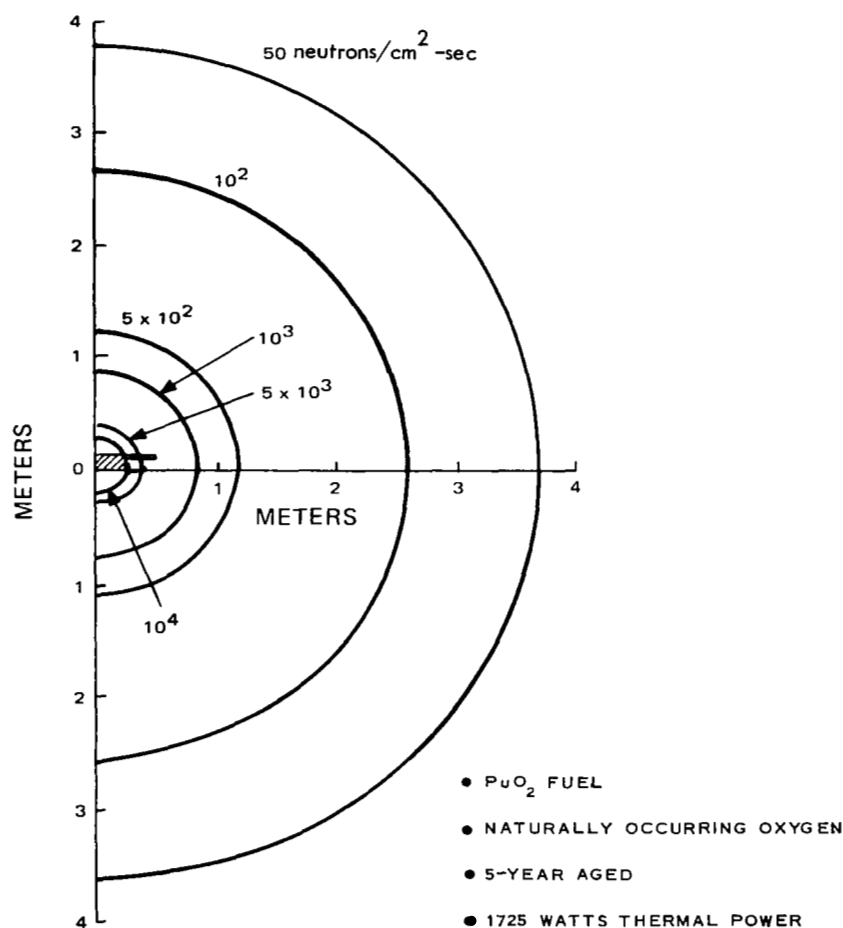
Figure 14. Neutron Isoflux Map of a Planar RTG

45
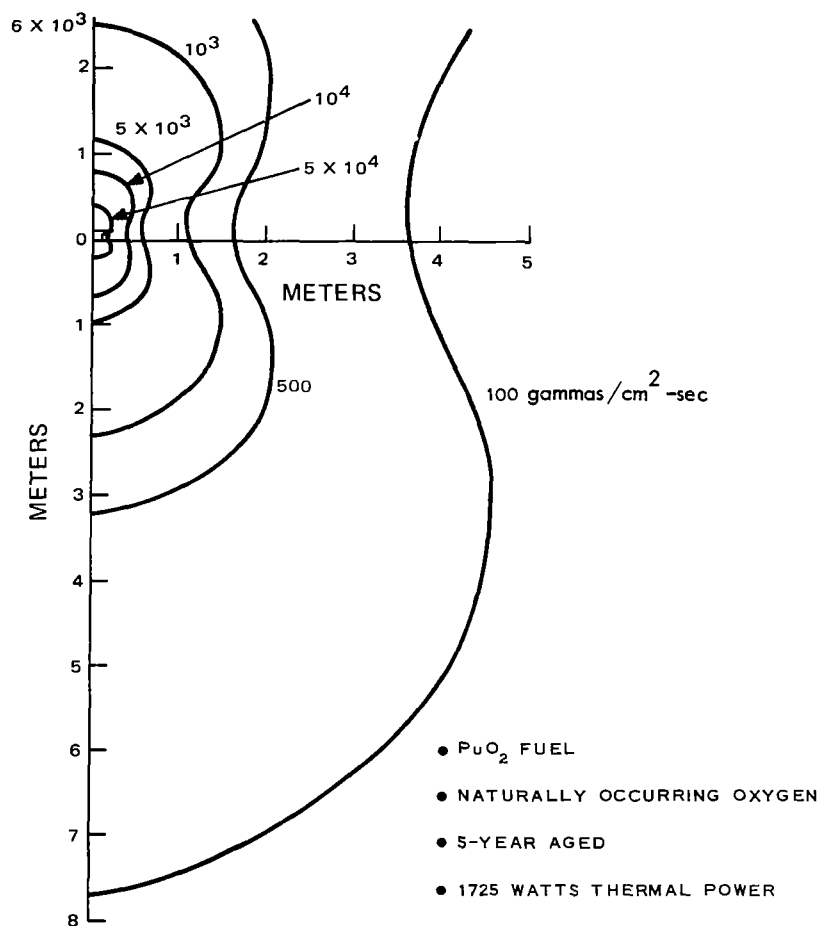
Figure 15. Gamma Isoflux Map of a Planar RTG

but are the result of more up-to-date information. The Phase A maps were based on emission spectra data for aged, 5-year-old Pu^{238} O_2 fuel with naturally occurring O_2 configured for a cylindrical RTG, with a beginning of life (BOL) thermal output of about 1520 watts. These calculations, aided by the QAD computer program, included buildup factors for the gamma flux.

In revising the Phase A maps, use was made of newer information from Mound Laboratory provided by data sheets dated July 1, 1967, and November 9, 1967. These newer reports indicate lower gamma fluxes throughout the energy spectrum. To test the validity of such data, Hittman Associates, Inc., calculated the expected fluxes from a SNAP-19 and compared the results with measurements made by the Martin Nuclear Division (Ref. 11). Excellent agreement was obtained if buildup factors were not included in the calculations. Dropping the buildup

46

factors can be justified on the theory that the gamma-ray mean free paths are much greater than the thicknesses of RTG construction materials, and, therefore, the buildup factors related to scattering effects are of negligible proportions.

Without the buildup factors used previously, the gamma flux estimates based on the newer data are about 25 percent of the original values. This difference is attributed to the two points just discussed:

(1) Use of buildup factors will increase the calculated gamma flux levels by factors in the range from 2.7 to 3.0.

(2) The recent re-estimates of the gamma flux account for the remaining differences between the revised and the earlier flux maps.

The revised neutron flux estimates, on the other hand, are nearly the same as those used in the Phase A study.

In applying the above radiation flux data to the calculation of dose levels from continuous exposure to the RTG's, the following assumptions were made:

(1) Since both neutrons and gamma rays are highly penetrating, the attenuating effect of intervening structure and packaging, in the path of the radiation reaching a component, will be neglected, since these will probably reduce fluxes by no more than a few percent.

(2) The ionizing dose in rads affecting components exposed to neutrons and gamma rays is dependent on the energy spectrum of the radiation source. The conversion factors used to calculate the ionizing dose from the RTG's are—

Neutrons to rads 3×10^8 neutron/cm^2 per rad

Gamma photons to rads 2.2×10^9 photon/cm^2 per rad

(3) The effectiveness of a particular kind of radiation in producing atomic displacements in the crystal lattice of a semiconductor (bulk damage) is generally based on the results of exposing representative samples under conditions simulating the anticipated actual environment. The results of recent experiments of this kind (Ref. 7) were used as the basis for estimating the bulk-damage effect from RTG neutrons in transistors. An average multiplying factor of 100 was used in converting neutron fluence to the dose in DENI's. Although bulk-damage effects can also be produced by gamma photons, these effects are so small in comparison

with those produced by neutrons in the present case that they can be neglected.

(4) The neutron and gamma photon output from the RTG's is assumed constant over the period used as the basis for calculating the ionization and bulk-damage dose levels. This time interval is taken as the 5-year mission period.

(5) The combined flux from the two RTG's is assumed to be twice that from a single RTG. If the distances from a particular component to the two RTG's is not the same, then the use of the shorter distance in calculating the dose can be taken as a worst-case condition.

Figure 16 shows the relationship between dose levels and distance from two planar 1725-watt (t) RTG's, based on the preceding assumptions. Curve A indicates the dose in rads from the combined effect of both neutrons and gamma photons. The major part of this effect comes from the photons, since neutrons have a relatively limited ionizing capability. Curve B gives the bulk-damage dose in DENI's. This results almost exclusively from neutron bombardment.

These calculations are based on the assumption that the fuel elements in the RTG's are arranged in a planar configuration. Gamma rays originating in the central elements of the fuel assembly will therefore be attenuated to some extent by the surrounding fuel elements. As a consequence, the gamma isoflux contours (see Figure 15) have a minimum value in the plane of the fuel elements.

If, as proposed in the Phase A study, the RTG fuel is arranged in a cylindrical form, the orientation of the RTG axis with respect to spacecraft components may result in somewhat higher dose levels for this configuration than was estimated for the planar type units. At the same distances from the two different types of RTG's, the gamma flux may be higher by a factor of as much as 25 percent. The neutron flux levels from the two types, on the other hand, will be essentially the same since the isoflux contours in both cases are nearly circular.

For a subsystem in an "exposed" internal location, a 25-percent increase in gamma flux from the RTG's will increase the total ionization dose by about 10 percent at a distance of 18 inches from the RTG's, about 4 percent at a distance of 36 inches, and about 1 percent at 78 inches. Transistor gain will be affected to a somewhat greater extent than is the case with the planar RTG, but the differences will be small and can be accommodated in the design with no difficulty.
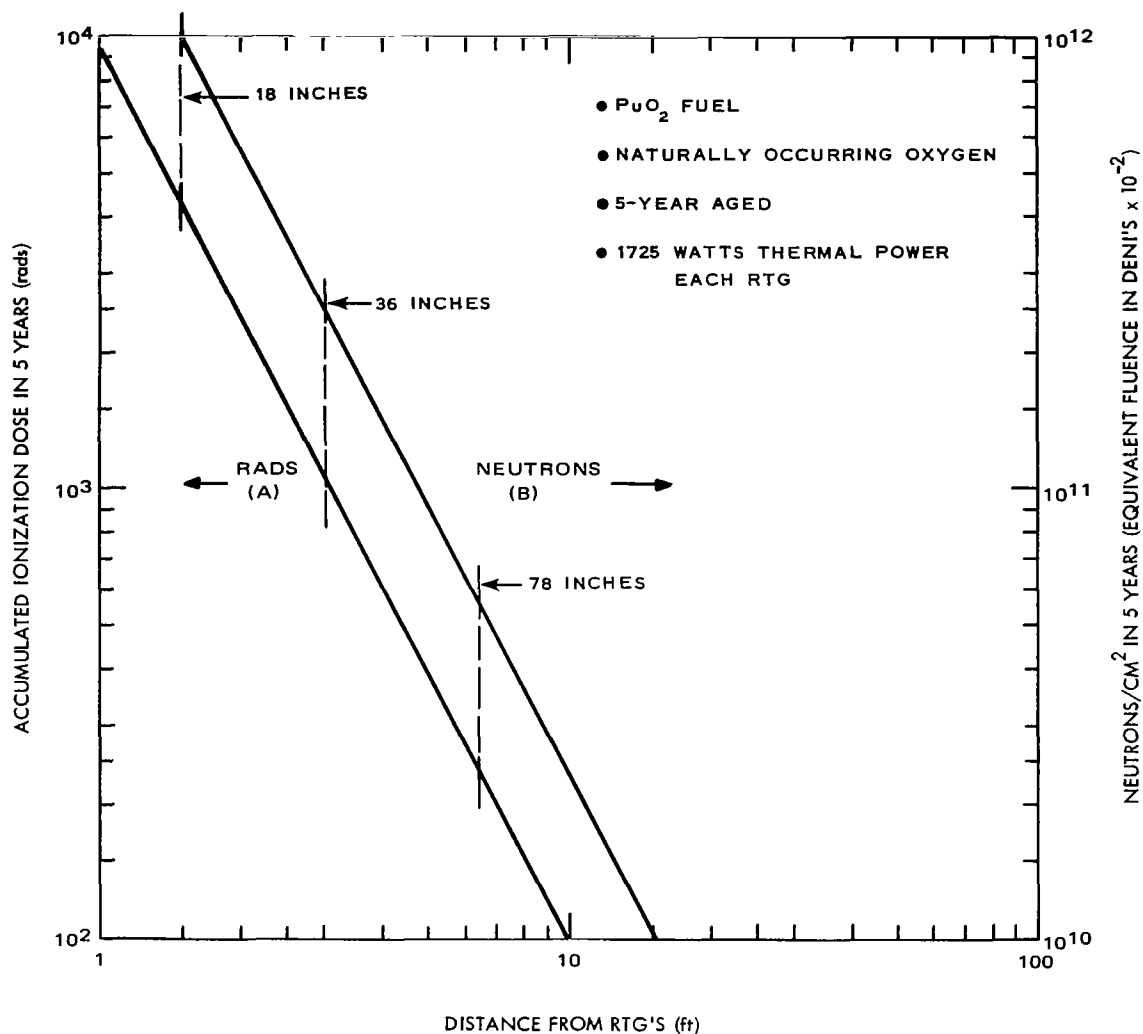
Figure 16. Neutron Fluence and Dose in Rads vs. Distance From Two Equidistant RTG's
For 5-Year Mission

E. Combination of Space and RTG Radiation

The major object of the evaluation of particle fluxes and their variation with shielding and distance from RTG sources, given in the preceding sections, has been to evolve a data format in which, for any component type and location, an estimate of the combined effects of the RTG and space radiation can rapidly be obtained, using a uniform set of ground rules. It is then possible to combine the environments for any location L_1, as shown in Figure 17, for any semiconductor component.

```
ESTIMATED              CALCULATE                    1
EXTERNAL SPACE         ATTENUATION            INTERNAL
RADIATION              FROM                   SPACE
                       STRUCTURAL             RADIATION
TABLE 1 OR 2           SHIELDING              DAMAGE
                       PRODUCED               (BULK)
                       AT
                       LOCATION L₁                          ADD 1 + 3
                                                            TOTAL
                                                            BULK
                                              2             DAMAGE
                                         INTERNAL           (DENI'S)
                                         SPACE
                                         RADIATION
                                         DAMAGE
                       FIGURES           (IONIZATION)       TABLE I
                       12 AND 13

ESTIMATED              CALCULATE                    3
RTG                    DISTANCE               RTG
RADIATION              ATTENUATION            DAMAGE
                       FACTORS                (BULK)
TABLE I                EXISTING
                       AT                                   ADD 2 + 4
                       LOCATION L₁                          TOTAL
                                                            SURFACE
                                              4             IONIZATION
                                         RTG                EFFECT
                                         DAMAGE
                       FIGURE 16         (IONIZATION)       TABLE I
```

Figure 17. Block Diagram of Analytic Steps to Estimate Internal Environment

In estimating the radiation dose affecting a particular component, the contributions from the various sources are reduced to compatible units of damage or effect and added arithmetically. The location of the component on the spacecraft will be of primary importance in determining the dose from the RTG's and from space radiation. The dose-vs-distance graphs in Figure 16 provide the information necessary to estimate the dose from the RTG's, assuming that no special shielding is added to attenuate the neutron and gamma photon flux.

In estimating the dose contribution from space radiation, the necessary data are taken from the damage profiles shown in Figures 12 and 13. As indicated previously, these profiles show how the anticipated dose from the space environment affecting a component will vary as a function of the thickness of a uniform spherical shell of aluminum surrounding the component.

The procedure for using the damage profiles to estimate the dose levels affecting sensitive components within a complex and irregularly shaped spacecraft system is called "Sector Analysis." This procedure, described in detail in Reference 9, involves the judicious subdivision of the solid angle surrounding a component location into a number of relatively small sectors, over each of which the total thickness of protecting walls and enclosures can be taken as uniform.

Such an analysis requires an accurate knowledge of the spacecraft geometry and physical characteristics. Data are required for the location of sensitive components, the thickness of intervening walls, and the kinds of materials used. The choice of the number of sectors and the solid angle included in each is generally a matter of judgment. Frequently the major part of the radiation flux reaching a particular component enters through a relatively small solid angle. By dividing this solid angle into five or six zones, the spectrum of the flux penetrating each zone can be determined with a reasonable degree of accuracy.

Past experience, from analysis of such satellite systems as TIROS M by this method, indicates that, with conventional component packaging for space, using aluminum boxes, the shielding provided by the enclosures and satellite structure surrounding a typical component in a moderately well-protected location ("average location") will be the equivalent of about 270 mils of aluminum. The use of 100 to 150 mils would be more conservative in estimating damage. That is, the doses reaching the component will be the same as if it were in the center of an aluminum shell 270 mils thick (see Figure 2). Similarly, the equivalent thickness of the shielding mass surrounding a component in a location with only minimum protection ("most exposed location"), such as a spot just within the outer skin of the spacecraft, will be only about 170 mils of aluminum. However, if, as in the case of Mariner and Ranger, the spacecraft has no overall enclosing "skin," and component boxes are, instead, slung on an open frame, then the effective equivalent shielding thickness is likely to be lower than this. A nominal 100 mils has been taken as the equivalent shielding for the "most exposed location" of internal electronic and mechanical parts on the NEW MOONS spacecraft.

In estimating the dose levels at specific locations within the spacecraft by the analytical method, it may be difficult to determine with adequate precision how much shielding is provided by the surrounding spacecraft structure including other components of irregular size and shape. Under such conditions, the error introduced in dose level estimates will depend to a large extent on the shape of the damage-profile curves. For a "flat" curve the error may be insignificant, but if the slope is very steep then even small errors in estimating approximately the shield thickness or angle subtended by a given shielding element at the point of interest will cause large errors in the corresponding dose level estimates.

Because of the steep energy spectrum model used for the space environment, the ionization damage profile for the NEW MOONS mission, as shown in Figure 12, has a fairly steep slope. It thus follows that dose level estimates based on the conventional sector analysis technique have a correspondingly large possibility of error. If particularly critical internal components are involved, then the experimental determination of shield thickness by laboratory techniques may be in order. Such techniques have been used, for example, in determining the protection against radiation provided by the Apollo command module using a gamma-ray source (Ref. 12). If added shielding is needed to avoid serious component degradation, then the more precise dose level information, acquired by such "dose mapping" methods, will serve to minimize the weight penalty involved in their procedure.

The values of equivalent shield thicknesses of 270 and 100 mils of aluminum formed the typical or "average" and exposed or worst-case space radiation conditions to be entered into Figures 12 and 13. The contribution of radiation from the two RTG's to the total dose was also calculated for three different distances of 18, 36, and 78 inches, as indicated in Figure 16. The 18-inch separation is taken as the minimum distance to a component, corresponding to an assumed worst-case condition with respect to radiation from the RTG's. The 36-inch separation represents an intermediate or average distance from the RTG's to a component, and the 78-inch separation is the distance involved in the spacecraft design described in Task V.

Table 4 provides a summary of these dose calculations for both ionization and bulk damage effects. Dose levels are given for various combinations of distance from the RTG's and shielding from space radiation. The shielding equivalent of a 100-mil-thick spherical aluminum shell is taken as a worst-case condition corresponding to a location on the spacecraft with minimum protection from space radiation. The 270-mil shield thickness corresponds to a more protected location in the interior region of any of the spacecraft subsystems. Table 5 indicates the contributions to the total dose from the various sources under worst-case conditions with respect to distance from the RTG's (18 inches) and shielding against space radiation (the equivalent of 100 mils of aluminum). The dominant contribution to the total dose under these conditions comes from the electrons presumably trapped in a radiation belt surrounding Jupiter, as indicated by the asterisked items in Table 5. However, it should be noted that the contributions from other sources are significant and if further analysis should change the environmental models, one of these might conceivably become the dominant source of predicted radiation damage effects instead of the trapped electrons.

The dose from the RTG's, for example, may become much larger if the pre-launch integration and check out procedure takes a substantial period of time and if the RTG's are in close proximity to sensitive spacecraft components during

Table 4

Combined 5-Year Dose Levels For Internal Locations

Radiation Source	Typical Internal Location*		Exposed Internal Location†	
	Ionization Damage Rads $\triangle 4$	Bulk Damage DENI's $\triangle 14$	Ionization Damage Rads $\triangle 4$	Bulk Damage DENI's $\triangle 14$
Space	0.074	0.002	3.23	0.020
RTG's at 18 inches	0.42	1.02	0.42	1.02
TOTAL	0.494	1.022	3.65	1.04
Space	0.074	0.002	3.23	0.020
RTG's at 36 inches	0.105	0.253	0.105	0.253
TOTAL	0.179	0.255	3.33	0.273
Space	0.074	0.002	3.23	0.020
RTG's at 78 inches	0.023	0.055	0.023	0.055
TOTAL	0.097	0.057	3.25	0.075

*Typical Internal Location = 270 mils equivalent all-around Al shield

† Exposed Internal Location = 100 mils equivalent all-around Al shielding

$\triangle 4$ — Multiply each number by 10^4

$\triangle 14$ — Multiply each number by 10^{14}

NOTE: This table assumes (1) No ground operations with RTG.

(2) Typical NEW MOONS mission and spacecraft.

(3) Typical electronic components.

Table 5

Estimated Worst-Case 5-Year Dose Levels From Space and RTG Radiation

Type of Damage Effect	Radiation Source	Particle Type	Estimated Dose With 100 Mils Aluminum Equivalent Shielding
Ionization	RTG at 18 inches	gammas plus neutrons	0.42×10^4 rads
	Earth and Jupiter Radiation Belts	protons / electrons*	0.004×10^4 rads / 3.2×10^4 rads
	Solar Flares	protons/(alphas)	0.024×10^4 rads
		TOTAL IONIZATION DOSE	3.65×10^4 rads
Bulk	RTG at 18 inches	gamma / neutron*	nil / 1.00×10^{14} DENI's
	Earth and Jupiter Radiation Belts	protons / electrons	0.00038×10^{14} DENI's / 0.0127×10^{14} DENI's
	Solar Flares	protons/(alphas)	0.0033×10^{12} DENI's
		TOTAL BULK DAMAGE	1.04×10^{14} DENI's

*Predominant Source of Dose or Damage

NOTE: (1) DENI calculated for p-type silicon, as in typical NPN transistors. Value differs for n-type silicon.

(2) Neutron spectrum assumed to be fission type.

(3) Ground operations before launch not included. See Table 1 for effects of ground operations.

this time. Table 1 shows the contributions to the total dose from a 9-month pre-launch exposure period but is not included in Tables 4 and 5 because only the flight portion of the mission is considered here.

SECTION III

THE PREDICTION OF DAMAGE EFFECTS IN SPACECRAFT SUBSYSTEMS

A. General

The prediction of damage effects in spacecraft subsystems depends primarily on the results of exposing representative components to simulated space radiation. In this manner, expected worst-case changes in component parameters can be related to estimated dose levels and the subsequent net effect on subsystem performance predicted. However, a component is as sensitive as its subsystem application dictates. If large changes in performance can be tolerated, the component is, by definition, less sensitive, and the subsystem is "hard" in this respect. If large parameter changes cannot be tolerated, a hardened subsystem can be achieved by such methods as selecting components which, while perhaps less efficient than the component of first choice, are relatively resistant to irradiation; operating devices in a mode which minimizes damage effects; and by placing particularly sensitive components as far as practical from the RTG's and in "sheltered" or shielded locations within the spacecraft. In extreme cases, limited supplementary shielding may sometimes also be justified, but, normally, only as a "band-aid" (i.e., small, local shield to close a small aperture). Measures such as these can raise the radiation hardness of a subsystem several orders of magnitude.

At the dose levels anticipated for the NEW MOONS mission, only a few types of electronic component will be appreciably degraded, so long as they are enclosed in normal electronic chassis and covers. If this condition is met, the degradation problem is limited to a number of low-frequency transistor types, a small, but statistically important proportion of high-frequency transistors including possibly a "maverick" or two, integrated circuits, some phototransistors and other optoelectronic devices, some ultra-sensitive types of MOS devices, some diodes, those SCR's which are equivalent to wide-base transistors, and certain optical materials which may be employed within the vehicle. As shown in Figure 1, Section I, resistors, capacitors, non-optical vacuum tubes, etc., are well outside the range of important degradation. The probable extent of the anticipated degradation of the more sensitive components in electronic subsystems has been estimated on the basis of a considerable body of available test data and experience. Detector subsystems, being in a unique class are considered separately in Section IIIC although the effects on the electronics of these subsystems will be the same as for the broad class of electronic subsystems. Materials problems are considered last, to the extent that current knowledge and experience in this area permits. In this category fall the surface

coating materials which are exposed to the full vigor of the space environment and are, in some cases, very sensitive to radiation.

In the paragraphs that follow, an attempt has been made to explain the physics of component failure and under what conditions failure can be expected. It is the objective of this section to outline the nature and scope of the component and subsystem problems which must be faced at the circuit and layout design stage to obviate the possibility of subsystem deterioration beyond acceptable limits during the very long mission. The circuit and layout designs must, of course, become more specific before close estimates of subsystem lifetimes and failure modes can be made.

B. Electronic Subsystems

1. Bipolar Transistors and Integrated Circuits

a. Physics of Radiation Damage. In a complex, long-life spacecraft containing many solid-state circuits, degradation of transistors will be the most widespread and serious problem of the designer. The damage takes the form of degradation of gain, β, and increase in junction leakage currents (I_{CBO}, etc.). A convenient way of expressing the damage done is in terms of increase in reciprocal of gain $1/\beta$. Loss of gain is attributable to two very different effects: the first effect is to permanent semiconductor lattice damage in the base region; this effect is frequently overshadowed in silicon planar transistors by the second effect, a surface-linked loss of gain, which sometimes starts at a space radiation flux level 50 times lower than that at which bulk damage becomes effective and hence at a much earlier time during a space mission (Ref. 13). This surface-linked loss of gain appears related to the leakage-current effect (Ref. 14). This damage to gain is more long lived than the leakage effect but is likewise affected by the biasing levels and the on-off duty cycle of the transistor. Unfortunately, the degree of the surface type of damage is not easily predictable and depends upon the details of the surface processing used. Each manufacturer uses a significantly different process and may even vary the processing within his plant and vary it from year to year. One regularity noted is that it is most effective at low operating current levels. A certain transistor, operated with a collector current of 10 milliamperes may not experience any appreciable loss of gain, while the same transistor, operated at 10 microamperes, may have fallen well below the tolerable level of gain. This current dependence corresponds well with a damage mechanism which involves the upper surface of the silicon wafer. Figure 18 shows a typical gain degradation curve for a set of planar transistors exposed to ionizing radiation from a Co^{60} source. *

---

*See paragraph 2 of this section for a brief discussion on similarity of Co^{60} and space radiation. Also see Reference 6. Bulk damage effects such as produced by neutrons from the RTG's are expected to be negligible at the anticipated fluence level.
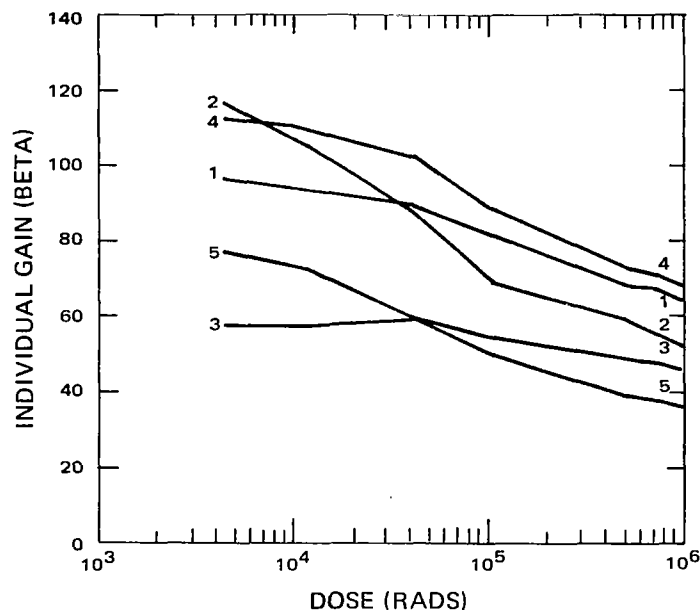
Figure 18. Gain Degradation in 2N2102 Transistors Exposed to Gamma Radiation from Co^{60} (I_c = 10 mA; 100% Duty Cycle) (Ref. 6)

Figure 19 shows the variability of surface damage and its insensibility to initial β among transistors of the same electrical type. The collector-base leakage current (I_{CBO}) can also be of serious proportions. For example, in some transistors, in the NEW MOONS mission conditions, the collector-base leakage current (I_{CBO}) value could increase by over a thousand times if bias were continually applied to the transistor for the entire mission period. Moreover, reasonable amounts of shielding would not necessarily completely eliminate
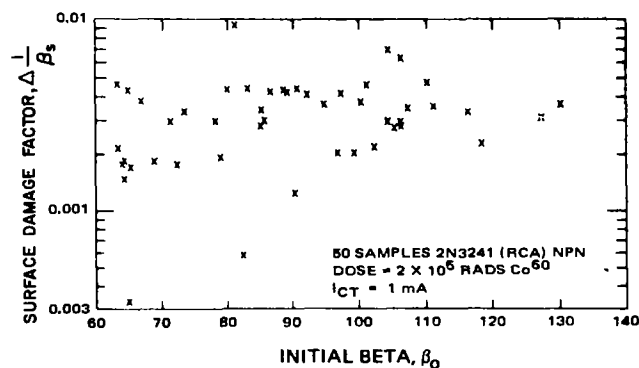
Figure 19. Damage Factor vs. Beta (Ref. 15)

this leakage problem, since the background of gamma rays or bremsstrahlung produced by the space radiation could still produce increases in I_{CBO}.

b. Transistor Degradation and its Impact on Circuit Design

(1) Degree of Damage

As has been noted in the preceding section, the assessment of the impact of transistor damage in a mixed radiation environment such as that of NEW MOONS requires many different calculations. Over the range of situations encountered in such a spacecraft, the impact of radiation can vary from negligible to very serious, depending on device location, on device geometry and processing, and on circuit application. Added to this, the surface effect in one batch of devices can vary by two orders of magnitude. Thus, the situation must always be analyzed in detail by means of an engineering analysis of up-to-date radiation test data and process details for all transistors of interest. Some techniques for making this analysis were developed by RCA over the past 5 years on several programs and now form part of the normal design procedure in effect at RCA-AED. In transistors, the principal changes in parameters caused by radiation damage as described above are (1) decrease in forward current gain (beta) and (2) increase in leakage current I_{CBO}.

Extensive research efforts at RCA and a number of other laboratories (Refs. 16 and 17) have brought about a clearer understanding of the damage mechanisms involved and a method for distinguishing between the two kinds of damage effects. In studying the effect of radiation on transistor forward current gain, it was found convenient to introduce a parameter called the "Damage Factor" defined by the equation

$$\Delta \frac{1}{\beta} = \frac{1}{\beta} - \frac{1}{\beta_0} \,,$$

where

β_0 is the initial value of beta, and

β is the value of beta after exposure to a specified dose level.

It was found that the combined effect of bulk and ionization damage on transistor gain could be described by the equation

$$\Delta \frac{1}{\beta} \, (\text{Total}) \;\; = \;\; \Delta \frac{1}{\beta_{\text{B}}} \, (\text{Bulk}) \; + \; \Delta \frac{1}{\beta_{\text{S}}} \, (\text{Surface}).$$

As mentioned, changes in gain and leakage due to ionization in transistors are not yet predictable by means of an analytical relationship as are bulk damage effects. Conceivably, continuing research on this problem may eventually provide such a relationship; but in the meantime, the result of exposing representative samples of selected transistor types to ionizing radiation seems to offer the only sound basis for predicting anticipated changes in transistor gain. An extensive series of such tests formed a major part of an investigation to determine whether sensitive components in the TIROS Operational Satellite (TOS) would survive the mission without causing out-of-tolerance performance. A radiation source ideally suited to the purpose is a Co^{60} gamma-ray facility since, in the dose range of interest, this radiation produces predominantly ionization damage; bulk damage is also produced but in insignificant amounts.

The above tests are then suitably analyzed so as to supply the circuit design engineers with worst-case degradation data on all approved transistor types in a form well suited for this purpose.

(2) Alternative Design Philosophies

The design engineer can then use these data in several ways. In the case of a new design, the radiation hardening philosophy, at its simplest, would be for the designer to choose only those devices for his circuits for which he could accommodate the given degradation without a loss in efficiency of his circuit design (this may involve the selection both of a particular manufacturer and electrical type number). In fact, most spacecraft circuitry is adapted from existing designs and in this case only a few available electrical types of device may fit the requirements electrically. The worst case of radiation-induced degradation in these may be too great to be accommodated suitably by means of circuit design. In this case, some positive hardening measure must be adopted. One such is special "pre-selection," within a given electrical type of device, for special resistance of the device to radiation. This approach is described in detail later. It has great advantages over the second possible measure, namely, relocation of the device to a more protected location or, least advisable, addition of slabs of dead-weight shielding. Depending on the demands made on the equipment, the problems due

to radiation may be very widespread or may narrow down to a few problem areas with clear solutions available. One conclusion can quickly be drawn from the above: in the design of a spacecraft, the evaluation of a given detailed electrical and mechanical design for radiation effects must be made early and thoroughly. This is because, while the changes required may be radical or may be insignificant, only thorough evaluation and testing of all transistor devices of interest to the designers, including testing of a number of alternative types, will give the designer an opportunity to produce electrical and mechanical designs which take account of the wide variety of possible device degradation values without impairing the overall efficiency of the design.

(3) Some Examples of the Impact of Device Degradation on Design

Both bulk and ionization damage effects can induce beta loss in the same transistor type, bulk damage generally predominating in transistors with a low-frequency gain-bandwidth product (f_T) and ionization damage in high-frequency transistors. The effect of ionization damage is also strongly dependent on the magnitude of transistor collector current, becoming much more severe at lower values of I_C, particularly at values below 100 microamperes.

Only a few transistors, serving specialized functions, such as power handling, will have low values of f_T. Most of the modern switching and amplifying types will have values of f_T above about 15 MHz. Above this level the predominant damage would be from the ionization effect. The degree of bulk damage will, of course, rise sharply as the devices are moved closer to the RTG units. Thus, clearly, power-handling subsystems should be located away from these sources of bulk damage and also a suitable amount of packaging placed around them to cut down the bulk-damaging component of the space environment.

To illustrate these effects, the estimates of transistor beta loss, in terms of the NEW MOONS mission, listed in Table 6 were prepared for two different types of transistor. The first, a type 2N1486 silicon NPN power transistor has a nominal gain-bandwidth product (f_T) of 1.25 MHz. Because of this relatively low value of f_T, most of the beta loss will come from bulk damage effects. The second, a type 2N2222A device, is a silicon NPN transistor with a gain-bandwidth product of about 400 MHz. Beta loss, due almost entirely to ionization damage effects, was calculated for several different values of collector current.

Table 6

Typical Transistor Degradation Data — 5-Year Mission

Transistor Type	Distance From RTG (inches)	I_c (mA)	Initial Beta	Typical Internal Location*		Exposed Internal Location*	
				Final Beta	I_{CBO} Change (μA)	Final Beta	I_{CBO} Change (μA)
2N1486	18	300	35	11.0	0.4	10.5	1.5
			60	12.7		12.0	
			·100	13.9		13.1	
	36	300	35	21.9		20.0	
			60	29.6		26.2	
			100	36.9		31.7	
	78	300	35	29.3		25.9	
			60	45.0		37.5	
			100	64.5	↓	50.0	↓
2N2222A	18	0.1	30	26	0.04	18	0.15
			60	45		27	
			120	73		34	
	18	1.0	50	44		24	
			100	78		39	
			150	106		58	
	18	10	70	64		27	
			140·	118		48	
			220	177	↓	80	↓

*Typical Internal Location = 270 mils equivalent all-around Al shielding

Exposed Internal Location = 100 mils equivalent all-around Al shielding

I_c = Transistor Collector Current

Beta = Forward Current Gain

I_{CBO} = Collector–Base Leakage Current with Emitter Open

A typical problem facing the circuit designer is to accommodate an anticipated beta loss without compromising the design in other respects. For example, severe beta loss such as that shown by the 2N1486 at 18 inches from the RTG's would probably require special treatment. One solution to this problem is to find a substitute transistor type having a higher f_T. Another possibility is to relocate the assembly incorporating the 2N1486. Doubling the distance from the RTG's would increase the final beta from 11 to 21.9 for an original beta of 35 and from 12.7 to 29.6 for an original beta of 60. If, in spite of such measures, beta loss is still larger than can be tolerated in a given circuit, then the use of two transistors in cascade would probably maintain adequate gain. The penalty would, of course, be the increased power requirements for the additional transistor.

It is seen above that the only way to determine the impact of a radiation environment of the NEW MOONS type is to test and thoroughly analyze the devices such as transistors known to be basically sensitive to radiation, followed by an analysis of how radiation-induced parameter changes in devices will be reflected in circuit and system degradation.

c. General Results from Transistor Radiation Tests. Radiation tests of electronic components conducted by RCA over the preceding 4-year period, primarily as part of the TOS program, have provided extensive test data on a wide variety of transistor types. Since the radiation levels estimated for the TOS and NEW MOONS missions are the same order of magnitude, some general observations derived from these tests are of use in evaluating the impact of radiation on the design of transistor circuits for NEW MOONS subsystems.

(1) The damage factor, $\triangle\, 1/\beta_S$, as a function of dose is essentially independent of the initial beta indicating, as expected, that this factor provides a suitable normalization for initial gain value. The data in Figure 19 illustrates this point. The relationship between final beta and initial beta of 50 samples of the RCA 2N3241 transistor after exposure to a dose of 2×10^5 rads appears to be completely random. This is in accord with the theory of surface recombination in transistors (Ref. 15).

(2) The relationship between the damage factor and collector current nearly always falls approximately on a straight line on log-log paper, as in Figure 20. The damage factor in the 1- to 10-microampere range is normally at least an order of magnitude larger

64
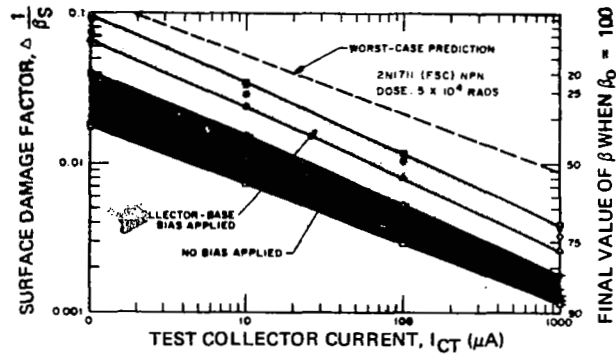
Figure 20. Degradation of Fairchild 2N1711 Transistors vs. Collector Current at Gamma-Ray Dose of 5×10^4 Rads (Ref. 15)

than the value at 1 milliampere. This, again, is in accord with the theory of surface recombination in transistors.

(3) Samples of the same transistor type from different manufacturers are likely to show marked differences in behavior.

(4) Samples of the same transistor type, even when from the same manufacturer, but from different batches, are likely to show substantial differences in behavior.

(5) Damage effects depend primarily on the total applied dose and may be almost independent of dose rate. This conclusion is based on data from RCA tests of the same transistor types exposed at dose rates differing by three orders of magnitude (Ref. 18). However, a small amount of annealing at room temperature appears to result in somewhat less damage when transistors are exposed at very low rates.*

---

*In-flight test data on the IMP-F spacecraft tend to support this observation although it is not considered definitive because a sufficient dose level has not been accumulated. A summary of a paper, ''Results from the Radiation Damage Effects on MOSFETs Experiment on Explorer XXXIV (IMP-F)'', by John L. Wolfgang, Jr., Flight Data Systems Branch, Spacecraft Technology Division, Goddard Space Flight Center, Greenbelt, Maryland, which contains these data is reprinted below.

SUMMARY

Metal Oxide Silicon Field Effect Transistors (MOSFETs) have been used extensively in the main spacecraft encoding systems on IMPs D, E, F, and G. Three of these payloads (IMPs D, E, and F) have amassed a combined total of over 174 million device-hours in orbit as of June 1, 1968. In order to correlate flight radiation damage with laboratory studies and to verify encoder shielding, an engineering experiment was flown on IMP-F. This experiment monitors 8 gate threshold

(6) Changes in collector-base leakage current (I_{CBO}) as a function of dose often exhibit a more irregular pattern than for gain. Transistors of the same type from the same manufacturer may differ by several orders of magnitude change in leakage current ($\triangle I_{CBO}$) with increasing dose. While most transistors show a general trend towards higher leakage currents as the dose level is raised, a substantial number, after an initial rapid rise, reach a peak and then show a gradual decrease. It is thus more difficult to devise a rational prediction for junction leakage effects under radiation. However, a fortunate trend has been observed in testing from 1965 to 1968, namely a reduction in the order of magnitude of I_{CBO} increases. Whereas, in 1964-65, $\triangle I_{CBO}$ values of 10^{-7} amperes were not infrequently observed in small devices (specified to operate at room temperature at I_{CBO} levels of less than 10^{-9} amperes), similar devices tested in 1967 and 1968 have rarely experienced changes of more than 10^{-8} amperes. This indicates that the manufacturers' efforts to improve collector-base junction passivation for general reliability reasons have also, fortuitously, suppressed the radiation-induced leakage phenomena.

d. The "Maverick" Problem. Although the great majority of transistor samples tested have followed a log-normal distribution pattern with respect to their ionization damage factor, there have been notable exceptions. Figures 21 and 22 show the results of two tests, each of which uncovered a case of one exceptionally radiation-sensitive transistor in a group. Similar tests by Peck and co-workers (Ref. 14) also indicated that an occasional "maverick" of this kind might be discovered in an otherwise normal group of transistors, all manufactured and processed in essentially the same manner.

To design all circuits to tolerate such abnormal sensitivity would penalize the design with respect to size, weight, power drain, and complexity. On the other hand, the effect occurs sufficiently frequently that the possibility of such an occurrence cannot be overlooked if high reliability, of the type required in a 5-year mission, is required.

---

readings and 6 drain-to-source leakage readings. These measurements are performed on devices distributed under three shielding thicknesses 0.25 gm/cm^2, 1.0 gm/cm^2, and 2.0 gm/cm^2.

After 60 orbits of IMP-F $\sim$9.5 x 10^{10} electrons/cm^2 (energy > 0.55 Mev) dose has been received by the 0.25 gm/cm^2 shielded devices. The gate threshold shift of the devices is lower than the threshold shift of similar devices, at the same dose of 1.5 Mev electrons in laboratory studies, indicating possible minor annealing is occurring over the highly elliptical orbit in flight. No measurable leakage has been noted in the devices during the first 60 orbits.
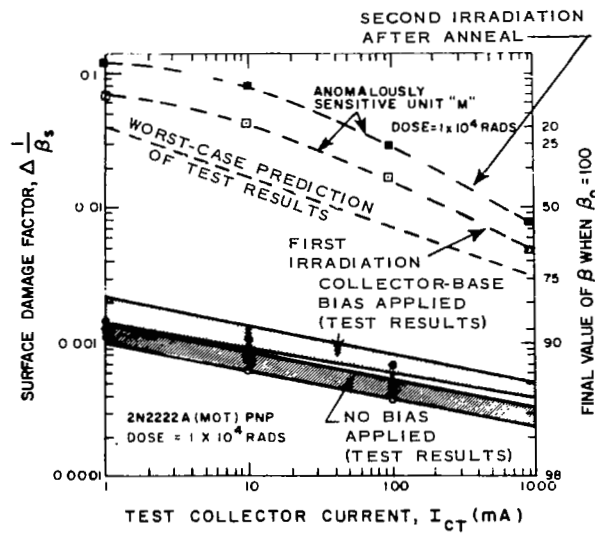
Figure 21. Result of Co^{60} Gamma Ray Irradiation of Motorola-Type 2N2222A Transistors (Damage vs. Collector Current)(Ref. 15)
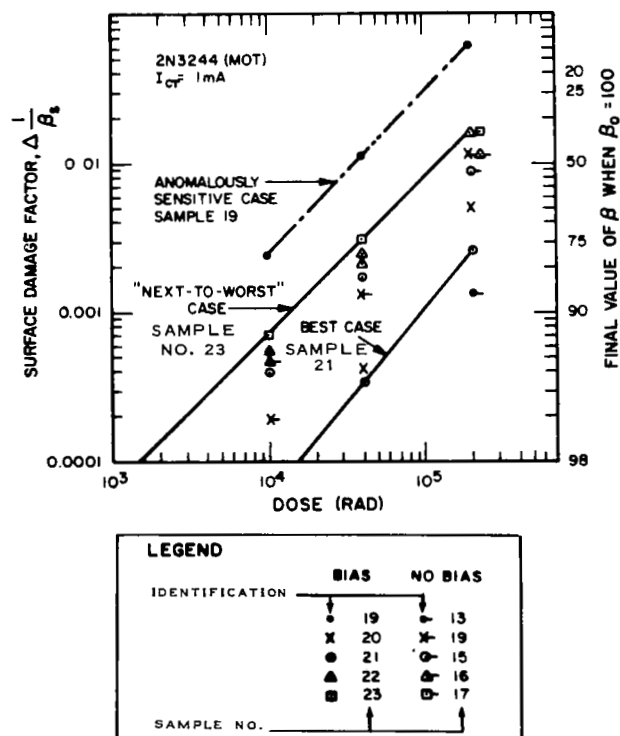
Figure 22. Degradation of Motorola 2N3244 Transistor vs. Co^{60} Radiation Dose, Showing Example of "Maverick" Device (Ref. 15)

67

The behavior of the "maverick" is so widely different from the norm that the occurrence of such a degradation effect could be catastrophic to a spacecraft mission. If degradation levels used in design are not to be set at an unreasonably high, and hence penalizing, level, the "mavericks" must somehow be eliminated. Some degree of improvement may be obtained by selection of certain device manufacturers; however, what is also needed is a relatively simple method that will identify the "mavericks" in a population, so that statistical methods for predicting transistor performance can be used with confidence on the remaining "normal" devices. Preliminary experiments forming part of a joint BTL-RCA program in 1964 (Ref. 19), showed that gamma-irradiated transistors could be restored to very nearly their original beta by a heat-treatment process. When these transistors were irradiated a second time, their behavior followed the same general pattern observed during the first irradiation. A procedure of this kind, which represents, in effect, a preselection process whereby these unusually sensitive devices could be identified and eliminated, is described in Section IV.

e. .Integrated Circuits and Germanium Devices. All the general considerations discussed here have been found to apply both to transistor or diode elements in integrated circuits as well as single or "discrete" transistors on individual silicon chips. Comments concerning passivation apply, of course, only to silicon devices, since grown oxide passivation is not used on germanium surfaces. The other elements of integrated circuits (resistors, capacitors) are not likely to contribute to radiation-induced degradation.

2. Metal Oxide Semiconductor (MOS) Devices

a. Physics of Radiation Damage. The principal effect of ionizing radiation* on MOS devices is a shift in the drain-current vs gate-voltage characteristic along the voltage axis. The slope of this characteristic, which represents the transconductance of the device, is not significantly affected until the dose level exceeds about 10^5 rads. Therefore, the effect constitutes a change in the operating region of the device rather than a true degradation in performance, as shown in Figure 23. However, unless the circuit is designed to adapt to these changes, the net result is a degradation of circuit performance that could be catastrophic. Such a case would occur, for example, if the threshold voltage of a p-channel changed from -1 to -11 volts, but the circuit was designed so that a -10 volt signal gate bias was used to command a fully "on" condition of the device. In a p-channel enhancement-type MOS device, such as the MEM-2017F, the gate voltage needed to turn on drain current (termed the threshold voltage, V_T) usually becomes increasingly more negative with increasing dose (the shift

---

*Bulk damage effects in MOS devices exposed to neutrons from the RTG's will be insignificant at the anticipated neutron fluence levels. See Figure 1.
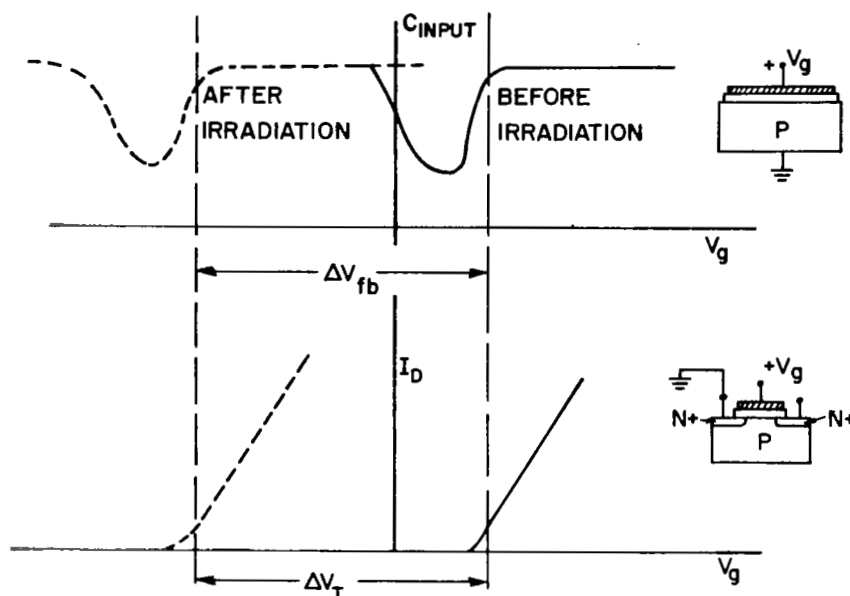
Figure 23. Changes in Operating Region of MOS Device Caused by Ionizing Radiation

is termed ΔV_T). This effect is also strongly dependent on the bias applied to the gate during the irradiation process (termed irradiation bias, V_I). At high values of negative V_I, the threshold voltage shift may be 10 times the value at zero V_I. However, at negative values of V_I, there may be a minimum in the V_T-vs.-V_I curve in the region of -2 to -5 volts. This, of course, constitutes an optimum biasing point for tolerance to radiation. The presently accepted model of how the negative shifts in threshold voltage occurs is as follows: the incident radiation creates electron-hole pairs in the gate-insulator film. The holes, having low mobility in the oxide get trapped almost immediately while the electrons shift under the action of an applied or built-in electric field. Many electrons recombine with a trapped hole; however, some of the electrons drift out of the oxide at the metal silicon-dioxide interface. This leaves behind a net trapped positive hole charge in the insulator. This trapped positive hole charge produces a negative image charge in the metal gate and the silicon. The negative image charge produced in the silicon implies a shift in the threshold voltage toward more negative voltage.

Detailed discussions of the probable causes of the radiation-induced threshold voltage shifts may be found in a number of recent articles on the subject (Refs. 20 and 21). Unfortunately, the degree of charge-trapping capability (i.e., the effective radiation sensitivity) of the oxide varies very widely with the oxide growth process used (Ref. 22). Therefore, although existing theory provides a satisfactory

explanation for the observed behavior of irradiated MOS devices, the magnitude of the shift in V_T cannot be predicted with the same certainty as can be attained, e.g., in predicting the degradation of silicon solar-cell performance under radiation. Thus, for any particular device type (or other group prepared by the same gate-oxide growth process) a radiation test is needed as the basis for predicting how a particular device group will be affected by a given space environment.* The broad variety of results observed in RCA-AED tests of a range of commercial devices is shown in Figure 24 (Ref. 23). RCA-AED has studied this problem intensively for several years. The present conclusion is that, with correct device selection and correct circuit design, even the existing commercial MOS
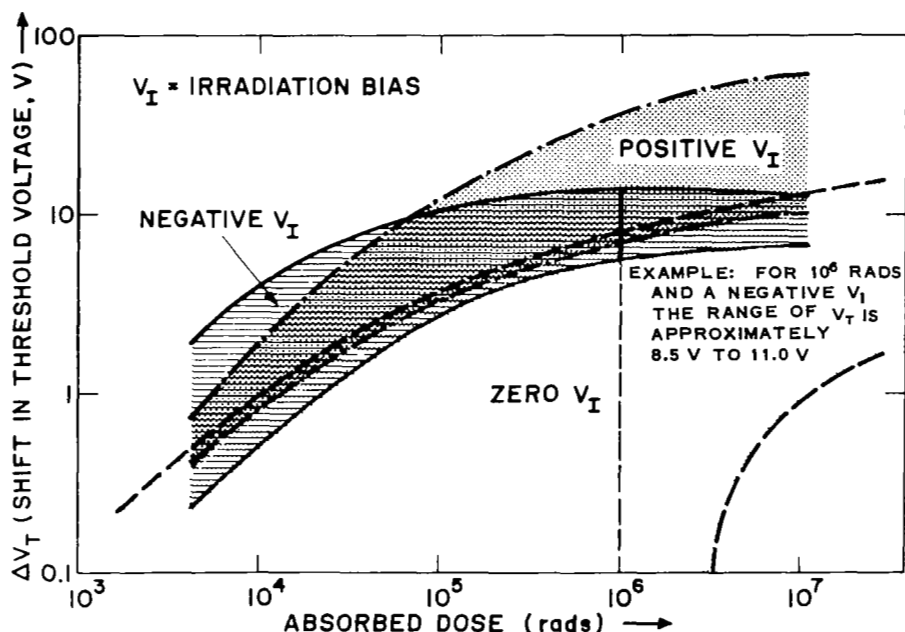
Figure 24. Typical Range of Threshold Voltage Shifts in MOS Devices

device can be used at the radiation levels expected in the NEW MOONS mission. Such devices have, indeed, already been used on AED-designed spacecraft under similar radiation conditions (Refs. 24 and 25). In addition, new types of gate insulator are being developed which should largely remove the problems described above.

    b. <u>MOS Device Tolerance Levels.</u> Exposures of MOS devices to gamma radiation have been made by investigators using the Co^{60} facility at the United States

---

*See footnote on p. 65 concerning IMP-F experience.

Signal Corps Fort Monmouth test site (Ref. 26) and the RCA Laboratories 1-MeV Van de Graaff generator (Ref. 22). Simulation of space radiation by gamma rays is justified on the basis that the predominant damage effect from electrons and protons in the devices in question will result from ionization of the same nature as that produced by gamma rays (Ref. 6).* The results of these tests have for some time been in general use by spacecraft circuit designers. The results of the gamma-ray tests lend themselves well to the radiation considerations present in the NEW MOONS mission.

Of particular interest in this application is the fact, as described above, that the shift in threshold voltage with radiation dose in MOS devices is strongly dependent on the material forming the insulating layer, its thickness and its area. Figure 25 shows the threshold voltage change as a function of dose for a particularly susceptible MOS device taken from a sample of four devices exposed to
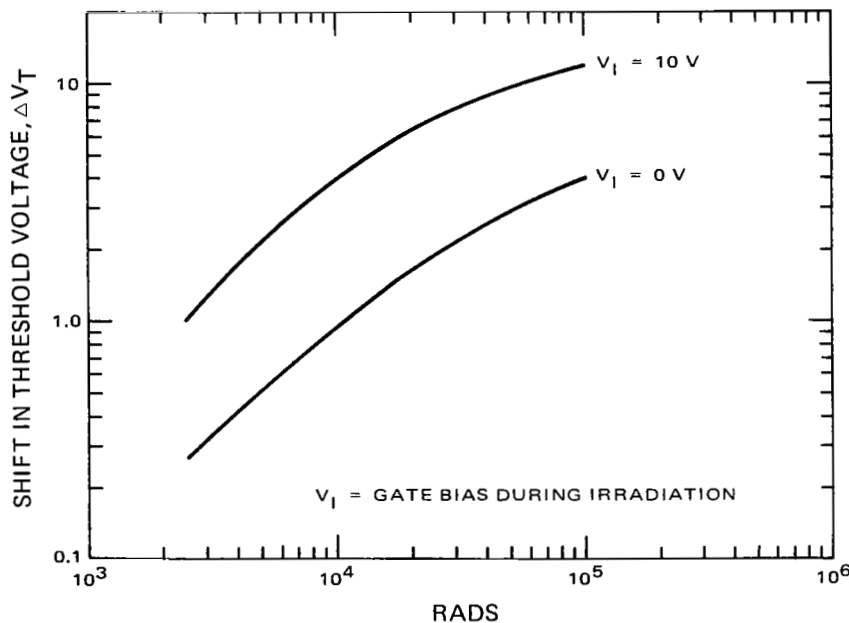
Figure 25. Typical MOS Transistor Worst-Case Changes in Threshold Voltage

gamma radiation from a Co^{60} source. The dependence on the bias applied to the gate during the irradiation process (V_I) to the extent of the shift in threshold voltage is also shown.

---

*For bulk effects a neutron source, such as a reactor, should be used.

Thus, even if MOS devices used on the NEW MOONS spacecraft have this high level of sensitivity to radiation, then the value of ΔV_T will be in the range from about 2 to 8 volts, depending on the effective level of gate bias throughout the mission.* This value assumes a dose level of about 3.6×10^4 rads, previously estimated as the worst-case combined ionization dose from space radiation and the RTG's. Note that bulk damage in the fluence range of interest has no effect at all on MOS device performance.

The possibility that threshold voltage shifts of such magnitude can cause the malfunction of circuits using MOS devices will not depend on the allowances made by circuit designers for this effect. This difficulty can often be avoided in logic circuits by applying sufficient drive voltage to the gates to accommodate the anticipated change in threshold voltage. Simply providing an "average location" for the circuit (7×10^2 rads) would, it is seen, also reduce the radiation problem to insignificant proportions. Precautionary measures of this kind will, therefore, allow the use of presently available MOS devices on the spacecraft. Moreover, recent research at AED has brought to light a number of MOS gate-insulator materials which, as well as being highly practicable for use in high-performance, mass-produced MOSFET's, are also very much less affected by radiation (Ref. 24). The one most likely to be widely used is pyrolytically deposited aluminum oxide, which exhibits ΔV_T shifts of less than 1 volt at 10^6 rads of ionizing dose and V_I values of -10 volts. It is reasonable to assume then, that the very useful attributes of MOS devices in logic and sensing circuits need not be sacrificed because of the NEW MOONS radiation environment.

c. Devices for Special Circuitry: FET's vs Bipolar Transistors. In some spacecraft subsystems, such as the scientific measurement circuits, some solid-state devices will be required to maintain their electrical parameters to very close limits (e.g., less than 5 percent) or, at the least, to degrade at a predictable rate. Thus, some devices will have to be selected and individually screened for low sensitivity and predictability. It is useful here to compare the problems of MOSFET's and bipolar transistors.

From the model of radiation-induced charge buildup in MOS structures which was discussed above, it could be seen that the amount of charge buildup, for any given fluence of radiation, will depend on the electric field in the oxide and the type and distribution of traps in the oxide. The silicon-dioxide insulating film, an amorphous material, is formed, in most cases, by thermal oxidation of silicon in the 1000 to 1200°C range. Consequently, the type and distribution of traps in the oxide will depend on such parameters as—

---

*It is expected that a cyclic bias sequence between two logic levels, about 0 and 10 volts, would give a shift in V_T of value intermediate between shifts produced by DC bias values of 0 and 10 volts.

72

(1) Oxidation temperature.

(2) Oxidation atmosphere (steam or dry oxygen).

(3) Impurity content of the oxidation atmosphere.

(4) Annealing treatments performed on the oxide after the oxidation has been completed.

Consequently, a fairly large degree of variability between different oxides with respect to their radiation sensitivity can be anticipated. Indeed, oxides prepared under almost identical conditions have shown fairly large differences in the amount of oxide charge introduced by radiation.

Since it has been found by RCA-AED (Ref. 18) that the variability in the charge buildup process over a single wafer is usually small, a useful screening technique would be to irradiate several devices from every wafer from which devices to be used on the spacecraft will be taken. On the other hand since the radiation-induced oxide charge can be annealed thermally (300°C for 1 hour), it may well be practical to use in flight the actual devices irradiated after they are restored to initial performance by annealing.

As described in Paragraph B-1a of this section, the bipolar transistor suffers from a "surface effect" in the passivating oxide layers which has features similar to the MOS oxide effect but depends more heavily on surface recombination phenomena. In addition, the bipolar transistor can suffer degradation from "bulk damage." The surface oxide properties of the bipolar transistor are normally much less well controlled than for the MOS transistor gate oxide. As a result, the repeatability of radiation sensitivity of MOS devices from a given MOSFET production line is much better than that for a given bipolar transistor production line.

d. General-Purpose Circuitry: MOS vs Bipolar Transistor. It is seen above that where the bipolar transistor suffers several damage effects, the MOS device suffers one; all of the effects in bipolar devices are prone to important variations (Refs. 15 and 27), whereas the effect in the MOS device is the more controllable at the present time. Thus, as an overall result, the amount of engineering analysis and test effort required to produce electronic circuits of uniform and predictable hardness is probably greater for the present generation of bipolar transistors than for the present generation of MOSFET's. However, the corrective action required is different in each case. The choice of device will probably be dictated mainly by the routine electrical requirements of the circuit undergoing design (impedances, current demands, etc.), and the corrective action will

be decided on grounds of ultimate effectiveness of the circuit, in terms of performance versus weight and power, before, during, and after the irradiation received in flight. Thus, both MOS and bipolar devices should be used, each in its correct place, radiation simply being regarded as a stress for which allowance is to be made. The complementary symmetry MOS (CMOS) flip-flop is particularly attractive for use in NEW MOONS spacecraft subsystems. This circuit element has one of the lowest standby power drains obtainable for electronic memory elements.

Recent tests (Ref. 28) of complementary symmetry MOS (CMOS) devices in a logic circuit configuration showed that these devices were still operable after exposure to 2×10^7 rads. Not all circuits will perform as well since survival at dose levels of this magnitude depends largely on how well the circuit can continue in operation in spite of the expected shifts in threshold voltage. With proper care in circuit design, CMOS devices can, therefore, be used as memory elements for the NEW MOONS spacecraft without danger of failure.

3. Junction FET's

The junction field-effect transistor (JFET) is a three-terminal device which overlaps in some of its uses with the bipolar transistor and the MOSFET. The "surface effect" in this device has been found, by test, to be small as compared to these other devices, while the "bulk effect" is also negligible. Thus, although the circuit applications of the JFET are somewhat limited, the device type can be used effectively at high radiation levels, at which the other devices are nearly useless. However, in the NEW MOONS mission, such a situation is unlikely to arise except in the following applications:

(1) Calibrated sensor circuits in which no change in device performance can be tolerated without loss of sensor accuracy.

(2) Devices which must be mounted very near to the RTG.

(3) Devices with near-zero protection from the direct space environment.

(4) Actual values of the Jovian radiation environment turn out to be several orders of magnitude greater than in the present model.

4. Effect of Radiation on Diodes

Devices of this kind that depend on the properties of a single crystal, but also have planar, passivated junctions, are subject to both bulk damage and ionization damage effects from particle and gamma photon irradiation. In the

usual space environment, the ionization-damage effect strongly predominates over the bulk damage effect at the dose levels typical of several years' exposure in a space environment. However, neutrons emitted by the RTG's will add substantially to the possibility of appreciable bulk damage effects particularly in wide base diodes.

The principal damage effects in these devices are limited to changes in leakage current and forward voltage drop. At the maximum dose levels listed in Table 5 the worst-case change in leakage current is not expected to exceed 20 percent, and the change in forward voltage drop is not expected to exceed 30 percent. Likewise, zener diodes experience very little change in zener voltage in the dose ranges of interest. Parameter changes of this magnitude will presumably have little effect, assuming that allowances for changes such as these have been made in the circuit design. These estimates are based on the results of tests by RCA (Ref. 9) and BTL. The RCA test program for diodes was conducted much along the same line as for transistors.

It may be concluded, therefore, as indicated in Figure 1, that diodes are, in general, not significantly affected by radiation at dose levels that cause significant degradation in most transistors.

5. Silicon-Controlled Switches

The range of devices termed silicon-controlled switches (SCS) can be regarded as a pair of back-to-back transistors, e.g., a p-n-p-n structure. At a certain point in degradation of gain in these transistors, the SCS will fail to "fire" or go into its low-conductance state. Tests (Ref. 9) of several types of these devices under conditions equivalent to several times the NEW MOONS mission radiation damage levels showed no noticeable change in their triggering characteristics. However, newer devices could, paradoxically, be more sensitive either to surface effects or to bulk damage. Thus, although serious effects are not expected, any SCS device employed in the spacecraft should be included in the radiation test series.

6. Effect of Electronic Component Performance Variation or Degradation on Subsystem Performance

In the previous paragraphs various mechanisms of component performance variations have been described, and indications were given of the types of variations or failures that can occur. In the text that follows, a description of a radiation test of a complete sawtooth generator circuit is given to illustrate the effect of radiation-induced component failure. The example given is that of an actual test performed for the TOS Radiation Test Program (Ref. 9).

a. <u>General.</u> Because of its importance in both Advanced Vidicon Camera System (AVCS) and Automatic Picture Taking (APT) camera systems (Ref. 9), a circuit of this type (complete sawtooth generator) was selected for irradiation as an operating assembly. The AVCS camera uses this basic circuit in both horizontal- and vertical-deflection generators, the APT camera only in the horizontal-deflection generator.

Survival of this circuit for the duration of the TOS mission was in question since it used several 2N930 transistors operating with collector currents in the 10-microampere range in high-impedance circuits. Other tests have shown that these transistors are particularly susceptible to radiation damage effects at these low currents. The two 2N930 transistors used in the differential amplifier in the vertical-deflection generator were selected for an initial β of 200.

The circuit assembly subjected to irradiation was a flight-qualified vertical sawtooth generator circuit module of the same type as that included in the AVCS camera system.

b. <u>Test Facilities and Procedure.</u> To operate the sawtooth generator during the test in the normal manner, a suitable sync generator was needed to supply input pulses at the specified rate of once every 6 seconds with a duration of 7.5 milliseconds. Special emphasis was placed on output pulse stability with respect to both amplitude and duration.

The sawtooth generator output was fed to a differential preamplifier to measure the positive and negative voltage swing of the sawtooth wave form. Voltage was applied to the generator through a clock-operated switch that periodically turned the power "on" and "off" to simulate the operating conditions for the TOS satellite. "On" time during the test was approximately 20 percent.

The sweep generator was located in the Co^{60} hot cell, but the voltage supplies and synchronizing generator were located outside the hot cell in the control room. Thus, they were not exposed to the gamma rays and could be checked during and after the experiment.

The initial exposure to Co^{60} radiation was at a dose rate of 2080 rads/hour for 49 hours. This rate was increased to 5800 rads/hour when a total dose of 1×10^5 rads was accumulated.

c. <u>Summary of Test Results.</u> At 4×10^4 rads, the output sawtooth amplitude had decreased by 2 percent. At slightly over 10^5 rads the circuit no longer produced a usable sawtooth. As determined by post-irradiation measurements,

failure was caused by one of the 2N930's in a low level differential amplifier. Beta of this transistor had dropped to 8 percent of its original value. A summary of post-irradiation test results is given in tabular form below. Experimental results are shown graphically in Figure 26.

2N930	Initial β	Final β	Initial I_{CBO} (A)	Final I_{CBO} (A)
Transistor No. 1	200	170	10^{-9}	2×10^{-9}
Transistor No. 2	200	16.6	10^{-9}	10^{-6}

d. Discussion of Test Results. The results of earlier radiation tests of individual 2N930 transistors indicated that if these devices were used in the sawtooth generator circuit there would be a strong possibility of circuit failure at low radiation dose levels. While some of the individual transistors* exhibited a relatively small loss of beta at 10^5 rads, others retained less than 1 percent of the original beta. This wide variation in susceptibility of these transistors to radiation is well illustrated by the post-irradiation measurements of the 2N930 transistors in the sawtooth generator circuits.

As a consequence of this early failure of the sawtooth generator due to a badly degraded 2N930, an effort was made to find possible substitutes. A radiation testing effort to find a suitable substitute was initiated. From these rather limited tests it was found that a 2N930 transistor produced by another manufacturer was a much better choice for this circuit. The relatively limited variation of beta loss with radiation shown by tests of six samples was considered a major advantage.

e. Conclusion. The above example is of a typical ultra-sensitive general-purpose circuit which might be used in the NEW MOONS Mission. Clearly, during mechanical layout of the vehicle, such a circuit would be specially considered for location, avoiding "most exposed" positions. Reference to Figures 12 and 16 show that by locating the circuit more than 24 inches from the RTG and in a not-too-exposed location, effectively building up local shielding to the equivalent of 200 mils of aluminum in all directions, would reduce the radiation level to 5×10^3 rads and hence solve the radiation problem with a good margin of safety (less than 0.02-volt shift in centering voltage).

---

*The individual 2N930 transistors tested and the 2N930 transistors used in the sawtooth generator circuit were all made by the same manufacturer.
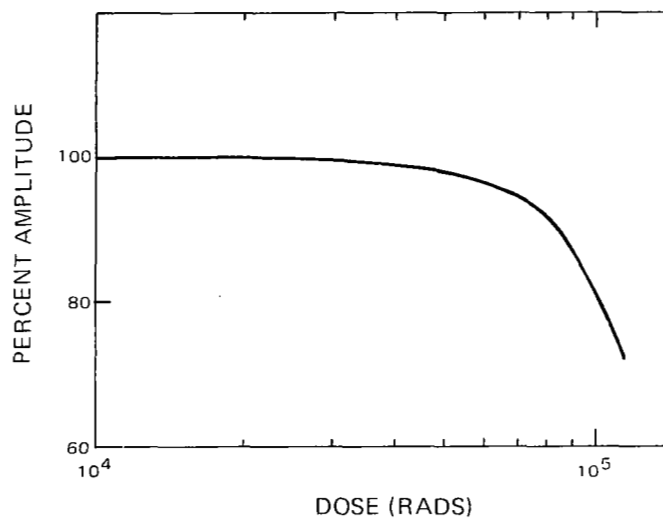
Figure 26A. Sweep Generator Amplitude as a Function of Dose
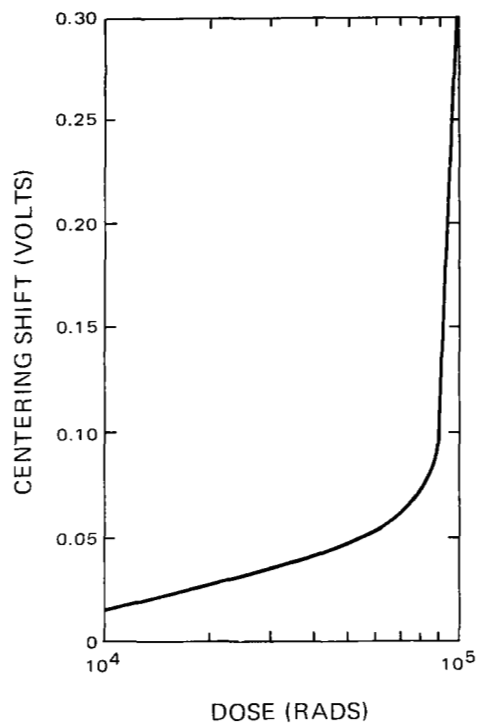
Figure 26B. Sweep Generator Centering Shift as a Function of Dose

This case illustrates that, in the NEW MOONS mission, radiation problems are real but with early anticipation need not have a serious impact on design freedom or ultimate design efficiency.

7. Subsystem Performance Deterioration for the NEW MOONS Mission: Comparison With State of the Art

The dose levels listed in Table 5 of Section II formed the basis for estimating the cumulative effect that the combined space and RTG radiation environment will have on sensitive Jupiter Probe electronic components and the resultant degradation of subsystem performance. As in the case just described, in designing the spacecraft subsystems, adequate allowances must be made for the anticipated component degradation to keep subsystem performance from deteriorating below tolerable levels. The radiation allowances must be combined with similar environmental specifications for other factors that can affect subsystem and device performance, such as temperature variations and aging. These specifications limit the choice of components available to the design engineer and impose constraints on the circuit design of spacecraft subsystems. If radiation damage strongly predominates compared with other deteriorating effects, then special measures may be needed to avoid failure. Such measures may include, for example, the addition of protective shields around particularly sensitive components. A detailed discussion of possible ways of protecting sensitive components is given in Section IV.

The potential magnitude of the difficulties to be encountered in the design of radiation hardened subsystems for the spacecraft can be evaluated on a broad general basis by comparing the estimated dose levels for the NEW MOONS mission with those previously calculated for other missions. Table 7 compares the worst-case dose levels (i.e., most exposed location and RTG's at 18, 36, and 78 inches) for the NEW MOONS mission with the dose levels previously estimated for several of the TIROS missions under similar worst-case conditions.

The TOS dose levels formed the basis for estimates of component degradation which were then used in designing TIROS subsystems to accommodate the anticipated radiation-damage effects. Because of the 1962 "Starfish" nuclear explosions in space, the radiation environment that formed the basis for the original TOS dose estimates was particularly severe. Special measures were taken to avoid failure including additional shielding for the protection of circuits in the camera electronics subsystem which were found to be unusually sensitive to radiation. The radiation environment in 1965 that was used as the basis for TIROS M dose estimates was much less severe because of the decay in the number of high-energy electrons trapped in the Van Allen belt at the time of the 1962 explosions.

79

Table 7

Comparison of Worst-Case Radiation Dose Estimates

Mission	Rads /4\	DENI's /14\
Jupiter Probe (5 years)		
RTG separation 18 inches	3.65	1.04
RTG separation 36 inches	3.33	0.273
RTG separation 78 inches	3.25	0.075
TOS		
6 months, 750 mi. (nautical) 1962 environment	190.0	.83
TIROS M and ITOS*		
6 months, 775 mi. (nautical) 1965 environment	10.0	.10

*Improved TIROS Operational Satellite.

/4\ Multiply each number in the column by 10^4

/14\ Multiply each number in the column by 10^{14}

As Table 7 shows, the estimated ionizing dose that will affect the NEW MOONS spacecraft components at a spacecraft-RTG separation distance of 18 inches is approximately a factor of 3 less than the dose level used as the basis for designing TIROS M subsystems and over 50 times less than the TOS levels.

The anticipated bulk damage affecting the spacecraft components situated at 18 inches from an RTG is, however, substantially above the levels calculated for the TIROS components. This condition is largely due to the effect of neutrons emitted from the RTG's and, therefore, depends on the distance between the RTG's and components sensitive to bulk damage. Fortunately, relatively few components of this kind (namely transistors or thyristors with very wide base widths) are normally included on a space-approved list of standard parts because of the limited need for such items, so that electronic subsystems with such

components can probably, with careful packaging, be located at distances from the RTG's much greater than 18 inches. For a 36-inch separation, the bulk damage is intermediate between the TOS and ITOS levels, and for a 78-inch separation, slightly below. The 78-inch separation was used as the basis for the spacecraft design study of Task V.

Assuming that the radiation-sensitive component types used for the NEW MOONS spacecraft will be generally similar to those included in the TOS series, radiation hardening subsystems to the required level as part of the NEW MOONS design program will present about the same problems encountered and solved for TOS. At the 78-inch separation distance postulated in Task V, the data in Table 7 indicate that the overall NEW MOONS radiation environment will probably be somewhat less severe than the TIROS M environment. However, the uncertainties in estimating the Jupiter environment, in particular, are considerably greater than the difference shown in Table 7. This indicates that the precautions used in evaluating radiation-sensitive components for the NEW MOONS spacecraft should be given at least as much attention and care as was done for TOS. The absence of any subsystem failures traceable to radiation damage on any of the satellites in the TOS series indicates that the measures taken to avoid such failures have been effective.

It should especially be noted that, while a "radiation specification"* was placed on every transistor used in the TOS/ITOS series, no serious design compromises resulted. Thus, unless allowances are to be made for contingencies not dealt with here (unexpectedly large Jupiter belts or solar flares, or RTG emissions; new "Starfish" belts about Earth), the application of a similar careful routine device/material evaluation should produce the required hardness level.

C. Detector Subsystems

The scientific payload of the NEW MOONS spacecraft will include detectors designed to measure even the relatively low levels of particle radiation in interplanetary space. To satisfy this requirement the background count level from RTG radiation at the detector locations should not exceed 10 counts per second from the two RTG's. The measures proposed for meeting this requirement are discussed in the Task IV report.

The radiation effects on the electronics supporting the sensor subsystem, however, must be treated in the same manner as described for electronic subsystems and components (Paragraph B of this section).

---

*See Appendix III for typical specification.

D. Materials

Particle radiation can cause significant changes in most bulk organic materials and in a limited number of bulk inorganic materials (prime examples are glasses, pigments, insulators, and many highly crystalline materials). The importance and magnitude of the effect depend, respectively, on the allowable tolerances to change in the property of interest (e.g., coefficient of friction, elasticity, light transmission, conductivity, etc.) and on the exact "mix" of the frequently very complex mixtures used for a given purpose (e.g., ratio of phenyl to methyl groups in a silicone elastomer). Thus, the only statements which can be made here concern the critical classes of materials and critical applications expected in the NEW MOONS mission.

The materials which will be most affected by radiation are those directly exposed to the space radiation or in direct contact with the RTG's. The material properties which are usually most sensitive to radiation are (1) optical absorptance or reflectance, (2) the properties determining material behavior such as elasticity, friction, viscosity, etc., and (3) electrical insulation parameters.

In the anticipated NEW MOONS environment, therefore, the principal problems in this respect will involve the thermal control coatings and optical windows. It is assumed that no organic insulating materials will be directly exposed to space radiation, since these would be adversely affected at the expected dose levels at the spacecraft surface. However, a metal covering over the insulating material as thin as 10 mils would provide adequate protection against the effects of direct exposure (see Figure 27).

The interconnecting electrical cables from the RTG to the spacecraft, however, require special attention because of the high operating temperature of the cables created by the proximity of the cables to the RTG. As shown in Figure 1 the estimated 5-year radiation dose level is sufficient to focus attention on electrical insulating materials when exposed externally. Moreover, the coupling of the high-temperature environment with the radiation environment requires that special attention be paid to organic insulators. A radiation hardening program such as proposed in this Report will uncover this need very early in a spacecraft program when a list of materials is furnished to the radiation specialist (see Figure 28). At this point in the program the necessary steps to obtain suitable materials, such as ceramic insulators or protective coatings, can be taken.

The properties of paint can also be significantly affected by ultraviolet radiation. However, paint formulations with improved resistance to UV have been developed and are generally used as thermal coatings on the outer surfaces of near-Earth satellites with partial success. In interplanetary space, however,
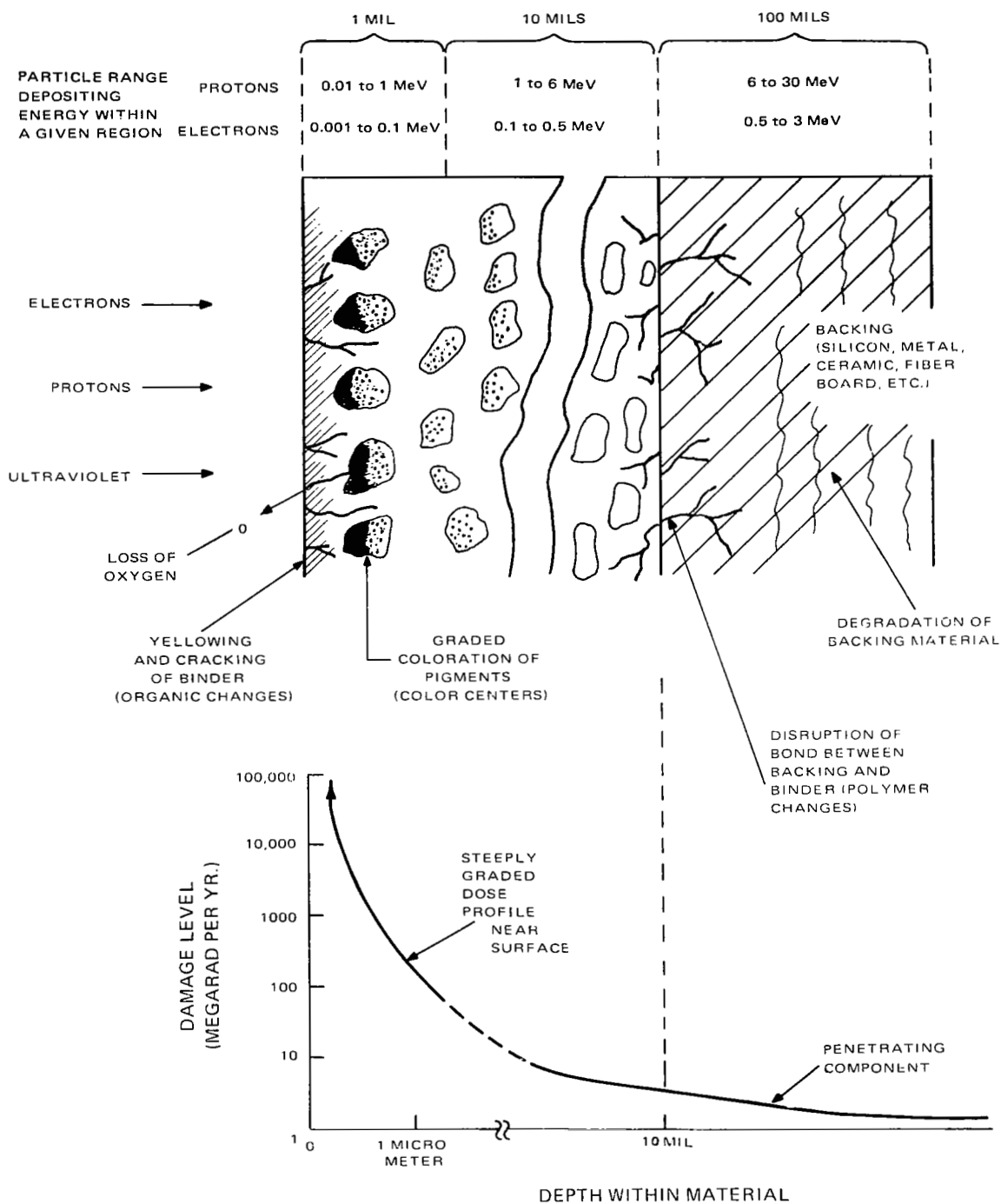
Figure 27. Damage Profile from Space Protons, Electrons, and UV in Coatings (1 to 5 years)

where the outer skin of the satellite will be exposed over a long period of time to a relatively large flux of low-energy protons and also to UV, the combination may produce unexpectedly large changes in the properties of thermal control coatings. As noted later in the text, limited experimental efforts to determine the nature and extent of such effects are currently in progress.

The radiation problem encountered in the surface region of spacecraft protective coatings is illustrated in Figure 27. A very large energy flux in the Van Allen Belts and in the interplanetary medium is concentrated in particles which are very easily stopped (ranges from 0.1 to 100 micrometers). Each particle may carry several thousands of electron volts of energy. This is all deposited in a very thin skin area of the coating. Thus, the absorbed energy density in this skin, i.e., the radiation dose, is very high. The additional photochemical effects of UV radiation aggravate the problem. Unfortunately, the important reflective and emissive processes of thermal control coatings take place in this damaged skin region.

1. Effect of Radiation on Thermal-Control Surfaces

There are many different mechanisms by which radiation affects thermal coatings, as shown in Figure 27. As indicated previously, the principal source of ionizing radiation at the surface of the spacecraft will be the low-energy protons from the solar wind.* These low-energy protons are particularly effective in producing ionization in a thin surface skin, a few micrometers thick, as shown in the lower view of Figure 27. Changes in the properties of this region can upset the thermal balance of the spacecraft. Doses in the first few micrometers of the spacecraft surface may exceed 10^8 rads. At this dose level, the change in reflectance would presumably be comparable to, or exceed, the effects listed in Table 8 (Ref. 29).

The coatings applied for thermal control of the NEW MOONS spacecraft may be different in composition from the types listed in Table 8. Thus, carefully combined environment tests to determine the changes in properties of the particular formulations used would be in order.

An in-orbit paint degradation test was performed for Lunar Orbiter V, with interesting and pertinent results (Ref. 30). The objective of this test was to obtain temperature data on four thermal-control paint coupons to evaluate degradation characteristics as a function of time. The test consisted of orienting the spacecraft on the sunline 1.5 hours prior to apolune for a period of 2 hours to

---

*Neutrons are relatively ineffective in producing ionization damage. Ionization damage is the principal cause of changes in the reflecting properties of paint. See Table 8.

Table 8

The Effect of Simulated Nuclear Radiation on Solar Absorptance of Solar Reflectors*

Material	Solar Absorptance α_s		Thermal Neutrons $E < 0.48$ eV (neutrons/cm^2)	Dose	
	Initial	Final		Fast Neutrons $E > 2.9$ MeV (neutrons/cm^2)	Gamma (Rads)
White Kemacrl Lacquer (Sherwin Williams M49WC17)	0.26	0.32	3.01×10^{15}	4.97×10^{15}	2.8×10^8
White Skyspar Enamel (A. Brown A423, Color SA 9185)	0.25	0.35	2.47×10^{14}	1.13×10^{15}	2.82×10^8
Fuller Gloss White Silicone Paint (517-W-1)	0.26	0.26	2.22×10^{14}	9.17×10^{14}	2.24×10^8
Inorganic paint, Ultrox pigment, Kasil 88 vehicle 80% pigment–vehicle ratio	0.07	0.13	9.9×10^{14}	1.44×10^{15}	1.02×10^8
Inorganic paint, Lithafrax pigment, Sodasil D binder, 80% pigment–vehicle ratio	0.10	0.23	8.9×10^{14}	1.47×10^{15}	1.09×10^8

*Based on Reference 29.

maximize the effect of solar radiation. The data points acquired at thermal equilibrium with no lunar infrared energy are shown in Table 9. Data from the prime mission are included to establish the starting reference and show the overall trend. Temperature correction was applied to account for solar constant changes and spacecraft heat sources.

During 122 days of exposure to the cislunar and lunar environments, the paint coupons degraded as follows: (see also Table 9)

(ST09)* S13G over B1056 final absorptance (α) = 2.420 times initial α

(ST15)* Hughes Organic final α = 2.345 times initial α

(ST16)* Silicone or Aluminum final α = 1.622 times initial α

(ST17)* Z93 final α = 1.481 times initial α

There is growing evidence that solar UV radiation, if applied in combination with "soft" ionizing radiation, has a more strongly deleterious effect on thermal-control surfaces than if these forms of irradiation are applied sequentially. Effects in vacuum are frequently worse than effects in air. Since it is suspected that the thermal control of both the Mariner and Lunar Orbiter vehicles was unexpectedly poor due to radiation-induced degradation caused by the solar wind and/or solar UV, this question should receive attention at all stages of NEW MOONS spacecraft design, especially where coatings of low absorptivity/emissivity ratio (i.e., white coatings) are involved. Such coatings are usually made from metal oxide powders. In white pigments of this type, the general degradation of binder and backing adds to the more serious darkening (increase in solar absorptance) of the pigment, due to the production of "color centers" and possibly also due to the photo-chemical decomposition of the oxides.

Detailed information regarding the changes in the properties of coated surfaces is only recently appearing in the literature. For example, significant results were obtained through a 3-year program sponsored by the NASA Goddard Space Flight Center (Ref. 10). A high-vacuum space-simulation facility was developed that allowed (1) simultaneous exposure of large arrays of temperature-controlled samples to electrons, protons, and ultraviolet radiation; and (2) high-resolution measurement "in situ" of total hemispherical sample reflectance and ultraviolet source irradiance. Twenty coating types (organic and inorganic paints and specular surfaces) were tested. All sample types were exposed separately to electrons or ultraviolet-rich electromagnetic radiation. Selected types were

---

*Characteristics of the paint samples used for this experiment are listed in Reference 30.

86

Table 9

Thermal Coating Experiment Data

Thermal Point	Mission Day								
	Spacecraft Unaligned						Spacecraft Aligned to Sun		
	213	218	224	230	236	244	271	300	335
ST09 (S13G over B1056)									
Telemetry (°F)	17.3	31.6	44.3	55.0	62.5	68.7	90.2	115.2	135
Temperature corrected (°F)	8.0	23.0	37.4	48.2	56.5	62.6	82.1	106.3	125.4
α_s	.189	.214	.240	.261	.278	.292	.339	.403	.458
ST15 (Hughes Organic)									
Telemetry (°F)	4.3	19.5	30.8	39.8	46.8	52.7	71.0	94.8	111.5
Temperature corrected (°F)	-9.5	6.5	18.5	28.2	36.0	42.2	60.5	82.7	97.8
α_s	.162	.186	.206	.223	.237	.249	.287	.341	.380
ST16 (Silicone on Aluminum)									
Telemetry (°F)	47.3	56.3	64.0	69.8	73.7	76.6	84.6	104.0	115.8
Temperature corrected (°F)	37.4	47.5	56.0	61.5	65.2	68.0	74.2	92.3	102.1
α_s	.240	.259	.277	.289	.298	.305	.320	.365	.389
ST17 (Z93)									
Telemetry (°F)	16.5	23.3	18.7	32.4	35.2	37.0	41.0	58.0	68.3
Temperature corrected (°F)	5.7	13.5	18.5	22.5	25.0	26.5	29.5	45.6	54.5
α_s	.185	.197	.206	.213	.217	.220	.225	.256	.274

exposed to both sequenced and simultaneously combined electron and UV radiation. Coatings were evaluated on the basis of threshold and profile of damage. Laboratory high-rate exposure to simulate low-flux electron effects of space was validated. Generally, types resistant to degradation from UV exposure were susceptible to electron-induced reflectance losses, and vice versa. Combined exposures revealed nonadditive synergistic effects and dependence upon the ordering of sequenced exposures. Current test practices for combined exposures were questioned, and the need for standardization examined.

These experiments contributed significantly to the state of the art by—

1. Identifying the thresholds and buildup of electron damage (50 keV) in many different types of thermal control coatings.

2. Verifying that no significant differences in effects of 50-keV electrons exist in coatings at 295°K, for exposures from peak space rates to those greatly accelerated rates used in the laboratory.

3. Establishing the vital need for "in situ" testing with low-energy electrons on the basis of substantial reflectance degradation and almost complete in-air recovery.

4. Exploring the differences in damage effects resulting from either simultaneous or sequential exposure to given intensities of UV and low-energy particle radiation.

5. Verifying preliminary data on the recovery of electron-induced reflectance loss by the subsequent exposure to UV-rich electromagnetic radiation.

6. Demonstrating significant differences in results obtained from different sequences of exposure to, as well as simultaneous exposure to, electrons and UV radiation.

The analytical techniques for determining radiation-dose profiles due to low-energy particles in the mixed-pigment binder layers of thermal coatings are not well developed. The effects constitute a major potential problem, for which quantitative prediction methods or corrective techniques must be developed.

However, for the NEW MOONS spacecraft, one alleviating factor must be borne in mind: the vehicle recedes from the Sun during the mission and thus has a reduced UV and solar-wind problem.

2. Optical Window Materials

Optical windows in all spacecraft have the common criterion that they must
be highly transmitting in a certain wavelength range or "spectral window." By
introducing new defects into the material, radiation can frequently introduce ab-
sorption bands into this "window". Such an effect is the strong "browning" of
common optical glasses ("brown" or "flint" glasses based on silica) by develop-
ment of a "color center" absorption band in the blue and UV region of the spec-
trum. IR, visible, and UV photometry can be hindered by this effect. Any glass-
vacuum envelopes (bulbs, TV tubes, photo cells, etc.) must be studied for this
effect. Likewise, lenses, filters, solar-direction sensors, etc., can be strongly
affected. In some applications, the effects can be alleviated by use of sapphire
and fused silica, both of which are very little affected in the dose range of interest.
If such materials cannot be used as the refractive elements themselves, it may be
necessary to shield the element with optically-ground slabs of the above materi-
als, acting as a clear "filter" on the optical axis. Such protective measures were
taken on TV camera lenses on early Nimbus and TOS satellite flights.

3. Organic Materials

Except where strongly exposed to space or RTG radiation, such as, perhaps,
the RTG-spacecraft interconnecting electrical cables, it is not expected that or-
ganic materials other than those used in optical applications (e.g., paint binder,
clear epoxy used as sensor covers, or light concentrators) will deteriorate ap-
preciably from radiation damage effects. Lubricants, sealants, potting com-
pounds, structural plastics, bearing surfaces, and hookup wire insulation nor-
mally withstand penetrating radiation doses in excess of 10^8 rads in vacuum
without gross degradation in their functions. Even glass-filled teflon bearings,
sometimes regarded as a special problem, should, at the 10^4 to 10^5 rad dose,
perform normally unless severe demands on performance are made (e.g.,
10,000 rpm bearings, etc.).

SECTION IV

THE RADIATION HARDENING PROGRAM

A. General

As summarized in Section I, a well organized radiation hardening procedure should be included as part of the normal NEW MOONS subsystem design activity to prevent out-of-tolerance spacecraft performance over the prescribed mission period. It is important to take into account the predicted effects of radiation damage even during the definition phase of the overall project so that optimum tradeoffs can be made early in the program when special requirements, such as the favorable location of radiation sensitive subsystems on the spacecraft, can readily be accommodated. It is thus imperative that a cooperative effort involving radiation specialists and systems and subsystem design engineers be instituted at the outset and continued throughout the program.

As outlined in the preceding section and illustrated by Table 7 the radiation environment estimated for the NEW MOONS mission is approximately of the same order of magnitude as that calculated for the TIROS M and ITOS missions. In addition, it is reasonable to assume that many of the subsystem types ultimately selected for use on the spacecraft will incorporate components and materials similar to those used on TIROS. There is, therefore, adequate reason to anticipate that a radiation hardening program, implemented early in the spacecraft-definition phase, should yield a "hardened" spacecraft capable of surviving the deleterious effects of the combined space and RTG radiation environment without imposing major design constraints or even requiring any weight penalties, being mainly concerned with very precise specification and control of semiconductor and other material compositions and the design of circuits with unusually high tolerance to drift in device parameters.

The two radiation hardening programs under consideration are essentially the same during their initial phases but differ primarily in the methods used to predict the effect of the actual radiation environment on the radiation-sensitive components included in the spacecraft. That phase of the two programs common to both are detailed in part B of this section. The two different component test methods used as the basis for predicting component behavior under space radiation conditions are detailed in part C of this section.

B. First Phase of the Radiation Hardening Program

The proper time to initiate a radiation hardening program, as shown in Figure 28, is early in the design program as the following information becomes available or can reasonably be forecast:

(1) Mission description.

(2) Space radiation damage profiles.
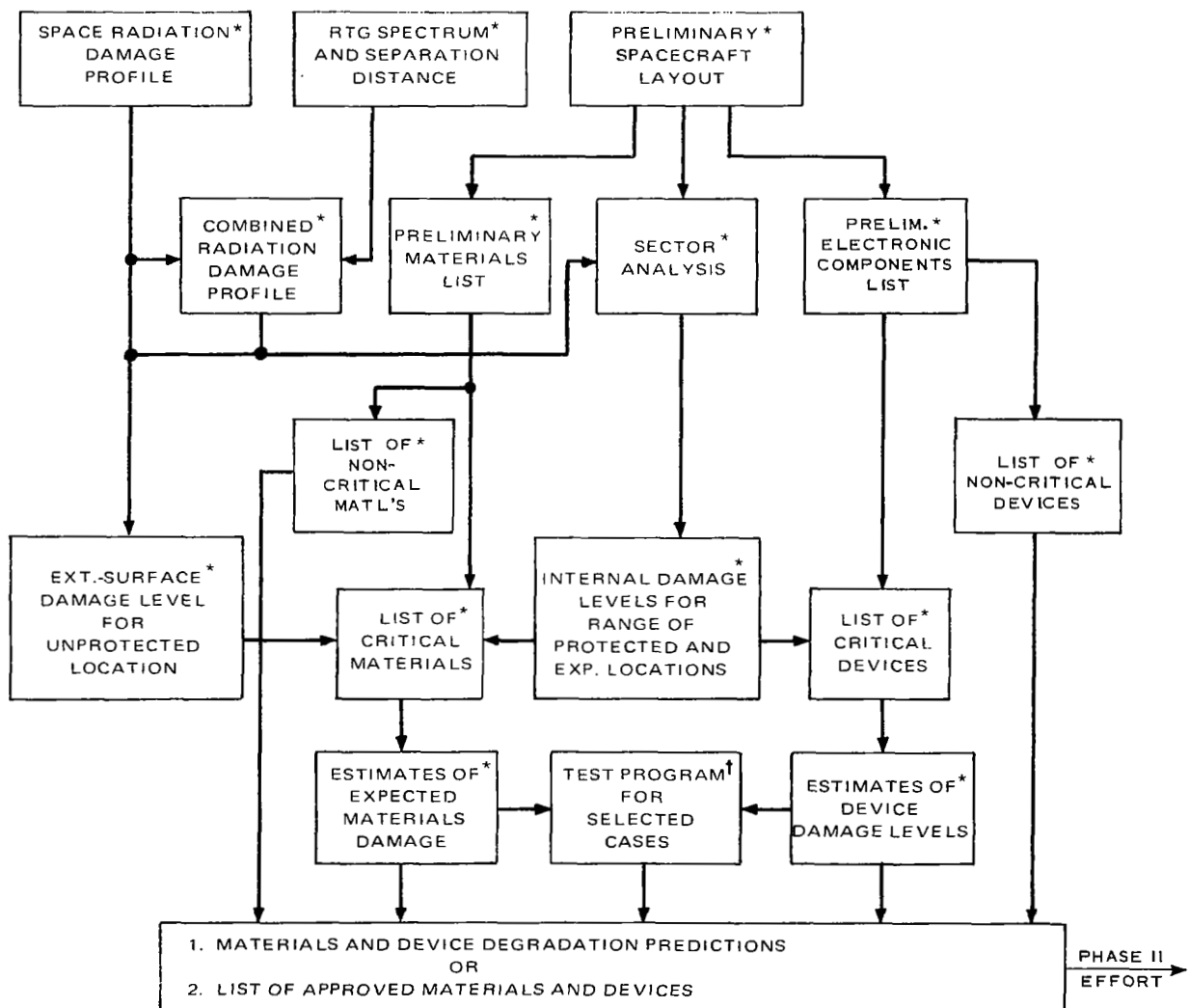
*THE STARRED ITEMS WOULD NORMALLY BE INCLUDED IN AN OVERALL PROGRAM DEFINITION PHASE
†THIS ITEM WOULD BE INCLUDED IN THE DESIGN AND DEVELOPMENT PHASE OF AN OVERALL PROGRAM.

Figure 28. Radiation Hardening Program, Phase I – Analysis

(3) RTG spectrum and spacecraft separation distance.

(4) Preliminary spacecraft layout.

(5) Subsystem performance specifications.

(6) Preliminary circuit analysis.

(7) Preliminary bill of materials.

1. Radiation Environment Affecting the Spacecraft External Surface

With the spacecraft-RTG separation distance established, a total value for combined space and RTG radiation can be estimated by summing the value derived earlier for space radiation (Section II) and the contribution of radiation from the two RTG's, thereby arriving at a value for any subsystem location for total ionizing dose (in rads) and total bulk damage (in DENI's). This is then an estimate of the external radiation environment to which exterior thermal coatings will be exposed.

2. Radiation Environment Affecting Components and Materials Inside the Spacecraft

The next step is to calculate the internal spacecraft-radiation environment. Radiation-damage profiles, as shown in Figures 12 and 13 (Section II), show how the anticipated dose from the total environment affecting a component will vary as a function of thickness of a uniform spherical shell of aluminum surrounding the component. Figure 2 (Section II) is a pictorial representation of this ideal case. The geometry of the shielding surrounding a component within an actual spacecraft, however, being a function of the spacecraft structure and internal packaging, is highly irregular. It is therefore necessary to perform a "Sector Analysis" to determine the actual range of radiation levels to which components at various locations within the spacecraft will be exposed.

A Sector Analysis requires knowledge of the spacecraft layout and physical characteristics. It is necessary to know the location of sensitive components, the thickness of intervening walls, and the kinds of materials used. A stepwise integration of the penetrating radiation over the full solid angle of 4π steradians is then performed to determine the radiation dose. A practical method for approximating this integration is to divide the total solid angle into small sectors over which the shield thickness can be considered uniform. The choice of the number of sectors and the solid angle included in each is generally a matter of judgement. Frequently, the major part of the radiation flux reaching a

particular component enters through a relatively small solid angle. By dividing this solid angle into five or six zones, the spectrum of the flux penetrating each zone can be determined with reasonable accuracy. To verify this procedure, consideration should be given to mapping a breadboard or prototype spacecraft using appropriate detectors.

The availability of both a preliminary circuit analysis, through which a list of critical components can be prepared, and a preliminary materials list, so that critical materials can be identified, will permit evaluation of the damage levels to which each component will be exposed through the working tools of the Sector Analysis and the combined radiation-damage profiles (e.g., by way of the spacecraft layout, the proposed location of a component is known, then by using the results of the Sector Analysis, the equivalent shielding afforded to a particular component or material by the spacecraft structure and packaging can be determined, and finally, once the equivalent shielding is known, the combined radiation-damage profiles, which show the relationship between the damage-producing capability of incoming particles and the shielding effect of intervening materials and structures, can be used to determine the flux to which a component will be exposed).

With the anticipated flux for critical devices and materials estimated, the next step in the radiation hardening program is to radiation test both materials and devices to determine the extent of degradation at the estimated dose levels.

C. The Radiation Test Program

1. Reasons for Testing

The need for materials and device testing to obtain degradation results has been discussed in Section III. Although there is a large quantity of radiation test data available these data should be used only as a guide in the initial selection of components and not as available design criterion. Due to rapid changes in the processing art for semiconductor devices, it is important to continually update test data and to evaluate newly developed devices. There are various reasons for this point of view:

(1) The persistence of use of a given solid-state device is very short, since new and improved devices are being made available at a rapid rate. The fact that a new device has improved electrical performance characteristics does not imply that its response to the effects of irradiation have also improved. The contrary is actually possible.

(2) Manufacturers are continuously working at improving processing techniques even in established, well-known electrical device types. A change in processing can radically alter the radiation-effects characteristics of a device, possibly for the worse, even though the nominal electrical characteristics which determine its JAN "2N" classification have not changed.

(3) Where established devices have undergone no change in manufacturing techniques, there is still the condition, due to poor reproducibility of semiconductor surface conditions and other device characteristics, that devices can vary from batch to batch in radiation-sensitivity. It is also well known (Refs. 9, 13, and 15) that even devices out of the same batch and with the same "day code" can vary.

(4) The same device type, manufactured by several different companies, can be distinctively different in response to irradiation. This difference can be put to good advantage if the characteristics of that device type are highly desirable; while test data on the device obtained from the first manufacturer tried might indicate undesirable results, a broader collection of test data covering other manufacturers could show from which manufacturer an acceptable device can be obtained. Thus, in planning a test program, a sampling of products from several manufacturers should be anticipated.

(5) There is a serious anomaly that is also a continual cause for concern: Arising unheralded, except through test results, is the anomalous degradation of a device that could be of any type number or any manufacturer. These "maverick" type of degradations occur for no well-understood reason. The "maverick" device has been described in Section III. The behavior of the "maverick" is so widely different from the norm (in the direction of excessive sensitivity to radiation) that the occurrence of such a degradation effect could be catastrophic to a spacecraft subsystem. Statistically, "mavericks" occur sufficiently frequently that the possibility of such an occurrence cannot be overlooked.

(6) Certain "bulk" materials, such as thermal coatings, optical windows, and some organics, where stability of properties is important, must also be tested carefully for damage effects in the properties of interest, for the following reason. The exact chemical mix of a commercial material will often vary from lot to lot and produce results similar to those described in Items 1 through 5 above. Such batch variations can have an important bearing on radiation hardness. Organic paints and glasses are important examples of such materials.

Other important advantages to be gained from a test program are discussed in the paragraphs that follow, where two alternate component test programs are described.

2. Solid-State Device Testing Program Based on Worst-Case Data

Small statistical samplings of each device (10, for example) must be exposed to an appropriate source of radiation in a manner to achieve the dose levels of interest within a reasonable time. As shown in Figure 29, the test results, in the form of degradation predictions, are then submitted to the design engineer. Based on worst-case data, the design engineer must decide if the predicted degradation of the device is within acceptable limits. The order of magnitude of damage to beta implied by a given value of $\Delta 1/\beta$ (explained in Paragraph III-B) can be obtained by consulting Table 10. If the predicted degradation levels are acceptable, appropriate quantities of the same device type from the same manufacturer can be purchased for subsequent circuit integration.

If the predicted degradation results are not tolerable, it can be seen in Figure 29 that there is an array of options available to the systems and subsystems design engineers. By way of example these options will be discussed as they apply to radiation hardening for ionization damage of a sensor electronics chain shown in Figure 30. These options are—

(1) Circuit redesign of the preamplifier.

(2) Circuit redesign of the sensor electronics chain.

(3) Relocation of the chain or a particularly sensitive part of the chain to a zone more protected from space radiation.

(4) Increase separation distance between the chain and the RTG's or provide shielding for the chain.

(5) Select "harder" component(s) for the chain circuits.

For the example noted, redesign of the preamplifier, option 1, can increase the "hardness" by an order of magnitude above the hardness level before redesign. Redesign of the electronics chain, option 2, to accept a preamplifier gain of 175 as compared to 300 can lead to an additional order of magnitude increase in hardness. If, however, the entire chain were relocated, option 3, from a lightly shielded zone of the spacecraft, such as might be represented by zone 3, to a zone which is very well protected by other components or subsystems, such as found in zone 5, then approximately 2 orders of magnitude
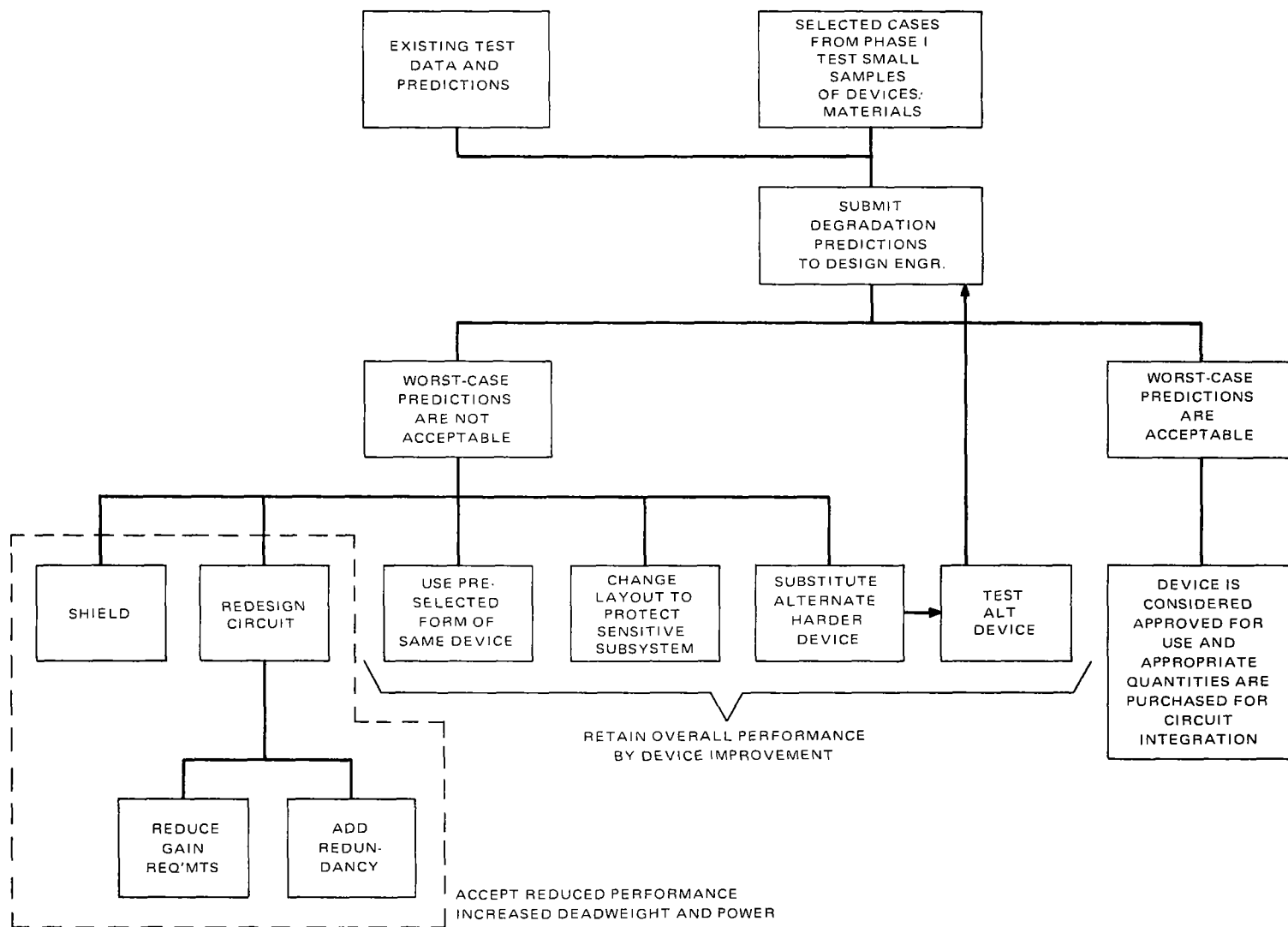
96

Figure 29. Second Phase of Radiation Hardening Program Based on Worst-Case Results

Table 10

Determination of Final Beta, Given Initial Beta and Damage Factor

(Based on $\Delta 1/\beta = 1/\beta - 1/\beta o$)

$\Delta 1/\beta$ \ βo	10	12	15	20	25	30	35	40	45	50	55	60	65	70	75	80	85	90	95	100	110	120	130	140	150	170	200	250	300	350	400
.0005	9.95	11.9	14.9	19.8	24.7	29.6	34.4	39.2	44.1	48.8	55.3	58.1	62.9	67.6	72.5	76.9	81.3	86.2	90.9	95.2	104	114	122	132	139	156	182	222	263	294	333
.0007	9.93	11.9	14.9	19.7	24.6	29.4	34.1	38.9	43.7	48.3	55.3	57.5	61.7	66.7	71.4	75.8	80.0	84.8	89.3	93.5	102	111	119	128	135	152	175	212	250	278	313
.001	9.90	11.9	14.8	19.6	24.4	29.2	33.8	38.5	43.1	47.6	52.1	56.6	61.0	65.4	69.9	74.1	78.1	82.6	87.0	90.9	99.0	107	115	124	130	145	167	200	233	256	286
.0015	9.85	11.8	14.7	19.4	24.1	28.7	33.2	37.7	42.2	46.5	51.8	55.0	59.2	63.4	67.6	71.4	75.2	79.4	83.3	87.0	94.3	102	109	116	122	135	154	182	208	227	250
.002	9.80	11.7	14.6	19.2	23.8	28.3	32.7	37.0	41.3	45.5	49.5	53.6	57.5	61.4	65.4	69.0	72.5	76.3	80.0	83.3	90.1	96.8	103	110	115	127	143	167	189	204	222
.0025	9.76	11.7	14.5	19.0	23.5	27.9	32.2	36.4	40.5	44.4	48.3	52.2	55.9	59.6	63.3	66.7	69.9	73.5	76.9	80.0	86.2	92.3	98.0	104	109	119	133	154	172	185	200
.003	9.71	11.6	14.3	18.9	23.3	27.5	31.7	35.7	39.7	43.5	47.2	50.8	54.4	57.9	61.4	64.5	67.6	70.9	74.1	76.9	82.6	88.2	93.5	99.0	103	112	125	143	159	170	182
.0035	9.66	11.5	14.3	18.7	23.0	27.2	31.2	35.1	38.9	42.6	46.1	49.5	52.9	56.2	59.5	62.5	65.4	68.5	71.4	74.1	79.4	84.8	89.3	94.3	98.0	106	118	133	147	156	167
.004	9.62	11.5	14.1	18.5	22.7	26.8	30.7	34.5	38.2	41.7	45.1	48.4	51.6	54.7	57.8	60.6	63.3	66.2	69.0	71.4	76.3	81.1	85.5	90.1	93.8	101	111	125	137	145	154
.005	9.52	11.3	13.9	18.2	22.2	26.1	29.9	33.3	36.8	40.0	43.1	46.2	49.0	51.9	54.6	57.1	59.5	62.1	64.5	66.7	70.9	75.0	78.7	82.6	85.7	91.7	100	111	121	127	133
.006	9.43	11.2	13.8	17.9	21.7	25.4	28.9	32.3	35.5	38.5	41.3	44.1	46.7	49.3	51.8	54.1	56.2	58.5	60.6	62.5	66.2	69.8	73.0	76.3	79.0	84.0	90.9	100	108	112	118
.007	9.35	11.1	13.6	17.5	21.3	24.8	28.1	31.3	34.3	37.0	39.7	42.3	44.6	47.0	49.3	51.3	53.2	55.2	57.1	58.8	62.1	65.2	68.0	70.9	73.2	77.5	83.3	90.9	97.1	101	105
.008	9.26	11.0	13.4	17.2	20.8	24.2	27.4	30.3	33.1	35.7	38.2	40.5	42.7	44.9	47.0	48.8	50.5	52.4	54.1	55.6	58.5	61.2	63.7	66.2	68.2	71.9	76.9	83.3	88.5	91.7	95.2
.009	9.17	10.8	13.2	16.9	20.4	23.6	26.6	29.4	32.1	34.5	36.8	39.0	41.0	42.9	44.8	46.5	48.1	49.8	51.3	52.6	55.3	57.7	60.0	62.1	63.8	67.1	71.4	76.9	81.3	84.0	87.0
.010	9.09	10.7	13.0	16.7	20.0	23.1	26.0	28.6	31.1	33.3	35.5	37.5	39.4	41.2	42.9	44.4	45.9	47.4	48.8	50.0	52.4	54.5	56.5	58.5	60.0	62.9	66.7	71.4	75.2	77.5	80.0
.011	9.01	10.6	12.9	16.4	19.6	22.6	25.3	27.7	30.1	32.3	34.3	36.1	37.4	39.5	41.1	42.6	43.4	45.3	46.5	47.6	49.7	51.2	53.5	55.3	56.5	59.2	62.5	66.7	69.9	71.9	74.1
.012	8.93	10.5	12.7	16.1	19.2	22.1	24.7	27.0	29.2	31.3	33.1	34.9	36.5	38.1	39.5	40.8	42.0	43.3	44.4	45.5	47.4	49.2	50.8	52.4	53.6	55.9	58.8	62.5	65.4	47.1	69.0
.013	8.85	10.4	12.6	15.9	18.9	21.6	24.1	26.3	28.4	30.3	32.1	33.7	35.2	36.6	38.0	39.2	40.3	41.5	42.6	43.5	45.3	47.0	48.3	49.8	50.8	52.9	55.6	58.8	61.4	62.9	64.5
.014	8.77	10.3	12.4	15.6	18.5	21.1	23.5	25.6	27.6	29.4	31.1	32.6	34.0	35.1	36.6	37.7	38.8	39.8	40.8	41.7	43.3	44.8	46.1	47.4	48.3	50.3	52.6	55.6	57.8	59.2	60.6
.015	8.70	10.1	12.2	15.4	18.2	20.7	23.0	25.0	26.9	28.6	30.1	31.6	32.9	34.1	35.3	36.4	37.3	38.3	39.2	40.0	41.5	42.9	44.1	45.3	46.2	47.9	50.0	52.6	54.6	55.9	57.1
.017	8.62	10.0	12.0	14.9	17.5	19.9	21.9	23.8	25.5	27.0	28.4	29.7	30.9	32.0	33.0	33.9	34.7	35.6	36.4	37.0	38.3	39.5	40.5	41.5	42.2	43.7	45.5	47.6	49.3	50.3	51.3
.020	8.33	9.67	11.5	14.3	16.7	18.8	20.6	22.2	23.7	25.0	26.2	27.3	28.3	29.2	30.0	30.8	31.5	32.2	32.8	33.3	34.4	35.3	36.1	36.9	37.5	38.6	40.0	41.7	42.9	43.7	44.4
.025	8.00	9.23	10.9	13.3	15.4	17.2	18.7	20.0	23.4	22.2	25.8	24.0	27.9	25.5	29.6	26.7	27.2	27.7	28.2	28.6	29.3	30.0	30.6	31.2	31.6	32.4	33.3	34.5	35.3	35.8	36.4
.030	7.69	8.82	10.3	12.5	14.3	15.8	17.1	18.2	21.9	20.0	20.8	21.4	22.0	22.6	23.1	23.5	23.9	24.3	24.7	25.0	25.6	26.1	26.5	27.0	27.3	27.9	28.6	29.4	29.9	30.4	30.8
.035	7.41	8.48	9.83	11.8	13.3	14.6	15.8	16.7	21.7	18.2	20.5	19.3	19.8	20.3	22.8	21.0	21.4	21.7	22.0	22.2	22.7	23.0	23.4	23.8	24.0	24.5	25.0	25.6	26.1	26.4	26.7
.040	7.14	8.11	9.38	11.1	12.5	13.6	14.6	15.4	21.4	16.7	17.2	17.6	18.0	18.4	18.8	19.0	19.3	19.6	19.8	20.0	20.4	20.7	21.0	21.2	21.4	21.8	22.2	22.7	23.1	23.3	23.5
.050	6.67	7.50	8.57	10.0	11.1	12.0	12.7	13.3	21.2	14.3	14.7	15.0	15.3	15.6	15.8	16.0	16.2	16.4	16.5	16.7	16.9	17.2	17.3	17.5	17.6	17.9	18.2	18.5	18.8	18.9	19.1
.060	6.25	6.98	7.89	9.09	10.0	10.7	11.3	11.8	21.0	12.5	12.8	13.0	13.3	13.5	13.6	13.8	13.9	14.1	14.2	14.3	14.5	14.6	14.8	14.9	15.0	15.2	15.4	15.6	15.8	15.9	16.0
.070	5.88	6.52	7.32	8.33	9.09	9.71	10.1	10.5	20.8	11.1	11.3	11.5	11.7	11.8	12.0	12.1	12.2	12.3	12.4	12.5	12.6	12.8	12.9	13.0	13.0	13.2	13.3	13.5	13.6	13.7	13.8
.080	5.56	6.12	6.82	7.69	8.33	8.85	9.21	9.52	20.5	10.0	10.2	10.3	10.5	10.6	10.7	10.8	10.9	11.0	11.1	11.1	11.2	11.3	11.4	11.5	11.5	11.6	11.8	11.9	12.0	12.1	12.1
.090	5.26	5.77	6.38	7.14	7.69	8.13	8.42	8.70	20.3	9.09	9.25	9.38	9.49	9.59	9.68	9.76	9.68	9.89	9.95	10.0	10.1	10.2	10.2	10.3	10.3	10.4	10.5	10.6	10.7	10.8	10.8
.100	5.00	5.45	6.00	6.67	7.14	7.52	7.81	8.00	20.1	8.33	8.46	8.57	8.67	8.75	8.83	8.89	8.95	9.00	9.05	9.09	9.17	9.23	9.29	9.34	9.28	9.44	9.52	9.62	9.68	9.72	9.76

increase in radiation hardness would be achieved without any redesign of either the preamplifier or the remaining circuits of the electronics chain. To determine the value of option 4, increase separation distance and/or shielding from the RTG's, it is necessary to evaluate the shield weight needed or the added weight accrued by lengthening the RTG booms and then examine the spacecraft inertia properties resulting from either of these modifications. An evaluation of these factors can then be compared with other available options to judge its suitability.

The selection of "harder" components, option 5, gives the system and design engineers two choices: (1) select an alternate device for testing in the reasonable hope of achieving better results (possibly, existing test data or device design principles* can be used as a guide in selecting an alternate that has been shown to be "harder") and use worst-case predictions for that device or (2) use a preselected form of the same device. This preselection technique was described briefly in Section IIIB and will be covered in greater detail in Paragraph C-3 of this section.

The worst-case program would appear to offer more economy in terms of program time and cost than the alternate preselection program described later in this section. There are, however, three possible penalties that may be incurred for the worst-case program that must be seriously weighed against the advantage of testing economy: (1) There is the possibility of a requirement for overdesign to insure reliability, which could mean the use of redundant devices or expensive, extra-high-rated devices. Either approach infringes upon economy of another sort—there is added weight (conceivably several pounds throughout all the circuitry), added power drain, and added design time. Added design time could be significant since redesign of one circuit can necessitate redesign of the subsequent circuits with which the first circuit is coupled, as shown in Figure 30. (2) There is also the possibility of having to accept reduced subsystem performance. (3) The third possibility arises from the fact that since the statistical population of "maverick" devices seems to average about 1 in a sampling of 100, the results of small sample tests could miss this worst-case possibility.

3. Testing Program Based on Component Preselection

a. The Preselection Concept. The "preselection" test program is predicated on testing the entire quantity of any device proposed for use, plus a percentage of extras. Then, based on test results and design criteria, in the form of specified allowable degradation, the acceptable devices are retained (those that degraded within acceptable limits) and the unacceptable devices set aside for other less critical uses. The samples that have been selected for

---

*e.g., narrower base width leads to smaller degradation from bulk effects.
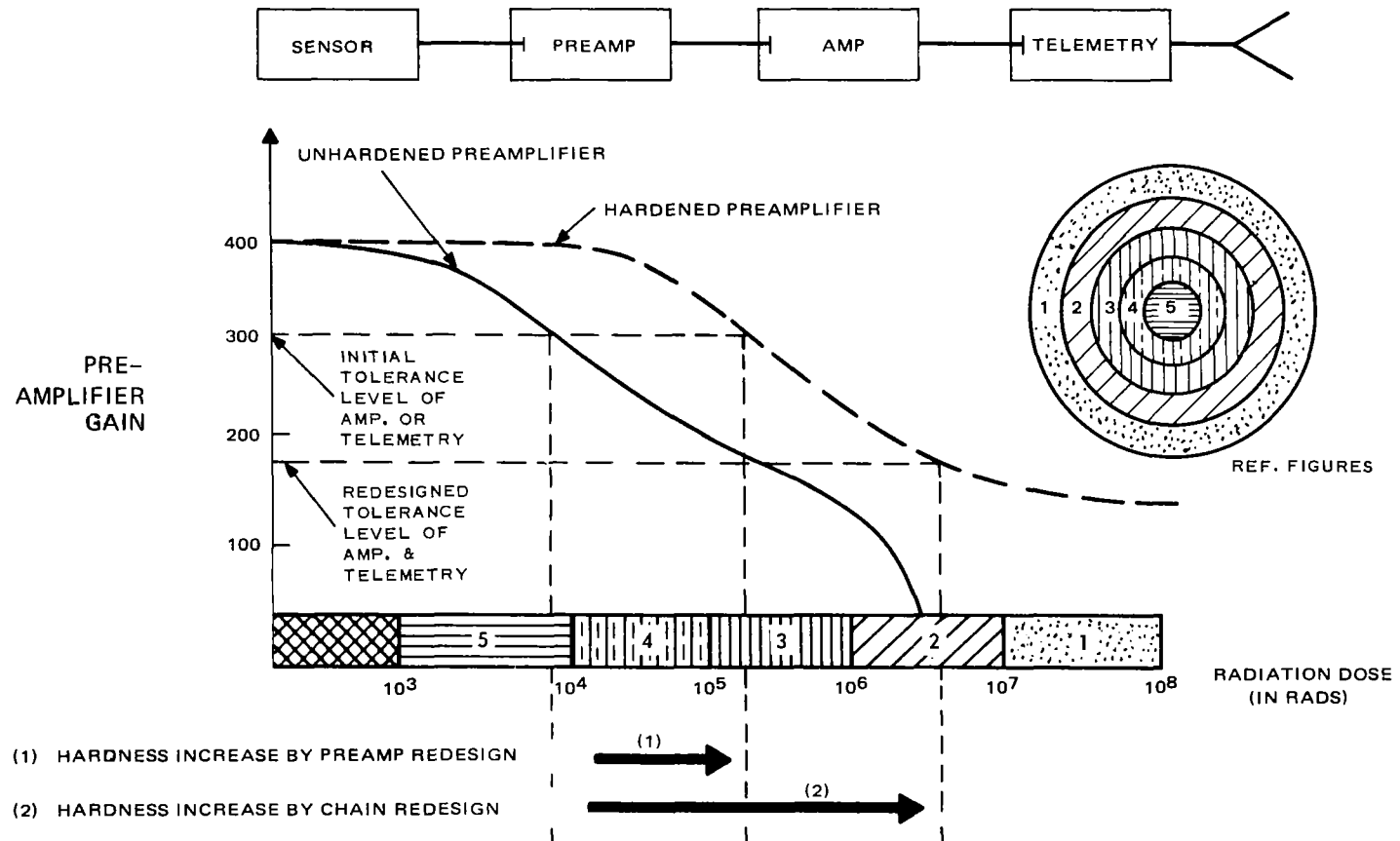
Figure 30. Hardening of Sensor Electronics Chain

use can then, through an annealing process, usually be restored to their original (pre-irradiation) electrical characteristics, without unacceptable loss of reliability. Any subsequent irradiation to the same dose levels, which would be the case in flight, will cause the devices to degrade to the same extent as during the test in the simulated environment (Refs. 14 and 15). This gives the engineer the added advantage of knowing in advance, exactly what the degradation will be.

Before describing a suggested test program based on the technique of component preselection, it seems useful at this time to discuss the basis for the concept, as it applies to radiation hardening.

Preliminary experiments, as part of the joint BTL and RCA ComSat Study Program (Ref. 19) showed that gamma-irradiated transistors could be restored to very nearly their original beta by a baking process. When these transistors were irradiated a second time, their behavior followed the same general pattern observed during the first irradiation. A procedure of this kind obviously offered the intriguing possibility of forming the basis for a preselection process whereby transistors prone to degrade beyond acceptable levels could be identified and eliminated. Life tests were conducted on annealed samples and the results showed essentially no effects of the irradiate-anneal procedures (Ref. 19).

More experiments to evaluate further the feasibility of an "irradiate-anneal" preselection technique of this kind were recently conducted (Ref. 15). Groups of transistor samples of various type were exposed to gamma radiation in the normal manner; they were then baked overnight at a constant temperature of 250°C and were then subjected again to the same irradiation conditions.

It was found that the times and temperatures used during annealing were not critical and could be varied over relatively wide limits without producing major differences in the results. Temperatures were generally in the range from 200° to 300°C, time from 4 to 24 hours (Ref. 15). Figure 31 shows typical beta versus dose curves obtained by repeated exposures of the same transistor to gamma radiation with an annealing process in between. Both of the transistors shown are low-power silicon planar devices with gain-bandwidth products of about 400 MHz. The 2N2222A is an NPN type and the 2N2907A is a PNP. The occurrence of a "maverick" can be seen in View A of Figure 31. For both transistors, the behavior of the test samples, including the "maverick," during successive irradiations followed the same pattern with generally decreased but with only minor deviations.

The variation of behavior within batches of transistors of the same type is summarized in graphical form in Figure 32. Differences in the initial values of beta at the beginning of successive exposures are indicated on the left of each view, differences in beta values after exposure to 5×10^4 rads on the right of each view. Each data point plotted along the horizontal axis, View A of
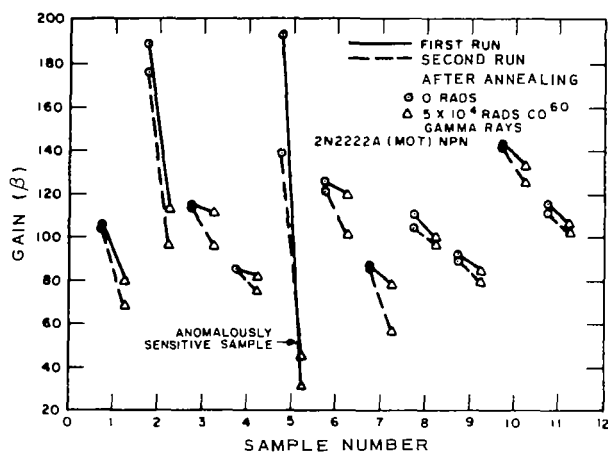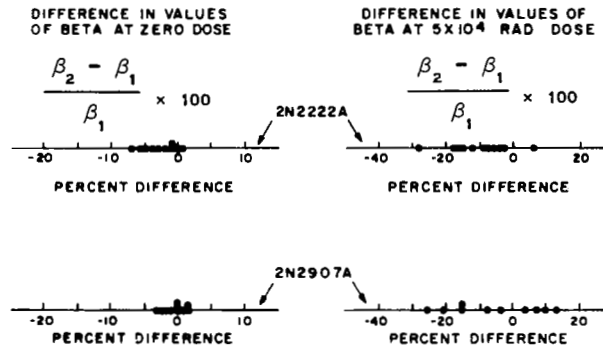
View A. 2N2222A Transistor (NPN)
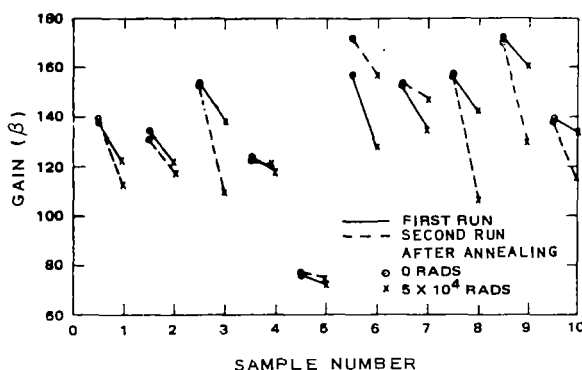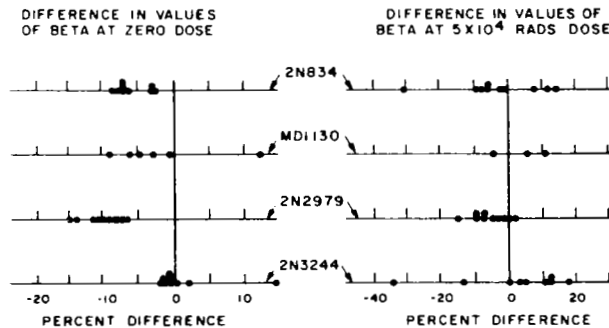

View B. 2N2907A Transistor PNP

Figure 31. Comparison of Beta Loss From Successive Irradiations
With Intermediate Annealing Step (Ref. 15)

Figure 32, shows in percent the difference in beta value of a transistor sample measured during successive exposure cycles. The grouping of the data points in these graphs indicates that most of the samples followed their original degradation pattern although a few showed slightly greater susceptibility to radiation damage.

Several other transistor types were studied in the same manner, including the 2N3244, 2N2979, 2N834, and the MD 1130 devices. The results of experiments with these transistors are presented in View B of Figure 32 in the same form as in View A. These data also show that the irradiate-anneal procedure provides a reliable indication of the behavior to be expected during a succeeding irradiation.

102

DIFFERENCE IN VALUES
OF BETA AT ZERO DOSE

DIFFERENCE IN VALUES OF
BETA AT 5×10⁴ RAD DOSE

$$\frac{\beta_2 - \beta_1}{\beta_1} \times 100$$

2N2222A

$$\frac{\beta_2 - \beta_1}{\beta_1} \times 100$$

PERCENT DIFFERENCE

PERCENT DIFFERENCE

2N2907A

PERCENT DIFFERENCE

PERCENT DIFFERENCE

A. 2N222A and 2N2907A

DIFFERENCE IN VALUES
OF BETA AT ZERO DOSE

DIFFERENCE IN VALUES OF
BETA AT 5×10⁴ RADS DOSE

2N834

MD1130

2N2979

2N3244

PERCENT DIFFERENCE

PERCENT DIFFERENCE

B. 2N834, MD1130, 2N2979, and 2N3244

Figure 32. Repeatability of Radiation Effect in Six Types of Transistors, Irradiated (1) as Received (β_1), and (2) After Irradiation to 5×10^4 Rads and Baking at 250°C for 16 Hours (β_2). Co^{60} Radiation was Used (Ref. 15)

b. The Preselection Test Program. For the preselection test program, shown in block diagram form in Figure 33, it is necessary to test the entire quantity of any device proposed for use plus a percentage of extras considered necessary to achieve the required number of acceptable devices. The test results should then be reviewed in terms of the design engineer's criteria, i. e., percentage of allowable degradation. The devices are then sorted to select all of those that are within tolerance. These devices would be baked to restore their initial electrical characteristics and supplied to engineering for subsequent spacecraft integration. If this approach can be accomplished safely, without incorporating reliability risks arising from the additional handling of the spacecraft-destined devices, it may offer a technique to deal with the "maverick" problem.

There are two possible test results other than an adequate yield of acceptable devices. The first is that the yield might be less than the number of
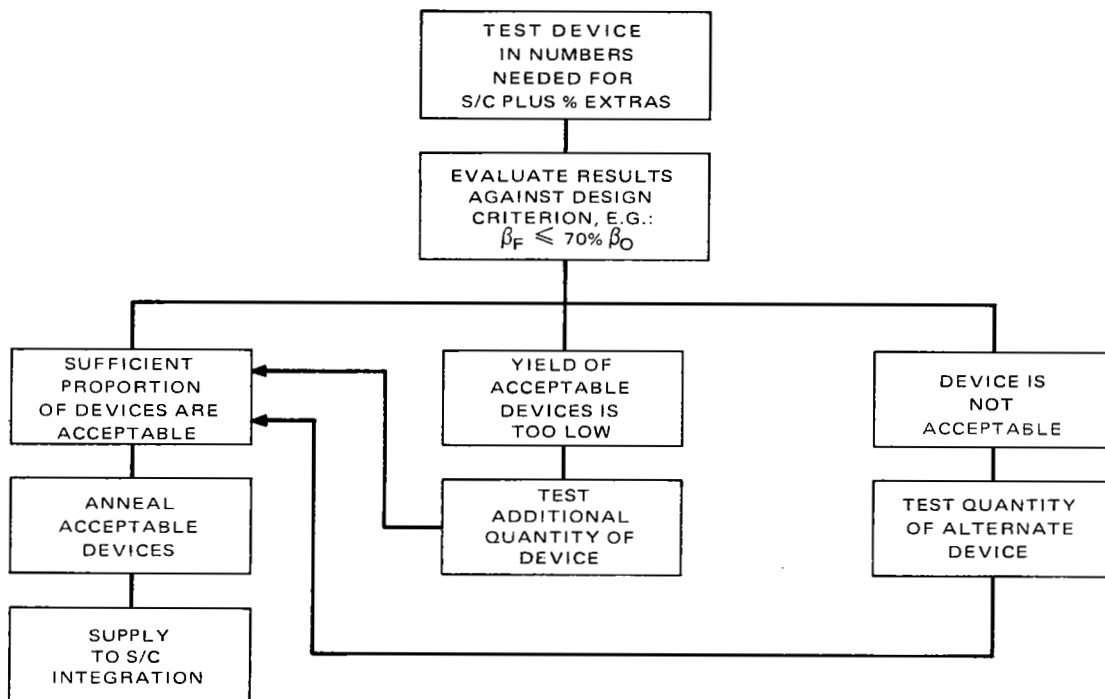
103

Figure 33. Test Program Based on Preselection Technique, Logic Diagram

devices required, thereby necessitating the radiating, testing, sorting, and annealing of an appropriate number of devices to achieve the required total. The second possibility is that the test results might be generally so poor that a substitute device must be tested. Although this last possibility indicates an undesirable extension of cost and schedule, it is worth noting that if a similar result occurs in the worst-case program, corrective action in terms of the alternatives shown in Figure 29 could lead to a commensurate penalty in cost and schedule with the additional undesirable situation where the design engineer is still working with predictions as a final outcome instead of space-qualified components. It is also worth noting that since the initial component selection would most probably be based on existing test data, the component choice would, of course, be that with the most desirable performance history, thereby almost eliminating the number of tests that might result in an unacceptable device. This aspect of statistical probability offers further interest in that, with wise initial component selection, the overriding probability is that a 100-percent yield could be achieved the first time.

The preselection approach, then, claims the following significant advantages over the worst-case approach:

(1) High reliability, in that the devices integrated into the spacecraft are space qualified for radiation in the same sense as all other environmental tests such as vacuum, humidity, etc.

(2) Potential weight savings in eliminating the need for redundant devices.

(3) Potential power savings in eliminating the need for redundancy or highly de-rated devices.

(4) Reduced overall design time in obviating the need to cope with cumbersome tradeoff techniques and/or circuit redesign in those areas where degradation levels are predicted to be either marginal or below tolerance. Reduced design time accrues also by virtue of not having to redesign those circuits that are coupled to the problematical circuit in order to accommodate reduced performance.

(5) Improved accuracy in circuit design since the design engineer can work with specific degradation levels instead of performance predictions where allowance would have to be made for variability.

4. Comparison of Worst-Case and Preselection Test Philosophies.

The worst-case approach offers a relatively quick and economic way of hardening an existing spacecraft. Its main virtue is that spacecraft integration does not have to await the performance of a somewhat lengthy screening program to acquire needed devices. In addition, last-minute circuit substitutions of electrically equivalent devices can be made (assuming that there are up-to-date predictions on the substitute device) without the time penalty entailed by a radiate-test-anneal cycle. However, there is always the possible reliability risk of a "maverick" device being incorporated into a critical circuit, and there is still the batch-to-batch variation to be compensated for in circuit design. The enonomy virtue dwindles somewhat in the light of the added possible burden to design time in those cases where redesign of a circuit, and possibly other related circuits, is necessary to accommodate those devices where worst-case levels are not acceptable and suitable electrically equivalent devices are not available. It appears that implementation of the worst-case test philosophy would be appropriate if the expected dose levels are relatively low, e. g., if a deployable RTG is used, in which case the $1/R^2$ law works in favor of the damage levels to which the spacecraft electronics will be exposed, or if the environment model for Jupiter is lowered by virtue of new scientific findings.

The preselection approach offers the option of high reliability. Although the costs (schedule-money) would obviously be greater, these costs could be obviated by a reduction in design time in that the criterion established by the

design engineer would be satisfied at the outset, relieving him of the problem of excessive circuit redesign and coping with difficult alternatives. The reduced weight and power are also important cost considerations. It appears that implementation of the preselection program would be most appropriate if anticipated radiation doses are relatively high, as would be the case if a close-to-body-mounted RTG is used in the final spacecraft configuration, or if conservatism in anticipated space and Jupiter environment is maintained or increased.

If the Sector Analysis when augmented by radiation mapping of the spacecraft indicates a fairly wide range of device problems, from minimal to critical, then a third "hybrid" approach might be worthy of consideration as a compromise between the disadvantage of the possible reliability risks and reduced performance inherent in the worst-case approach and the disadvantage of greater costs inherent in the preselection approach. It may be reasonable to worst-case test those devices in protected locations or where performance deterioration is only semi-critical. In exposed areas and where failure might be catastrophic, preselection procedures could solve the reliability problem.

The predicted performance of a subsystem based on component characteristics derived from radiation testing, while generally satisfactory, does not exclude life testing of selected subsystems. These tests should be conducted as soon as a prototype is available.

SECTION V

CONCLUSIONS AND RECOMMENDATIONS

A. General Conclusions Based on Radiation Susceptibility Analysis

The use of a carefully planned and controlled radiation hardening procedure which is already implemented during the Definition Phase of the NEW MOONS Spacecraft Program can ensure survival of the spacecraft over the postulated 5-year mission without excessive degradation from exposure to the combination of space and RTG radiation. This can be done successfully even if the two RTG units are mounted within 18 inches of electronic subsystems that contain semiconductor devices sensitive to radiation damage effects. Results of the study contributing to these conclusions include the following:

(1) Neutron flux from the RTG's will be the principal source of bulk-damage effects in semiconductors, particularly transistors. This difficulty can be avoided to a large extent by using only those transistor types having a relatively large gain-bandwidth product ($f_T > \sim 50$ MHz).

(2) Space and RTG radiation both contribute significantly to the anticipated ionization dose affecting sensitive components. The maximum anticipated dose is about a factor of 5 below the level used to estimate damage effects in typical Earth satellites such as the TIROS series.

(3) In calculating the ionization dose, a major difficulty is the uncertainty involved in the estimates of the near-Jupiter radiation environment. As indicated by item (2), however, an order of magnitude increase in the Jupiter radiation flux could be accommodated without serious consequences. The electron flux could, therefore, be an order of magnitude larger since it predominates over the proton flux. Alternatively, about the same effect would be produced by an increase in the Jupiter proton flux by about three orders of magnitude. These estimates assume that the energy distribution of the particles will not change significantly. However, if the spectra become harder, that is, having proportionately more high-energy particles, then the allowable increase in number will be reduced.

With a detailed semiconductor component list, component layout, and list of bulk materials, it is possible to calculate subsystem degradation rapidly and fairly accurately and thereafter to assess the extent of component testing

107

necessary to provide the data needed to predict component degradation or achieve component preselection. However, the prediction of subsystems performance based on component behavior does not exclude proof-of-principle testing or life testing of selected subsystem.

To validate shielding estimates provided by the spacecraft structure and intervening subsystems, mapping internal dose patterns on a breadboard and/or prototype spacecraft should be considered. This may be done for a selected sector where a particularly sensitive subsystem is housed or on the entire spacecraft.

The degradation predictions arising from the worst-case component test program will provide much of the necessary data for a tradeoff study where the effect of degradation situations can be balanced against the addition of shielding, component or circuit alteration, reduction of mission demands, etc.

Preselected space-qualified components can be obtained through a preselection program that employs a radiate-test-anneal cycle for most solid-state devices.

It is recommended that the choice between the alternative component test programs outlined here be predicated on the final spacecraft-RTG configuration which will be necessary to establish the magnitude of the radiation effects problem.

In general, however, while experience with similar radiation hardening programs suggests that, for the radiation levels anticipated, the impact of radiation on overall spacecraft design will not be dominating, it should be considered a "new environment" subject to a careful consideration as a design parameter, especially in subsystem layout, parameter drift considerations, materials choice and finally, test verification.

B. Impact of Radiation Effects on NEW MOONS Program Time and Cost

1. General

The inclusion of radiation as a design parameter in a sophisticated, long-life spacecraft has, inevitably, some time and cost implications. Recent research and development makes it somewhat more simple than in the past to assess these implications. Engineering a "hardened" spacecraft requires the collaboration of engineers and physicists and good general dissemination of

unfamiliar design concepts throughout a spacecraft design organization. Once this basic understanding is present in an organization, the cost for a given degree of "hardening" can be approached with a fair degree of accuracy.

Several important functions of a radiation hardening activity are noted in the following paragraphs with a very brief description of each activity.

2. Mission Analysis

A physicist will be required to assess the radiation fluxes to be met in the mission and the penetration characteristics of these fluxes in typical spacecraft materials.

Also needed is a determination of the estimated radiation flux from the RTG's that will reach the detector subsystems to ensure that tolerable "noise" levels will not be exceeded.

3. Spacecraft Sector Analysis

Information derived from spacecraft layouts and drawings showing the location of individual subsystems as well as the internal construction of the subsystems will form the basis for applying the "Sector Analysis" technique to estimate the extent of the "natural" shielding surrounding radiation-sensitive components at various locations throughout the spacecraft. If added shielding seems necessary then the amount needed can be determined more accurately by using X-ray techniques to measure the extent of the "natural" shielding surrounding a component. This effort will start early in the Definition Phase of the program and will continue as new and more detailed information regarding the internal physical arrangement of the spacecraft becomes available.

4. Component Damage Analysis

Determining the effect of the anticipated environment on each spacecraft component, particularly the semiconductor devices known to be sensitive to radiation, will constitute a critical part of the radiation hardening program. Information of this kind will form the basis for determining the measures that must be taken as part of the subsystems design effort to maintain performance within tolerable limits over the entire mission period. When bills of materials and parts become available, an extended search for radiation test data on such parts will be needed followed by a test program (item 6) to fill gaps in existing knowledge. Again, this effort should start as soon as possible during the Definition Phase of the program when preliminary parts data become available.

5. Circuit/System Degradation

Design engineers must "add on" to their existing design time an allowance for analyzing the impact of the above device/material degradations on their system. Start of this phase may be delayed by lag in step 4.

6. Component Test Program

The identification of critical parts and materials on which no adequate test or prediction datum exists leads to an unavoidable testing effort to supply a basis for prediction. A typical program, as performed by AED for the TIROS project is shown in Figure 34. About 600 devices of over 100 different types were tested to establish worst-case degradation levels under Van Allen belt radiation. In the present case, some neutron tests may also be required. The program shown involved engineers and physicists continuously for several months. The results and implications of such a test may be disseminated rapidly as obtained if the correct background analysis techniques and working relations are already set up between testing device, evaluation, and design personnel, thus shortening time delays radically.

7. Screening Test

If, as is advisable, each flight unit of certain critical devices is pre-tested or "qualified" under radiation before integration into the spacecraft, then such tests must be scheduled into the device-procurement cycle. Allowing for the need for recycling certain items because of poor yield or catastrophic failures, the procurement cycle could be lengthened by well over a month. As a rule, the device vendor cannot supply such a service and the user must anticipate the need for in-house testing and resultant added lead time in procurement. Research and development on the preselection technique to be used can, of course, remove uncertainties as to the cycle time involved.

8. Final Corrective Action

As with step 5, the ensurance of optimum tolerance to radiation in the final design requires the cooperation of design engineers and radiation physics personnel. An "add on" to design engineers' time is thus required as well as consulting time from radiation experts. Proof-of-principle overall tests of selected prototypes of a particularly sensitive subsystem might be included in this part of the program. Finally, as mentioned earlier, it may be thought advisable to design monitors of dose levels in selected spacecraft locations in the same sense as temperature is monitored on spacecraft. Such monitoring subsystems could be designed within a few months by an engineer-physicist team.

ITEM	ITEM DESCRIPTION	JANUARY				FEBRUARY				MARCH		
		5-8	11-15	18-22	25-29	1-5	8-12	15-19	22-26	1-5	8-12	15-19
1	RECEIVE APPROVAL & ORDER PARTS		████	████	████							
2	COMPL. TEST SPECS & CIRCUIT MODIF. SPECS	6 ████	13 ██									
3	PREPARE, CHECKOUT & MODIFY TEST APPARATUS		████	████								
4	PREPARE IRRAD. MEAS. OF ALL TEST ITEMS			████	26 ██							
5	COMPLETE INSTALL. & CHECKOUT-TEST SITE			████	26 ██							
6	TEST RUN NO. 1 Co^{60}				27 ██	2 ██						
7	POST-IRRAD. MEAS. (TEST RUN NO.1)					3 ████	11 ██					
8	TEST RUN NO. 2 Co^{60}					3 ████	████					
9	POST IRRAD. MEAS. (TEST RUN NO. 2)						11 ██	████				
10	POST IRRAD. CHECKOUT ALL TEST APPARATUS								23 ██			
11	TEST RUN NO. 3 (1 MeV ELECTRON ACCELERATOR)						10 ██	16 ██				
12	POST IRRAD. MEAS. (TEST RUN NO. 3)							████	24 ██			
13	DATA REDUCTION											
14	ANALYSIS AND INFORMAL REPORT								████	████	████	████

Figure 34. Radiation Test Program for TOS Spacecraft (1965)

9. Conclusions

A well-planned radiation analysis effort need not add greatly to the time required to bring a spacecraft from concept to launch phase, since the work involved can be dovetailed with the routine design process. However, the services of "radiation effects" personnel grounded to some degree in radiation physics, test procedures, and design engineering are required. Several engineers will probably be required to share the tasks described. Total labor involved will depend on (a) severity of "internal" environment, (b) number of types of components involved, and (c) degree of reliability required in design.

C. Development Program

1. Radiation Sensitivity of New Solid-State Components

New solid-state components, new junction geometries, new semiconductors, and new insulators will be considered for use. In particular, the incorporation of new dielectric materials (silicon-on-sapphire substrates, ceramic isolation, photodiode/phototransistor optical links, silicon nitride encapsulation, etc.), is likely to bring with it new radiation problems (e.g., trapped-charge buildup in sapphire substrate leading to inversion layers in semiconductor). Thus, to achieve the quick reaction time demanded in making device evaluations, a steady radiation-testing activity, anticipating the radiation susceptibility work of NEW MOONS, is recommended. In this way, a list of standard "space-qualified" components can be kept up to date, and problems caused by new effects can be followed up by device-physics R&D work before the effect becomes a bottleneck to efficient and timely spacecraft design.

2. Device Preselection

The work on screening techniques described has generated an understanding of "maverick" and batch variability effects in transistors and established feasibility of the technique. However, the general applicability of the technique to all sensitive but otherwise spaceworthy devices has yet to be studied, while the most economical and reliable method of applying the technique must still be determined.

3. Stable Exterior Coatings and Components

a. _General Solar Wind Phenomenology._ The very short stopping distances of interplanetary solar wind particles makes the analysis of effects due to them difficult. Further basic study on the interaction of these particles with surfaces is required. Such questions as the relative amounts of atomic displacement, sputtering, and ionization produced must be addressed.

112

b.   Development of Stable External Materials.   Materials directly exposed to low-energy trapped and solar particles have a special materials problem. Such materials as organic binders for paints, paint pigments, insulators for cables, potting compounds for electrical harness, etc., will receive surface doses above 10^8 rads.   The problem will be acute if white (low α/ϵ) coatings are required.   For example, color-center formation in white pigments by protons and UV probably caused the changes of α_s by a factor of 2 and corresponding temperature rises in white paints observed during the 3-month missions of Lunar Orbiter.   Current technology has not produced good space-stable coatings which will retain thermal, optical, and electrical properties under such conditions.   In addition, recent experiments indicate that the combined effect of particle and ultraviolet radiation may be very much greater than the effect produced when the two different types of radiation are applied in sequence. Thus, further development of such materials is required and recommended for long interplanetary missions.

4.   Experimental Mapping of Shielding Afforded by Spacecraft Structures and Components

Statements in Sections IIC and IVC and the material of Section IID indicate that for magnetically trapped electrons and protons of the type expected in NEW MOONS mission environments, the role played by component box covers, device encapsulations, and the neighboring structures in providing mutual protection for the active solid-state components inside them is very significant.   This being so, variations in the layout of the electronic packages can have a strong impact on the "hardness" of the overall system (see, for example, Ref. 13, Figure 10). Thus, it is important to examine several different layouts in order to determine the optimum layout for "hardness" in a given space situation.   The mapping of radiation doses in each component location, if done by individual manual calculation, for many space situations would be extremely time consuming.

An experimental method can be devised which conserves time and effort. Equipment mockups, in several layouts, could be constructed, a radiation detector placed inside various component boxes and a suitable radiation source placed outside to simulate the space radiation.   This preliminary "mapping" of layouts for mutual radiation protection could ultimately produce significant savings in weight by eliminating shielding which might otherwise have to be added to protect sensitive but under-protected electronic components.

If it is decided to monitor radiation dose in flight, lightweight, low-power dosimetric systems should be developed at this stage which will telemeter radiation damage status of the spacecraft in a compact data format which does not occupy telemetry bandwidth unduly.

5. Computation of Shielding Effects

The experimental mapping, described in the foregoing section, requires an essential accompanying capability. This is the capability to compute, rapidly and accurately, the space radiation flux and doses which emerge after passing through a slab shield of a given material and thickness (see Section IIC-6). New computations are needed for every change in spacecraft trajectory around Jupiter. Thus, the process should be computerized. Only a limited range of programs is at present available for this purpose. Furthermore, as accurate prediction curves for the degradation of key devices are evolved, the dose and damage levels computed above could be automatically converted into degradation levels for devices behind a given thickness of shielding. Such programs are not yet available for internal electronic components. Finally, the fact that, in real life, shielding around a component is nonuniform could be included in a computer program by making independent shielding calculations for several sectors of the 4π solid angle about a given component location. Such calculations would be particularly important for critical components such as MOS transistors and for determining the feasibility of certain close-flyby missions with respect to radiation degradation of the spacecraft system as a whole. *

6. Other Recommendations

Radiation-hardened products are being pursued by the Department of Defense (Reference Article in ELECTRONICS NEWS, Monday, Feb. 24, 1969, by Ron Williams, Dallas, entitled "Standing Up to Radiation"). New study contract for radiation-resistant products to component and subsystem companies are being released. Companies include Texas Instrument, Motorola, Fairchild Semiconductor, and Signetics. It would seem appropriate to coordinate with the government agencies involved and their contractor to ensure optimum use of relevant data for NEW MOONS missions.

---

*V. Danchenko, Goddard Space Flight Center, has previously indicated the importance of this requirement in mission analysis.

ACKNOWLEDGMENTS

REFERENCES

1. Vette, J. I., "Models of the Trapped Radiation Environment," Volume I, <u>Inner Zone Protons and Electrons</u>, NASA Special Publication 3024, 1966.

2. Webber, W. R., "An Evaluation of the Radiation Hazard Due to Solar-Particle Events," Boeing Report DZ-90469, The Boeing Company, Seattle, Washington, December 1963.

3. Ness, N. F., "The Magnetosphere and Its Boundary Layer," in "Proceedings of the Second Symposium on Protection Against Radiation in Space " (ed. Arthur Reetz, Jr.), Washington, D.C., Oct. 12-14, 1964, NASA Special Publication 71, 1965.

4. <u>Space Materials Handbook</u> (ed. C. G. Goetzel, J. B. Rittenhouse, and J. B. Singletary), New York: Addison-Wesley Publishing Co. Inc., 1965.

5. Hamman, D., et al., "Space Radiation Damage to Electronic Components and Materials," REIC Report No. 39, Battelle Memorial Institute, Columbus, Ohio, January 31, 1966.

6. Holmes-Siedle, A. G., Liederbach, F., and Poch, W., "The Prediction of Space Radiation Effects on Transistors and Solar Cells," IEEE Catalog No. F63, Institute of Electrical and Electronics Engineers, New York, N.Y., 1966.

7. Brucker, G. J., "Correlation of Radiation Damage in Silicon Transistors Bombarded by Electrons, Protons, and Neutrons," Toulouse Conference on Radiation Effects in Semiconductors, March 1967.

8. Cooley, W. C., and Barrett, M. J., "Handbook of Space Environmental Effects on Solar Cell Power Subsystem," Exotech, Inc., Report No. TR-014, Exotech, Inc., Alexandria, Va., September 9, 1966, p. 12.

9. TOS Radiation Program Report, "Analysis and Evaluation of Test Results," RCA Corp., Princeton, N.J., under Contract No. NAS 5-9034 with Goddard Space Flight Center, Greenbelt, Md., September 1965.

10. Brown, R. R., Fogdall, L. B., and Cannaday, S. S., "Electron Ultraviolet Radiation Effects on Thermal Control Coatings," AIAA 3rd Thermophysics Conf., Los Angeles, Calif., June 1968.

11. Hittman Associates, Inc., Baltimore, Md. Memorandum No. HA-3404-2087, under Contract No. NAS 5-9548 with Goddard Space Flight Center, Greenbelt, Md., February 12, 1968.

12. Ross, R., Krumbein, A. and Beaulieu, A., "A Gamma Ray Probe System for Determining the Shielding Effectiveness of the Apollo Vehicle," in "Proceedings of the Second Symposium on Protection Against Radiation in Space " (ed. Arthur Reetz, Jr.), Washington, D.C., Oct. 12-14, 1964, NASA Special Publication 71, 1965.

13. Holmes-Siedle, A. G., "Space Radiation—Its Influence on Satellite Design," RCA Engineer, July 1965.

14. Peck, D. S., et al., "Surface Effects of Radiation in Transistors," Bell Syst. Tech. J., 49:95, 1963.

15. Holmes-Siedle, A. G., and Poch, W. J., "A Prediction and Selection System for Radiation Effects in Planar Transistors," IEEE NSRECON, Missoula, Montana, July 1968, Trans. of IEEE on Nuclear Science, NS-15:213, 1968.

16. Brucker, G. J., Dennehy, W. J., and Holmes-Siedle, A. G., "High-Energy Radiation Damage in Silicon Transistors," Trans. of IEEE on Nuclear Science, NS-12:69, 1965.

17. Brucker, G. J., Dennehy, W. J., and Holmes-Siedle, A. G., "Electron-Induced Surface Damage in Silicon Transistors," Proc. of the IEEE, 53 (11): 1800, 1965.

18. Dennehy, W. J., Holmes-Siedle, A. G., and Zaininger, K. H., "Interrelation of Space Radiation Sensitivity and Process Techniques in MOS Devices," RCA Corp., Princeton, N.J., Final Report under Contract No. NAS 5-10177 with Goddard Space Flight Center, Greenbelt, Md., July 1967.

19. RCA Astro-Electronics Division, Moorestown, N.J., and AT&T Bell Telephone Laboratories, Murray Hill, N.J., "Commercial Communications Satellite," Final Report to Communications Satellite Corporation, Washington, D.C., March 1, 1965.

20. Holmes-Siedle, A. G., and Zaininger, K. H., "A Survey of Radiation Effects in MOS Devices," RCA Review, 18(2):208-240, 1967.

21. Gordon, F., and Wannemacher, H., "The Effects of Space Radiation on MOSFET Devices and Some Application Implications on Those Effects," Trans. of the IEEE on Nuclear Science, NS-13:262, 1966.

22. Dennehy, W. J., Holmes-Siedle, A. G., and Zaininger, K. H., "Interrelation of Space Radiation Sensitivity and Process Techniques in MOS Devices," RCA Corp., Princeton, N.J., Final Report under Contract No. NAS 5-10177 with Goddard Space Flight Center, Greenbelt, Md., July 1967.

23. Dennehy, W. J., Holmes-Siedle, A. G., and Zaininger, K. H., "Techniques for the Reduction of Radiation Sensitivity in MOS Structures," in "Solid State Device Conference," Manchester, England, Inst. Phys., October 1967.

24. Waxman, A., and Zaininger, K. H., "Al_2O_3-Silicon Insulated Gate Field Effect Transistors," Applied Physics Letters, 12(3):15, 1968.

25. Holmes-Siedle, A. G., and Zaininger, K. H., "Physics of Failure of MOS Devices Under Radiation," Trans. of the IEEE on Reliability, R-17(1):24, 1968.

26. "TIROS M Radiation Program," RCA Radiation Test Internal Report RAP-6811, RCA Corp., Princeton, N.J., May 21, 1968.

27. Messenger, G. C., and Steele, E. L., "Statistical Modeling of Semiconductor Devices for the TREE Environment," IEEE NSRECON, Missoula, Montana, July 1968, Trans. of IEEE on Nuclear Science, NS-15:133-139, 1968.

28. Poch, W., and Holmes-Siedle, A. G., "Evaluation of RCA Complementary Symmetry MOS Logic Devices," RCA Radiation Test Internal Report RAP-69B, RCA Corp., Princeton, N.J., February 1, 1969.

29. Space Materials Handbook (ed. C. G. Goetzel, J. B. Rittenhouse, and J. B. Singletary), New York: Addison-Wesley Publishing Co., Inc., 2nd Edition, 1965.

30. The Boeing Co., "Lunar-Orbiter V—Extended Mission Spacecraft Operations and Subsystem Performance," NASA Contractor Report 1142, August 1968.

APPENDIX I

RADIATION ENVIRONMENT OF THE JUPITER FLYBY
FOR VARIOUS NEAR-JUPITER TRAJECTORIES

by

T. P. Sciacca, Jr., and R. S. Marriott
Goddard Space Flight Center

Trajectory Data

by

R. Groves
Goddard Space Flight Center

The postulated space radiation environment for the Outer Planets Explorer (OPE) mission is based upon data from various sources* and is tabulated in Table I-1. The radiation environment produced by four RTG's used as the electrical power source for the OPE spacecraft is also included in Table I-1 and is given in more detail in Table I-2.

A study was made of the change in accumulated dose as a function of the near–Jupiter trajectory. The various trajectories considered relating distance from Jupiter to time from closest approach are illustrated in Figure I-1. To obtain flux curves for a specific near–Jupiter trajectory Figure I-1 is used in conjunction with the curves in this report. Figures I-2 and I-3 are examples

---

*Discussed in Section II of this report.

Table I-1

Design Fluence for the Environment Radiation
of the OPE Mission

		Energy (MeV)	Particles/cm^2	Adjusted Fluence[‡]
Space Environment*	Electrons	>5.0	1.0×10^{10}	1.0×10^{11}
	Proton[†]	>0.1	5.0×10^{13}	5.0×10^{14}
		>30.0	1.5×10^{8}	1.5×10^{9}
RTG Environment●	Neutrons	2.5	Approx. 3.0×10^{11}	3.0×10^{11}
	Gammas	2.5	Approx. 4.0×10^{12}	4.0×10^{12}

* The radiation totals include the (1) near-Earth, (2) Earth-to-Jupiter, (3) near-Jupiter environments.

[†] The proton estimate could vary as much as two to three orders of magnitude.

[‡] The adjusted fluence for space environment includes a factor of safety of 10.

● RTG Environment = 4 RTG for 8 years at approximately 1700 watts each.

of the proton flux for a trajectory of 7 R_{JA}* and 7.4 R_{JA}[†] respectively. Figures I-4, I-5, and I-6 are examples of the electron flux for trajectories of R_{JA}, 5 R_{JA}, and 3 R_{JA} respectively. The area under these flux curves (i.e., Figures I-2 through I-6) represent a fluence for a specified trajectory; hence, by integrating and multiplying the result by 2 (the curve is actually one half of the flux as it is symmetrical about the ordinate) the fluence as a function of a specific trajectory is obtained. Considering the uncertainties of the Jupiter environment the results obtained indicate that the fluence is relatively insensitive, within an order of magnitude, to changes in the trajectories considered.

---

* R_{JA} is the altitude from Jupiter's surface in terms of Jupiter's radius.

[†] The trajectory of 7.4 R_{JA} used in this report.

Table I-2

Radiation Environment Produced by RTG's

Particle	Flux	Fluence—8-Year Mission	MeV
Neutrons			
Center line of RTG to nearest electronic package	250 neutrons/cm^2-sec.	2.52×10^{11} neutrons/cm^2	2.5
Center line of RTG to center of spacecraft	150 neutrons/cm^2-sec.	1.51×10^{11} neutrons/cm^2	2.5
Center line of RTG to experimental package on booms	15 neutrons/cm^2-sec.	1.51×10^{11} neutrons/cm^2	2.5
Gammas			
Center line of RTG to nearest electronic package	8×10^3 gamma/cm^2-sec.	4.03×10^{12} gamma/cm^2	2.5
Center line of RTG to center of spacecraft	4.5×10^3 gamma/cm^2-sec.	2.27×10^{12} gamma/cm^2	2.5
Center line of RTG to experimental package on booms	1×10^3 gamma/cm^2-sec.	7.56×10^{12} gamma/cm^2	2.5

NOTE: No Shielding Assumed
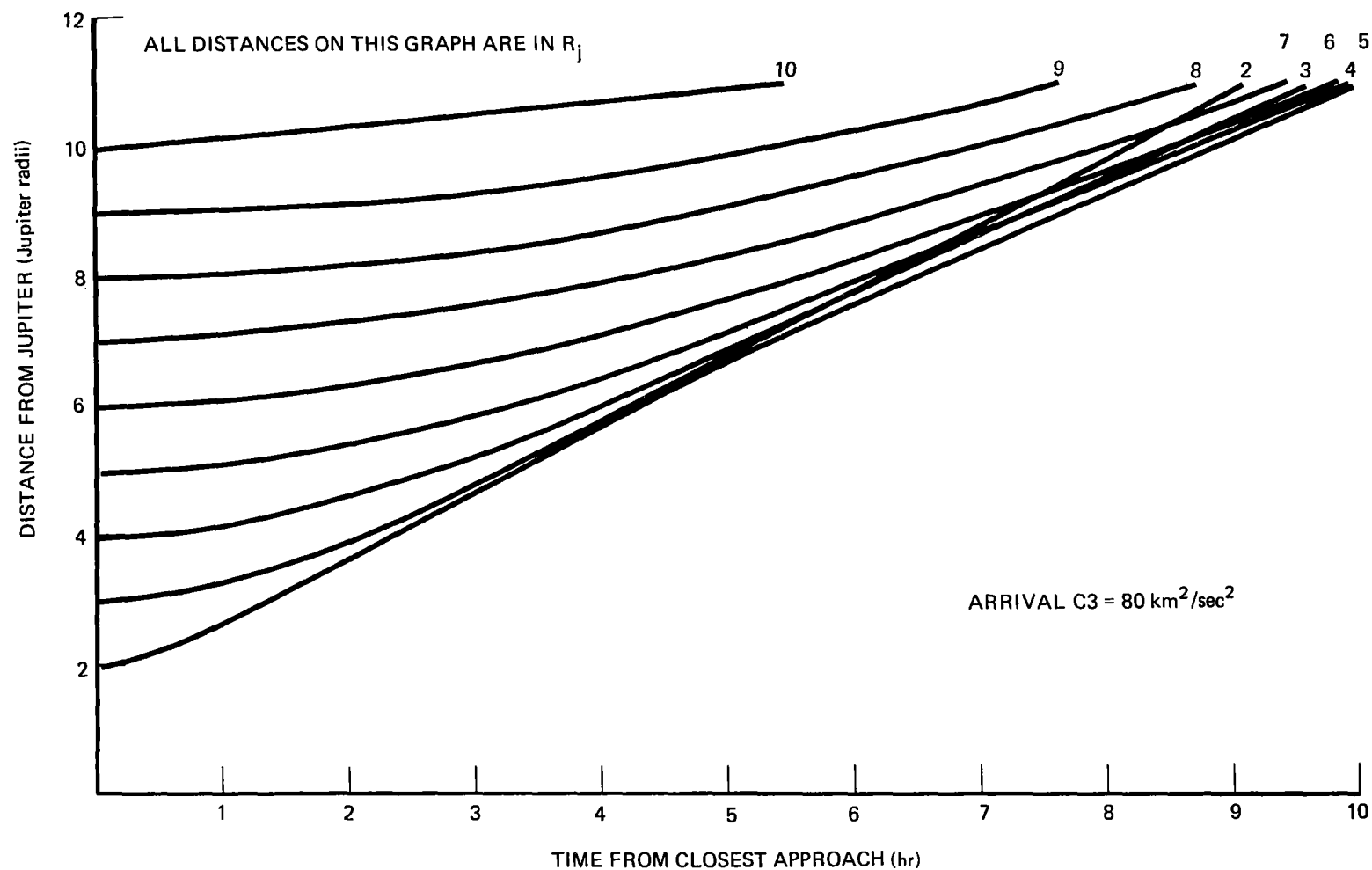
Reference Geometry:
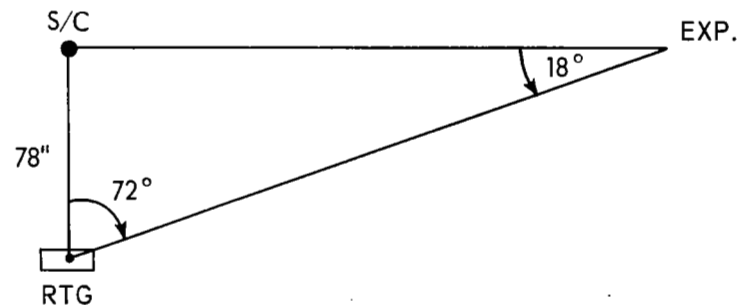
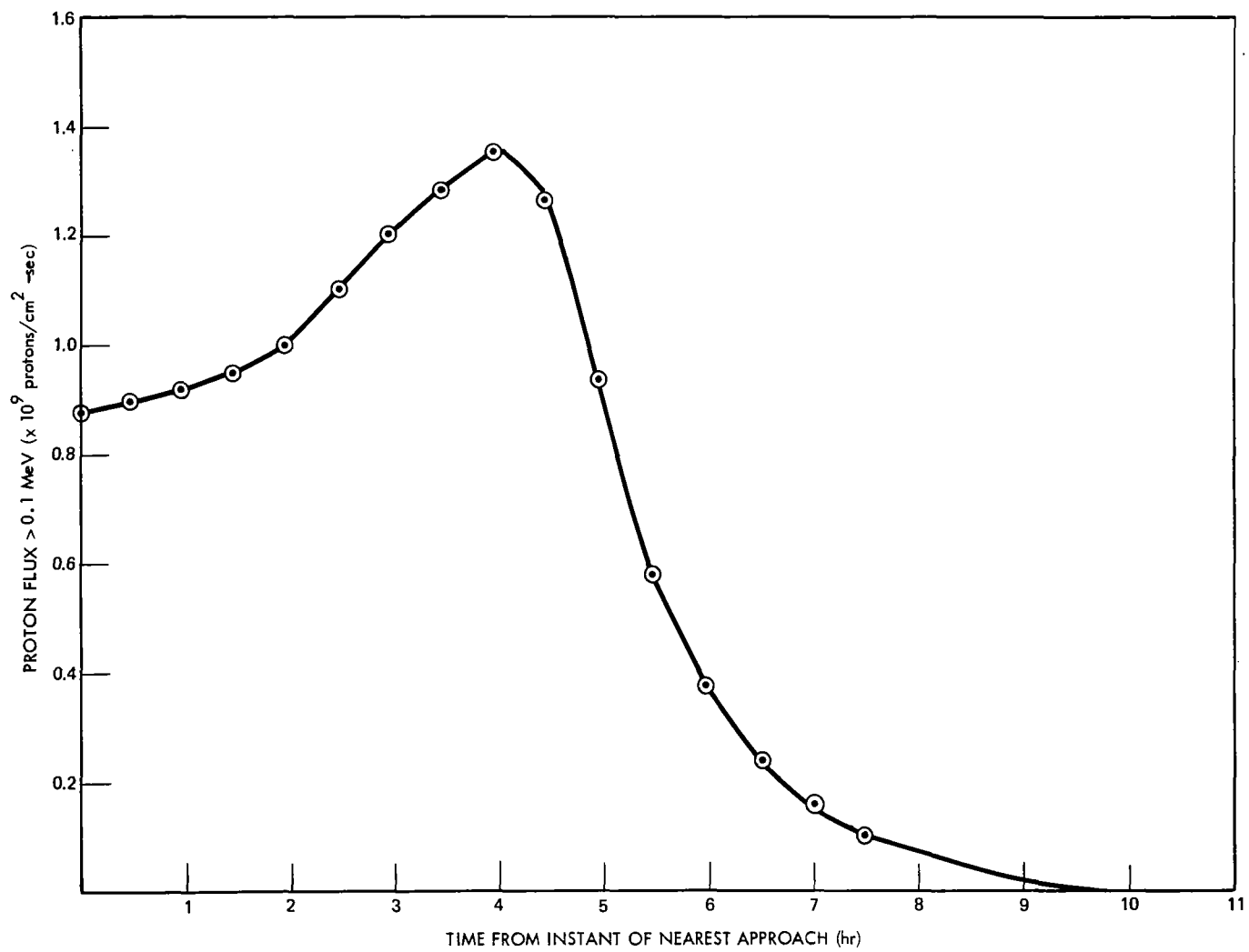Figure I-1. Distance From Jupiter vs. Time From Closest Approach

Figure I-2. Proton Flux vs. Time for Trajectory of 7 R_{JA} (Closest Approach)
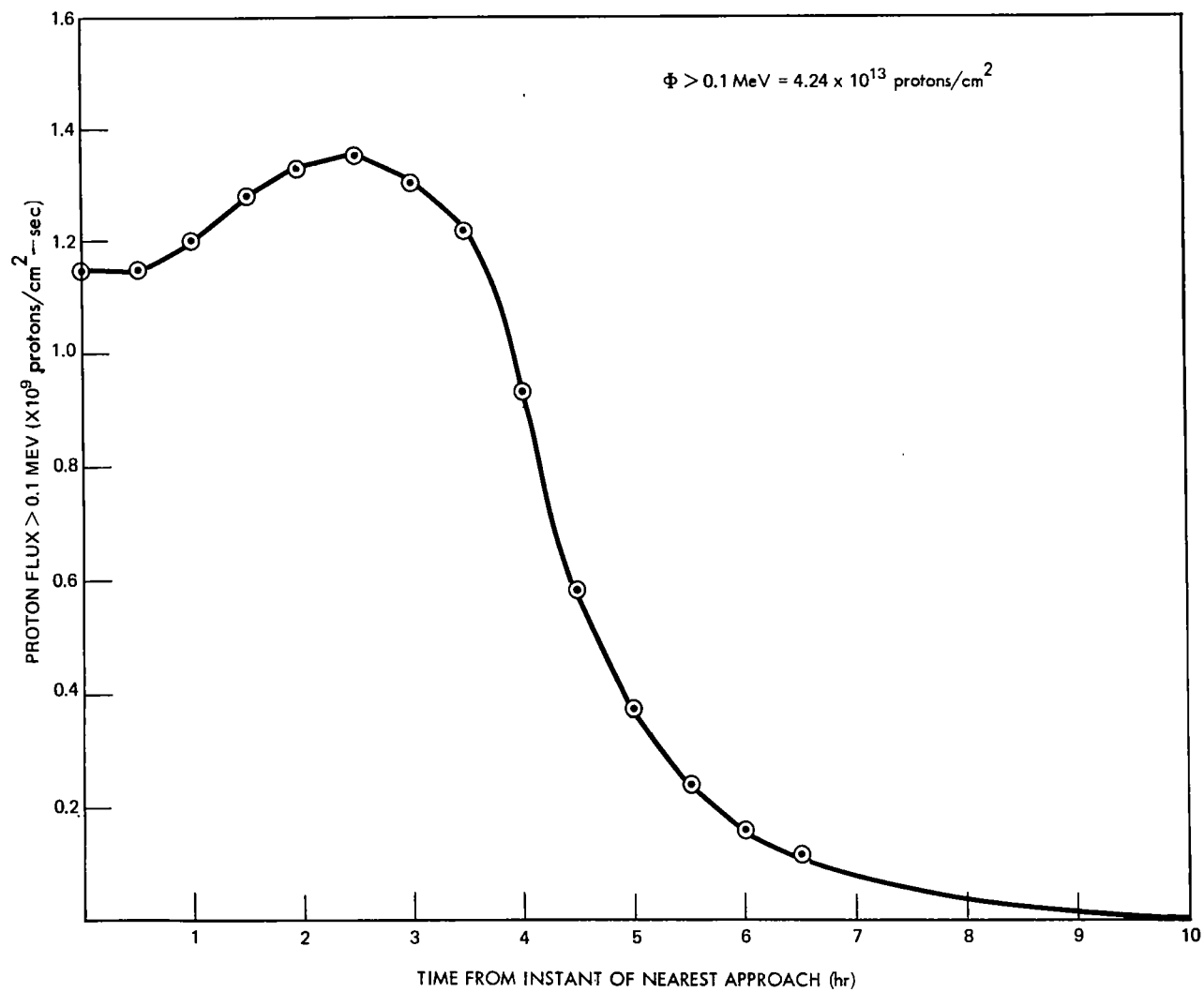
Figure I-3. Proton Flux vs. Time for Trajectory of 7.4 R_{JA} (Closest Approach)
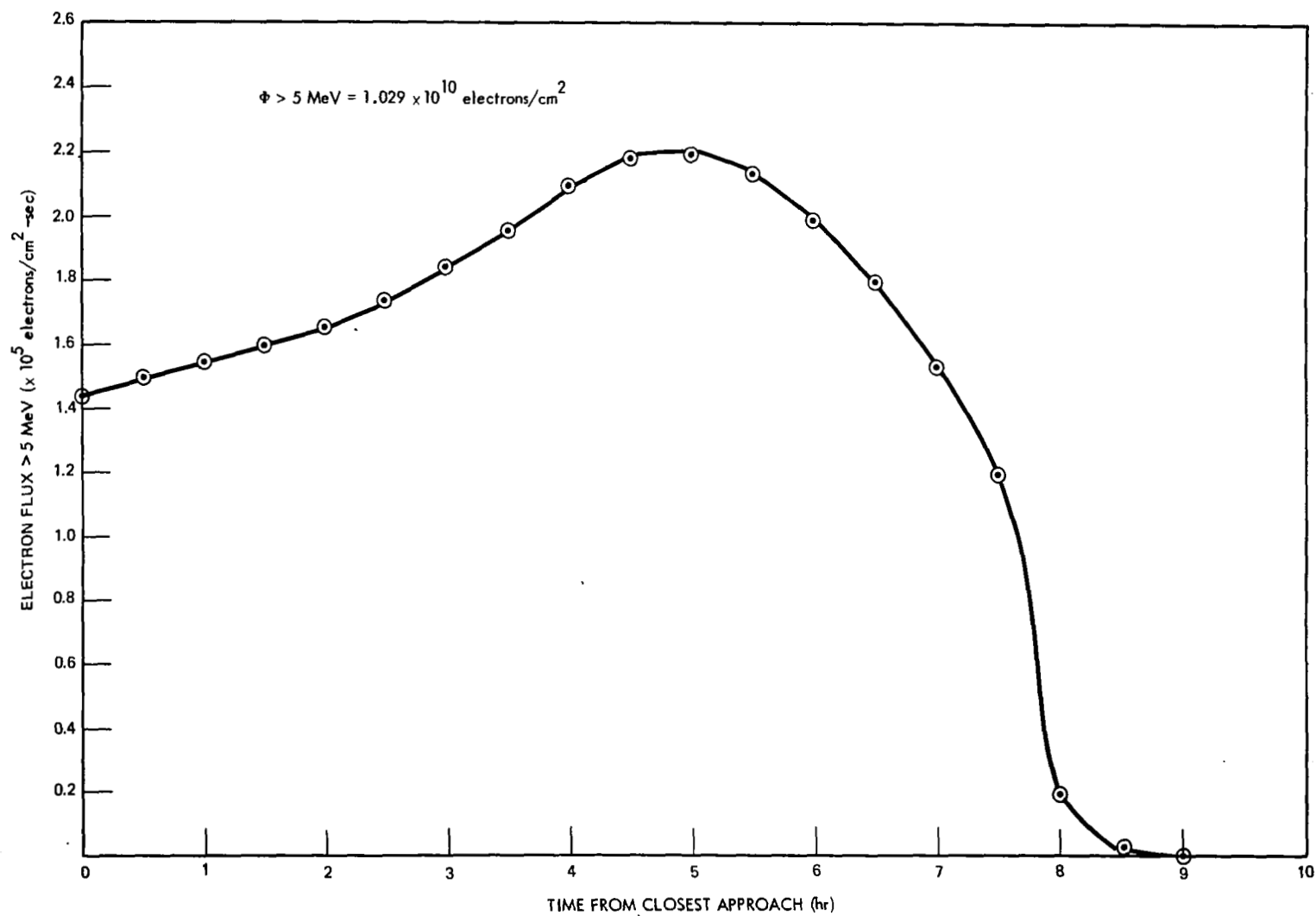
Figure I-4. Electron Flux vs. Time for Trajectory of $7R_{JA}$ (Closest Approach)

$\Phi > 5\ \text{MeV} = 1.029 \times 10^{10}\ \text{electrons/cm}^2$

ELECTRON FLUX > 5 MeV ($\times 10^5$ electrons/cm^2 -sec)
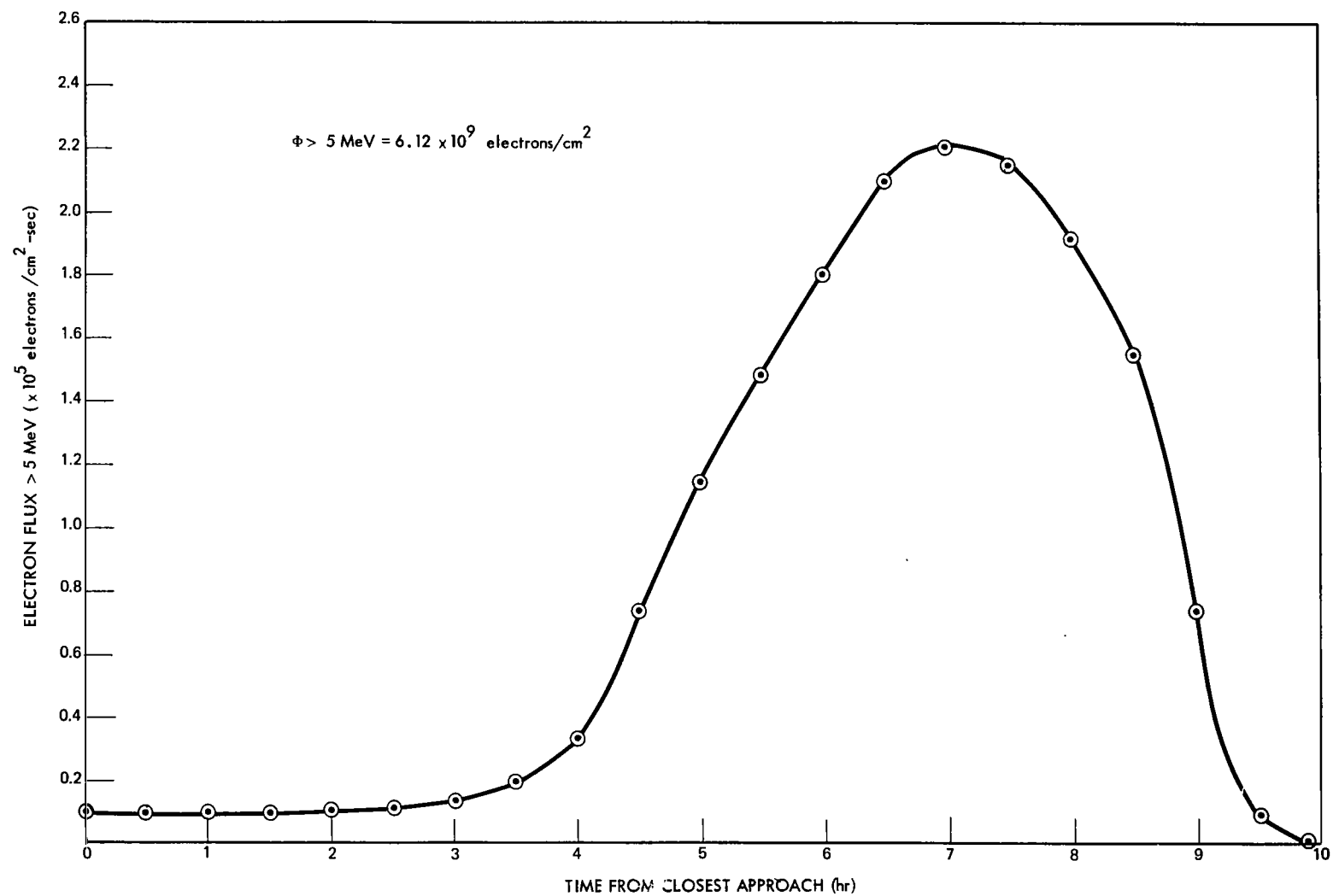
TIME FROM CLOSEST APPROACH (hr)

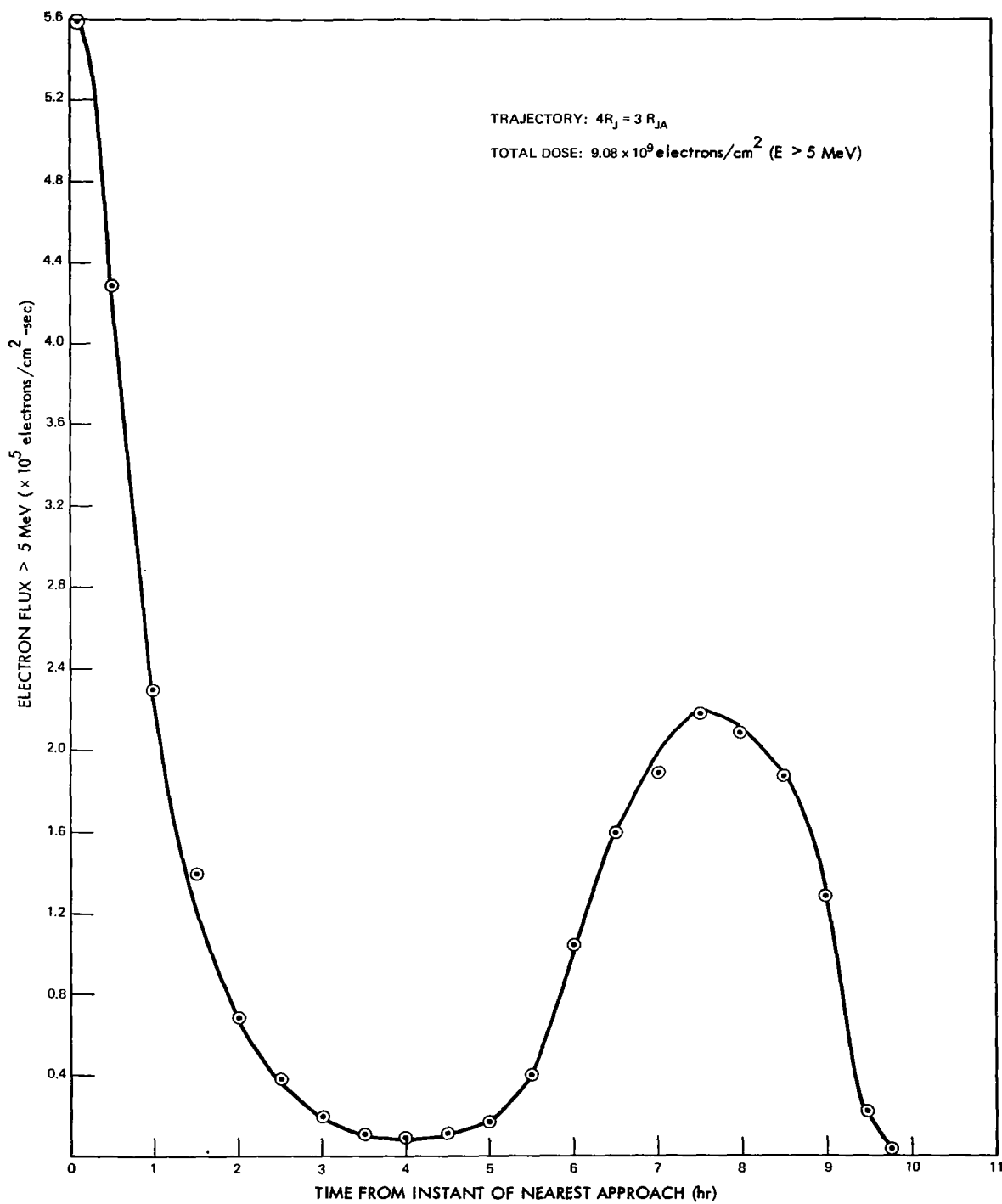Figure I-5. Electron Flux vs. Time for Trajectory of $5\,R_{JA}$ (Closest Approach)

Figure I-6. Electron Flux vs. Time for Trajectory of $3R_{JA}$ (Closest Approach)

APPENDIX II

FUEL DATA AND DERIVATION OF ISOFLUX MAPS*

by

Dale Harris
Goddard Space Flight Center

K. Campe
Hittman Associates

I. Introduction

Among the objectives of Task IIA are the assessment of the susceptibility
of the model mission configurations to the nuclear radiation environment of an
onboard RTG and the evaluation of the possible modifications and radiation
hardening programs which may be required for a successful deep-space flight.
In support of these objectives, a study was performed with respect to the PuO_2
fuel properties and the radiation fields surrounding a planar RTG.

A compilation of the physical, chemical, and nuclear properties of PuO_2
has been made on the basis of the latest available experimental and theoretical
data. The properties are presented in tabular and graphical form in Section II.

Section III contains a discussion of the relative biological hazards of PuO_2
microspheres and PuO_2 cermets. In addition, an evaluation is made of the feasi-
bility of O^{18} depletion from PuO_2 and the associated reduction in neutron emis-
sion rates.

The RTG gamma and neutron radiation fields are given in Section IV. They
are presented graphically in the form of isoflux contour maps. A separate map
was constructed for each of the three selected RTG power levels, i.e., 50, 75,
and 100 watts(e). The effect of O^{18} depletion is discussed in conjunction with
the isoflux data. A description of the nuclear fuel data and the method of analysis
is also included in Section IV.

---

*Prepared Under Contract by Hittman Associates for RCA AED.

Conclusions and recommendations with respect to PuO_2 cermets, O^{18} depletion, and the accuracy of the RTG radiation field analysis are presented in Section V. A list of references cited in this appendix appears on page 163.

II. Pertinent Properties of Selected State-of-the-Art RTG Fuel

A. Physical Characteristics of Pu^{238} Oxide Microspheres

1. <u>Composition</u> (Ref. 1)

   a. Oxygen
   12 percent by weight (calculated)

   b. Plutonium
   Depends on age of fuel (see Figure II-1)

   c. Uranium
   Depends on age of fuel (see Figure II-1)

2. Specific Power (80 Percent Pu^{238} Isotope Purity: (Ref. 1)
   Theoretical $Pu^{238}O_2$ density)

   a. 0.40 watts/g

   b. 12.13 Curies/g

3. <u>Power Density (Bulk Power Density)</u> (Ref. 1)

   2.6 $\pm$ watts/cm^3

4. Mechanical Properties (Ref. 2)

   a. Hardness of Sintered $Pu^{239}O_2$
   $\sim$1163 kg/mm^2

   b. Crush strength of $Pu^{238}O_2$ Microspheres
   1 to 3 kg/sphere

5. <u>Thermophysical Properties</u>

   a. Density of Individual Microspheres (Ref. 3)

   Theoretical 11.46 g/cm^3
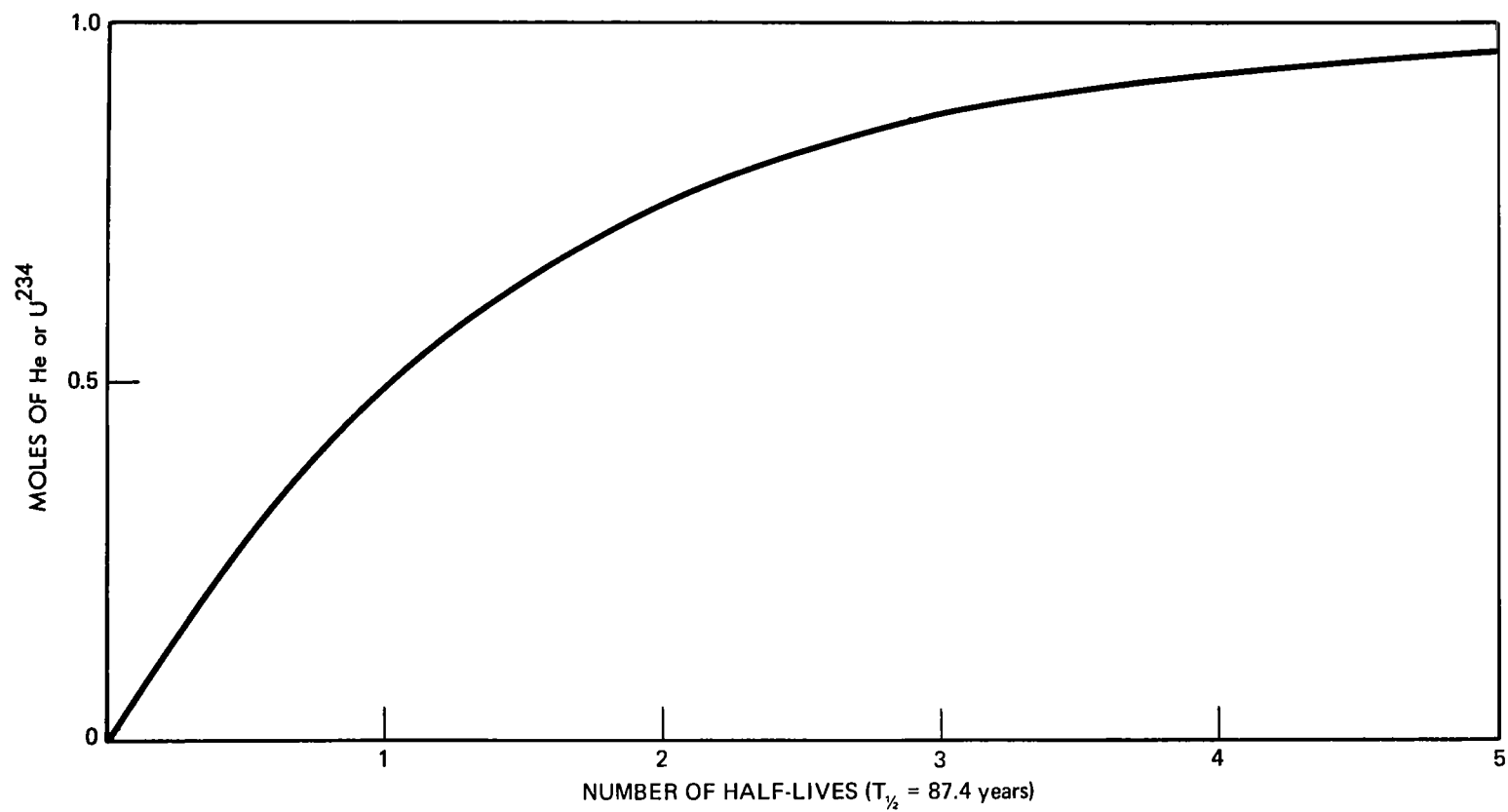   Production grade 8.9 to 10.1 g/cm^3

Figure II-1   Moles of He or U^{234} Produced From the Decay of 1 Mole of Pu^{238}

b. Linear Thermal Expansion Coefficient for Pu^{239}O$_2$ Microspheres (see Figure II-2) (Ref. 4)

c. Bulk Density

>6.2 g/cm^3 (varies inversely with particle density and inversely with void volume between particles)

d. Heat Capacity (Ref. 5)

16.4 cal/mole-$^\circ$K at 25°C for Pu^{239}O$_2$ microspheres

e. Enthalpy (Ref. 5)

$H^\circ_{298} - H^\circ_0$ = 2600 cal/mole for Pu^{239}O$_2$ microspheres

f. Temperature of Phase Transformation (Ref. 6)

Melting point for Pu^{238}O$_2$ microspheres is 2240°C ± 30°C

g. Absolute Entropy

19.7 cal/$^\circ$K-mole at 298°K (Ref. 3)

h. Entropy of Formation

$\Delta S_F{}^{298}$ = -416 cal/$^\circ$K-mole (Ref. 3)

i. Latent Heats of Phase Transformation

ΔH_{fus} for Pu^{239}O$_2$ = 15.2 kcal/mole (Ref. 7)

ΔH_{vap} for Pu^{239}O$_2$ = 133.8 kcal/mole (Ref. 4)

j. Vapor Pressure for Pu^{239}O$_2$ (Ref. 4)

log P (atm) = A - (B/T), where A = 8.072,
B = 29240, and T is the temperature in degrees Kelvin

k. Thermal Conductivity for Pressed and Sintered Pu^{239}O$_2$ (Ref. 8)

Figure II-3 gives thermal conductivity values as calculated from experimentally determined thermal diffusivity of pressed and sintered Pu^{239}O$_2$. The temperature correction of the PuO$_2$ density is based on the reported coefficients of linear thermal expansion. The specific heat of PuO$_2$ is assumed to be the same as UO$_2$
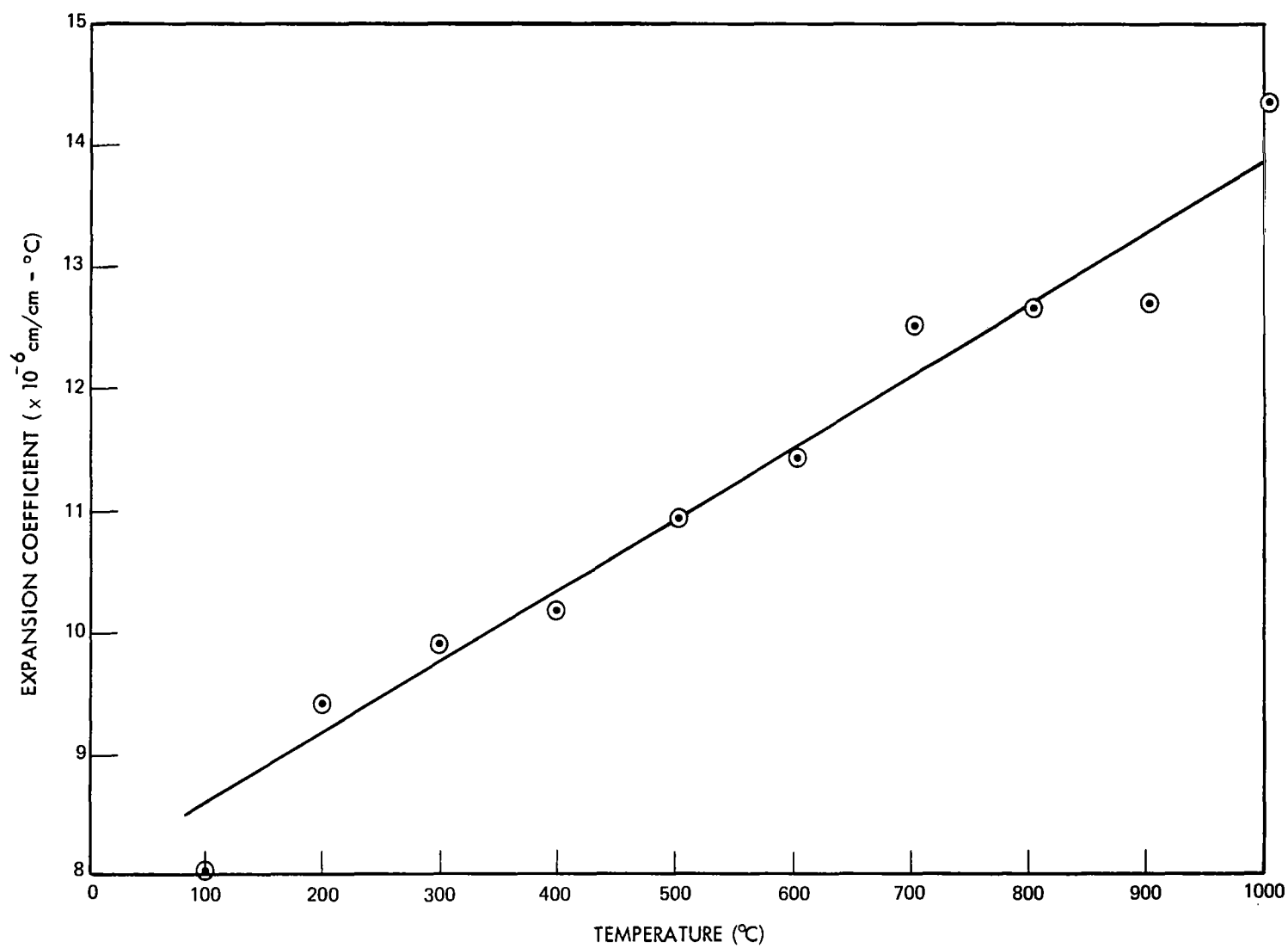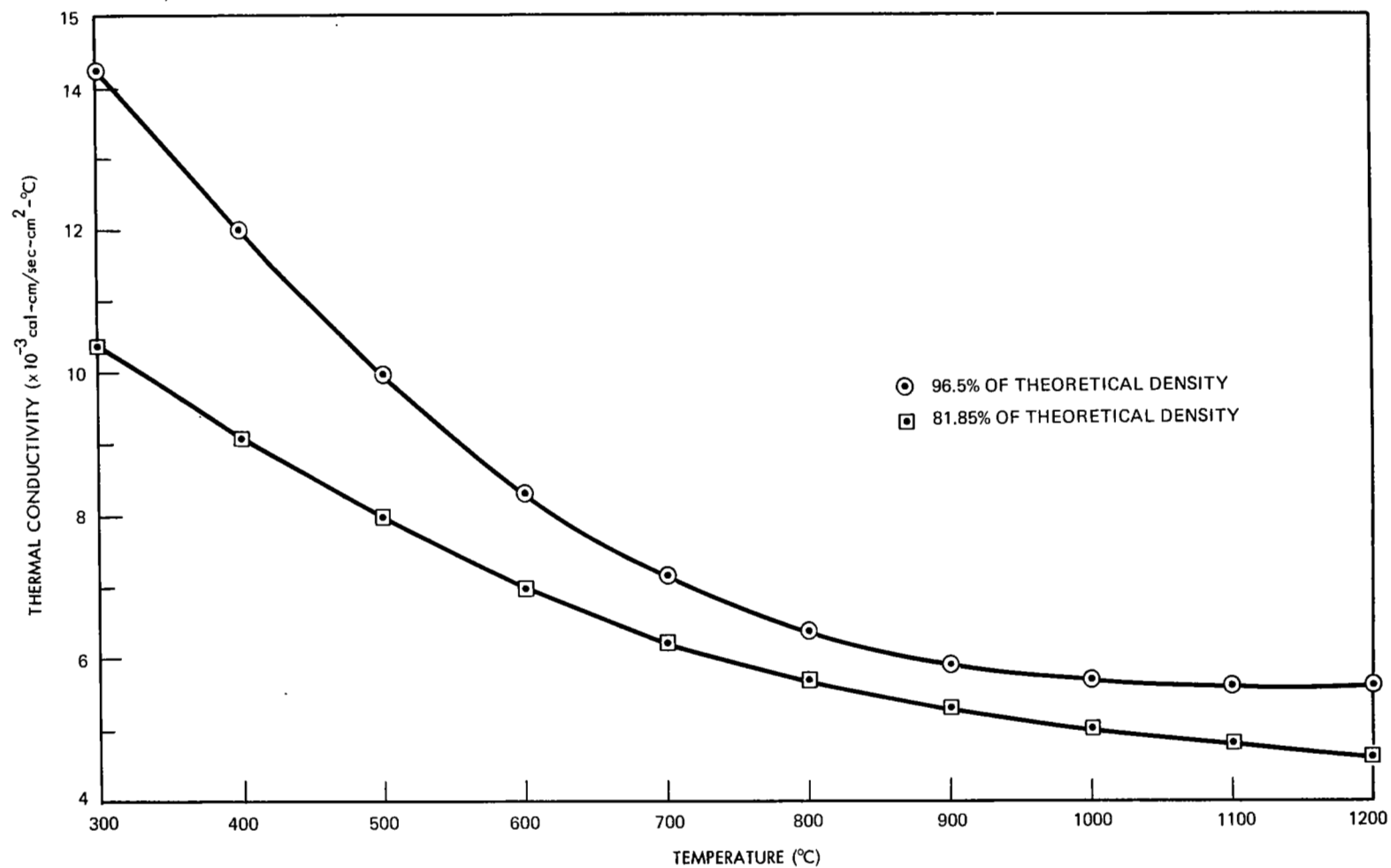
Figure II-2. Linear Thermal Expansion of Pu^{239}O$_2$ Microspheres

Figure II-3. Thermal Conductivity of Two Densities of $Pu^{239}O_2$

l.   Thermal Diffusivity for Pressed and Sintered $Pu^{239}O_2$ (Ref. 8)

The thermal diffusivity values of $Pu^{239}O_2$ reported in
Figure II-4 have an accuracy of ±5 percent

m.   Viscosity of $Pu^{239}O_2$ (Ref. 1)

32 Centipoise (±25 percent) at melting point (calculated)

n.   Surface Tension of $Pu^{239}O_2$ (Ref. 1)

525 dynes/cm (±15 percent)

o.   Crystallography: $Pu^{238}O_2$ (Ref. 6)

FCC structure   (Ref. 6)
Space group Fm3m
Lattice constant 5.400 Å
Ionic radius 0.90 Å

6.   <u>Electrical Properties</u>   (Ref. 3)

Electrical Resistivity of $Pu^{239}O_2$
800 ohm-cm at 1250°K
4×10^{12} ohm-cm at 298°K by extrapolation

B.   <u>Chemical Properties of Pu^{238} Oxide Microspheres</u>

1.   <u>Heat of Formation of Pu^{239}Oxide</u>   (Ref. 9)

-252.9 kcal/mole at 25°C
-253.3 kcal/mole at 1200°C

2.   <u>Free Energy of Formation of Pu^{239} Oxide</u>   (Ref. 9)

-240.4 kcal/mole at 25°C
-192.3 kcal/mole at 1200°C

Free energy of formation can be calculated from an empirical
equation

$$\Delta G_f^\circ = (-253480 - 3.45T \log T + 52.58T) \text{ cal/mole}$$

19

17

15

13

11

9

7

5

3

THERMAL DIFFUSIVITY ($\times 10^{-3} cm^2/sec$)

⊙ 96.5% OF THEORETICAL DENSITY
▣ 81.85% OF THEORETICAL DENSITY

200   400   600   800   1000   1200

TEMPERATURE (°C)
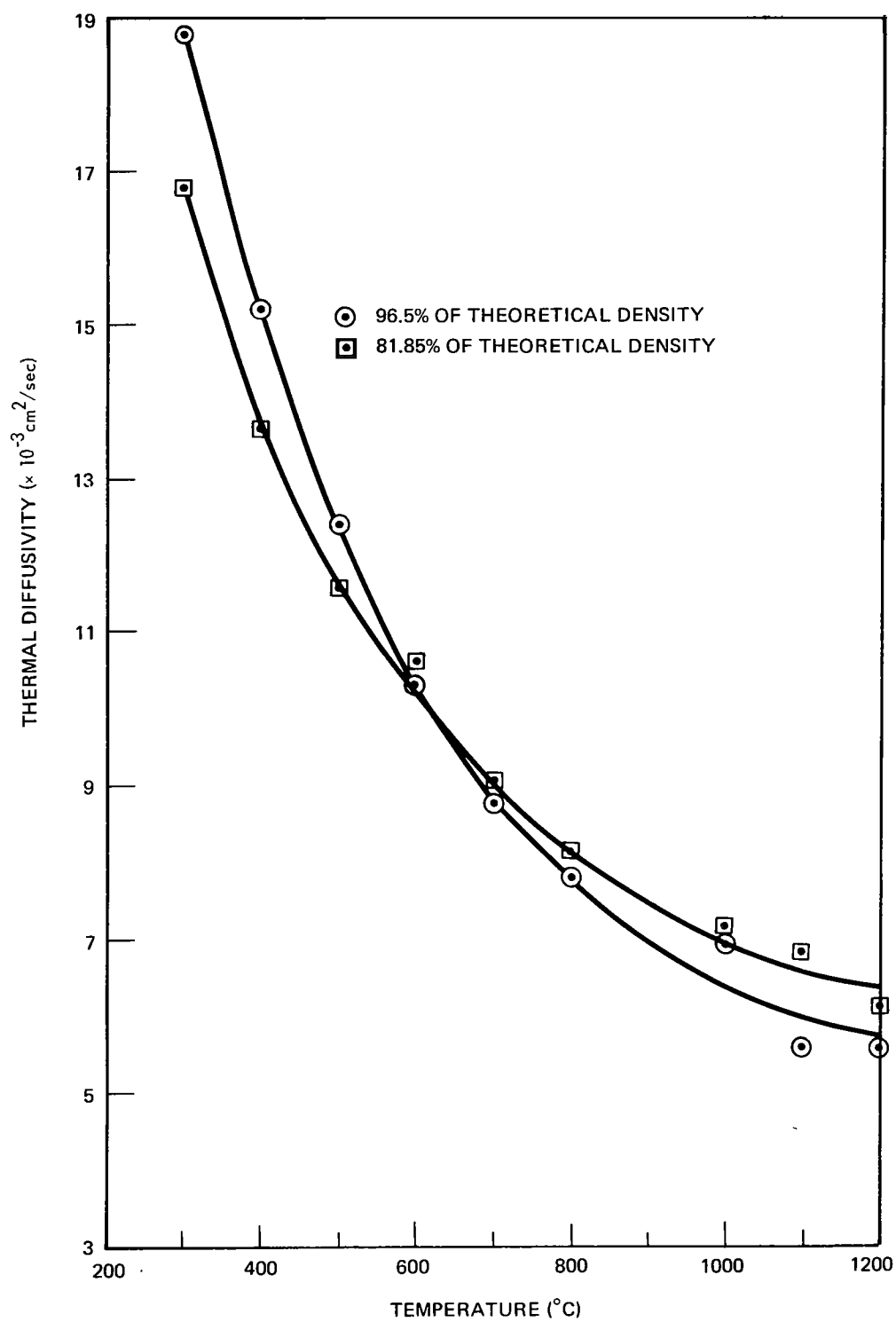
Figure II-4. Thermal Diffusivity of Two Densities of $Pu^{239}O_2$

136

Table II-1

Standard Free Energy Change for PuO_2-Metal Reactions
Between 1000° and 2000°K (Ref. 10)

Metal	Temperature Range (°K)	Reaction	ΔF for Temperature Range Listed (kcal)
Ni	1000–1728	$Ni + 2PuO_2 \rightarrow NiO + Pu_2O_3$	+62, +57
Mo	1000–2000	$Mo + 4PuO_2 \rightarrow 2Pu_2O_3 + MoO_2$	+96, +149
Fe	1000–1812	$Fe + 2PuO_2 \rightarrow Pu_2O_3 + FeO$	+49, +39
W	1000–2000	$W + 4PuO_2 \rightarrow 2Pu_2O_3 + WO_2$	+98, +80
Cr	1000–2000	$2Cr + 6PuO_2 \rightarrow 3Pu_2O_3 + Cr_2O_3$	+81, +58
Nb	1000–2000	$2Nb + 10PuO_2 \rightarrow 5Pu_2O_3 + Nb_2O_5$	+134, +90
Ta	1000–2000	$2Ta + 10PuO_2 \rightarrow 5Pu_2O_3 + Ta_2O_5$	+100, +56
Ti	1000–1933	$2Ti + 6PuO_2 \rightarrow 3Pu_2O_3 + Ti_2O_3$	−7, −28
	1000–1900	$2Ti + Pu_2O_3 \rightarrow 2Pu + Ti_2O_3$	+34, +37
Zr	1000–2000	$Zr + 4PuO_2 \rightarrow 2Pu_2O_3 + ZrO_2$	−23, −34
	1000–1900	$3Zr + 2Pu_2O_3 \rightarrow 3ZrO_2 + 4Pu$	+4, +28
Be	1000–1556	$Be + 2PuO_2 \rightarrow Pu_2O_3 + BeO$	−23, −27
	1000–1556	$3Be + Pu_2O_3 \rightarrow 2Pu + 3BeO$	−33, −23
Th	1000–2000	$Th + 4PuO_2 \rightarrow ThO_2 + 2Pu_2O_3$	−53, −63
	1000–1900	$3Th + 2Pu_2O_3 \rightarrow 4Pu + 3ThO_2$	−88, −58

3.   Compatibility with Materials of Containment*

Results to date show $Pu^{238}O_2$ microspheres to be compatible with all materials tested on a short-term basis. Free energy change values for reactions between PuO_2 and metals can be used as an aid in selection of potential encapsulation material (Table II-1).

Table II-1 shows the dissolution of PuO_2 in distilled water and sea water.

*Paprocki, S. J., et al., "The Chemical Reactivity of PuO_2 with Reactor Materials", BMI-1580, 1964.

Table II-2

Dissolution of Microspheres in Distilled Water and Sea Water (Ref. 12)

Number of Particles	Total Surface Area (mm^2)	Type Water	Temperature	Sample Rate of Release* (μg/day-mm^2)
446	34.81	Florida sea water	Ambient	1.02×10^{-8}
515	43.58	Florida sea water	Ambient	1.23×10^{-8}
628	54.69	Florida sea water	Ambient	1.00×10^{-8}
917	82.69	Distilled water	Ambient	1.52×10^{-8}
518	46.32	Distilled water	Ambient	1.27×10^{-8}
885	76.79	Distilled water	Ambient	1.49×10^{-8}

*Rate of release based on 22 months exposure; test is continuing

C. Nuclear Properties of Pu^{238} Oxide Microspheres With Natural O^{18} Content (Ref. 11)

1. Radiation

Type		Energy (Mev)	particles/watt-sec
Alpha	1	5.495	$\sim 8.04 \times 10^{11}$
	2	5.452	$\sim 3.12 \times 10^{11}$
	3	5.353	1.45×10^{9}
	4	5.204	5.59×10^{7}
	5	5.004	7.82×10^{4}

| Type		Energy (Mev)	particles/watt–sec
Beta		Stable	
Gamma	1	0.810	~2.24×10^5
	2	0.776	~5.59×10^5
	3	0.203	4.47×10^4
	4	0.1531	1.12×10^7
	5	0.0998	1.01×10^8
	6	0.00435	4.25×10^8
	7	0.017	
	8	6.45 (due to Pu^{238})	
	9	6.95 (due to Pu^{239})	
	10	2.61 (due to Tl^{208})	
	11	Other low–energy gamma rays due to impurities	
Bremsstrahlung		Negligible	
Neutrons:		Neutron emission primarily due to (α, n) reactions with O^{18}. Best available average value is ~2×10^4 neutrons/sec–g Pu^{238} (see Figure II-5 and Table II-3)	
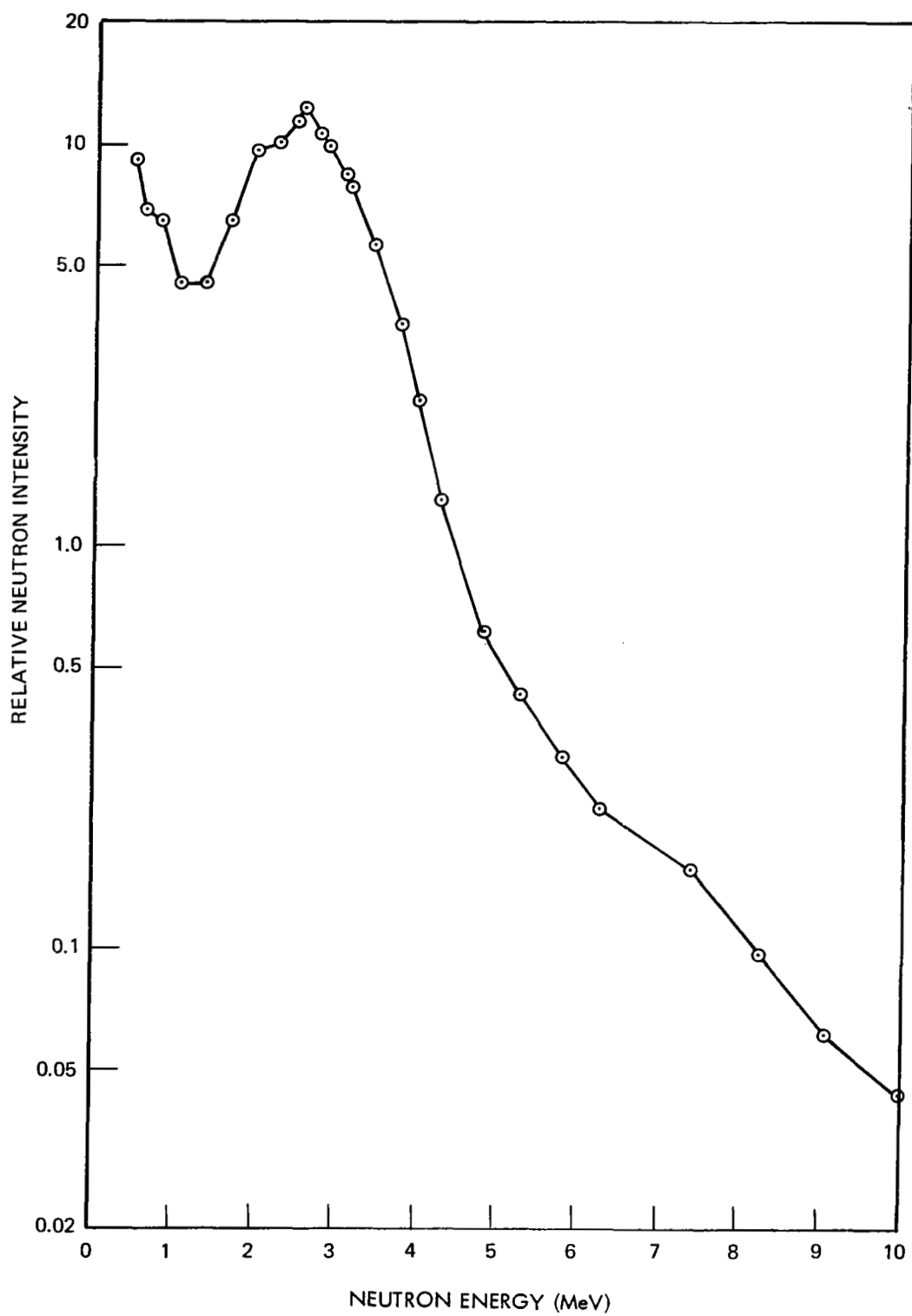
Figure II-5. Neutron Energy Spectrum for PuO_2 Microspheres With Natural O^{18} Content

Table II-3

Data Plotted in Figure II-5

Energy (MeV)	Neutron Intensity	Energy (MeV)	Neutron Intensity
0.48	9.1	3.12	7.8
0.59	6.8	3.42	5.6
0.80	6.5	3.72	3.9
0.99	4.5	4.00	2.4
1.34	4.5	4.28	1.3
1.66	6.5	4.82	0.62
1.96	9.7	5.3	0.43
2.24	10.0	5.8	0.30
2.48	11.4	6.3	0.22
2.51	12.1	7.4	0.16
2.78	10.6	8.3	0.096
2.81	9.9	9.1	0.062
3.03	8.7	10.0	0.044

III. Fuel Form Modifications

A. Cermets

The current status of Pu^{238} fuel forms is an area of major concern to the NEW MOONS Program. Presently, only the PuO_2 microsphere form is available for use. This fuel has a number of unacceptable characteristics with regard to safety. It has been shown that if released at high altitudes, the microspheres will break up into inhalable size particles which could result in unacceptably high lung burdens. Particle degradation also occurs if the fuel is impacted or stepped upon. If released at ground level, the fuel can be suspended and carried by winds creating an inhalation hazard and a highly contaminated downwind footprint pattern. A number of alternate fuel forms have been postulated which prevent the generation of inhalable particles and subsequent atmospheric transport.

One promising fuel is a matrix consisting of PuO_2 microspheres and either a high melting point metal or a ceramic. The Battelle Memorial Institute, under contract with the AEC, is presently engaged in the preliminary investigation of such cermet or ceramic fuels. Matrix materials, such as molybdenum and magnesia, are being considered. Little information has been reported on the status of this development work, so nothing can be said as to when these improved fuels will be made available. If successfully developed in time to be factored into the NEW MOONS Program, such fuels would provide an additional safety backup of some significance.

B. Depleted Oxygen Fuel Form

Plutonium-238 dioxide (PuO_2) decays by alpha emission. Neutrons are generated by spontaneous fission and by (α, n) reactions between the emitted alpha particles and the oxygen atoms.

The neutron emission rate for PuO_2, made with naturally occurring oxygen, can be as high as 6 times that of high-purity Pu^{238} metal for equal quantities of Pu^{238} (Ref. 11). Examination of the emission spectra of aqueous solutions of Po^{210} (Ref. 13) have indicated that O^{18} is the major source of (α, n) neutrons with Po^{210} alphas. Polonium-210 experimental results are applicable to Pu^{238} since the α energies are very similar (5.3 MeV and 5.5 MeV, respectively). The cross section for the (α, n) reaction with O^{18} exceeds the cross-section (α, n) reactions with all other materials except beryllium. Further examination of (α, n) cross sections has

142

revealed that the cross section of O^{17} is less than 10 percent of the cross section for O^{18}. Therefore, most of the neutron emission from PuO_2 appears to result from the (α, n) reaction with O^{18}.

Based on the above, it appears that a substantial reduction in neutron emission is possible if a major portion of the O^{18} isotope is depleted from the oxygen used to produce the PuO_2.

One effective method of preparing oxygen depleted in O^{17} and O^{18} is thermal diffusion of oxygen gas. The required apparatus is simple, and separation factors are large. Since O^{16} is initially at a high concentration, there are no initial transport problems, and more complex distillation methods to gain capacity at the feed end of the system are not necessary.

Mount Laboratory used a simple thermal diffusion column system to prepare oxygen depleted in O^{17} and O^{18} (Ref. 11). Two experiments were performed. Oxygen was depleted to an intermediate composition in the first experiment and a portion of the resultant material further depleted in the second experiment.

Using a portion of the first experiment product, analysis utilizing a mass spectrometer indicated a decrease in O^{18} content from 0.204 percent to 0.1 percent. Carbon dioxide (CO_2) manufactured with the depleted oxygen was separately analyzed to determine the mass 46 content ($C^{12}O^{16}O^{12}$). This measurement indicated an O^{18} content of 0.15 percent and was felt to be more accurate than the direct measurement technique.

Another portion of the first experiment's product was depleted further in O^{18} in a second experiment. Carbon dioxide samples, prepared with this product, indicated less than 0.005-percent O^{18} content. National Bureau of Standards measurements indicated that O^{18} content had been reduced to 0.0016 ± 0.0005 percent.

An estimate indicated that the O^{17} content had been reduced from a natural abundance of 0.039 percent to 0.0033 percent.

Oxygen samples were prepared with various amounts of O^{18} content ranging from essentially no O^{18} to the natural abundance of O^{18}.

Metal buttons of 80-percent Pu^{238} were measured for specific neutron emission rate. The buttons were converted to plutonium hydride and immediately exposed to five oxygen samples. When the reaction was completed, each of the samples was encapsulated, and the quantity of Pu^{238} in each sample was determined by calorimetry.

The oxide samples were counted individually using a recently calibrated detector. The results of the sample are presented in Table II-4 and Figure II-6. Note that oxide samples prepared with negligible amounts of O^{18} showed very little increase in specific neutron count over the original metal. The specific neutron count of samples containing O^{18} indicated an approximately linear increase in neutron emission with increasing O^{18} content.

The experiments performed indicated that a substantial portion of the neutron emission of PuO_2 is due to the (α, n) reaction of plutonium alphas with O^{18}. PuO_2 prepared with O^{18} depleted oxygen had a neutron emission rate about one-sixth of that from natural oxygen fuel form.

The availability of O^{18} depleted PuO_2 is dependent only on the availability of O^{18} depleted oxygen. There are several feasible methods for depleting oxygen in the O^{18} isotope, including the previously described method used by Mound. The increase in cost due to producing the fuel form would be small when compared to the total fuel cost. The physical, chemical, and mechanical properties of the fuel form should remain essentially unchanged. The decrease in neutron emission will yield an equivalent decrease in neutron dose rate.

Table II-4

Neutron Emission Rate From Pu^{238} Containing Varying Quantities of O^{18}

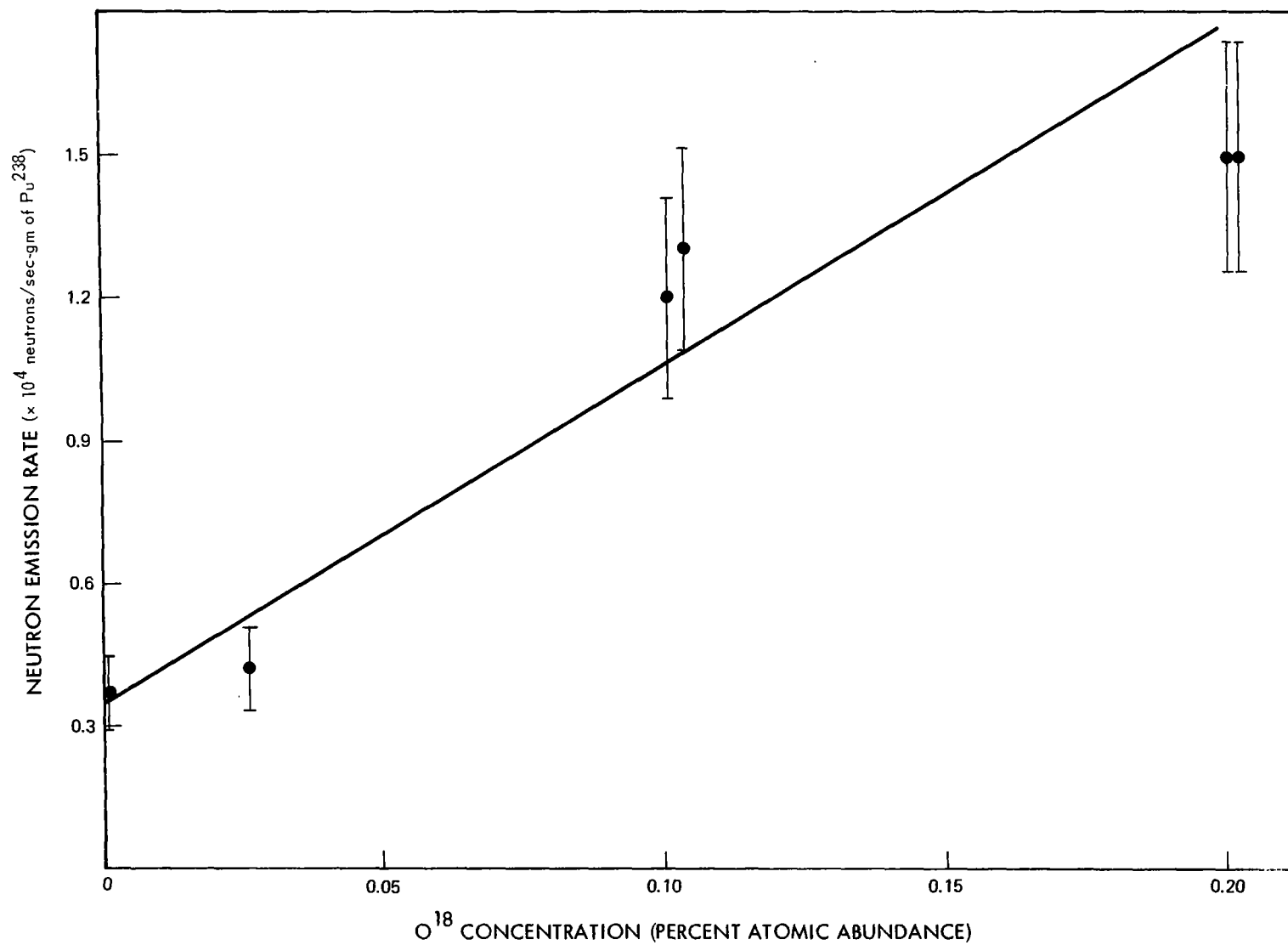| Source Number	Weight of Isotope (g)	Metal Emission Rate (neutrons/sec-g of Pu^{238})	O^{18} Contents (%)	Oxide Emission Rate (neutrons/sec-g of Pu^{238})	
				Measured	Computed
1	2.36	9.8×10^3	0.20	1.5×10^4	1.8×10^4
2	2.10	4.3×10^3	0.103	1.3×10^4	1.1×10^4
3	2.04	3.6×10^3	0.027	4.2×10^3	5.4×10^3
4	1.79	3.6×10^3	0.0016	3.7×10^3	3.7×10^3
5	1.43	4.6×10^3	0.101	1.2×10^4	1.1×10^4
6	1.68	4.6×10^3	0.202	1.5×10^4	1.8×10^4

Figure II-6. Neutron Emission Rate as a Function of O^{18} Concentration (17-Percent Error Bars)

IV. RTG Radiation Field Mapping

A. Radiation Isoflux Data

The radiation analysis was performed for three planar RTG power levels: 50, 75, and 100 watts(e). The results, in the form of gamma and neutron isofluxes, are presented for each power level graphically in Figures II-7 through II-12. A phantom outline of a planar RTG is included in each figure for orientation. The magnitudes associated with each contour have the units of particle flux, as indicated in Figures II-7 through II-12.

The isoflux contours can be used to evaluate the total gamma and neutron particle fluxes at any point in the vicinity of an RTG. If the point in question happens to lie between a pair of contour lines, interpolation can be used to estimate the magnitude of the flux.

The same isoflux contours are applicable to multiple RTG configurations. The total gamma or neutron fluxes at a selected point can be obtained by superposition. The procedure is to determine the relative positions of the point in question with respect to the RTG's. In effect, the same point will have several sets of coordinates, one for each RTG. Every coordinate set yields a flux magnitude on the isoflux map, and the summation of all the magnitudes represents the total flux at the point due to all the RTGs in the system. Figure II-13 gives an example of the method for a two-RTG system.

A noticeable feature of the gamma isoflux lines is the characteristic contour indentation in the "horizontal" plane of the RTG. This reflects the self-absorption effects of the PuO_2 fuel. The overall spatial distribution of the PuO_2 fuel among the spherical capsules approximates a planar configuration. The amount of self-absorption is greatest when viewing the fuel plane "on edge", hence the indented contours. The neutron isoflux lines are not indented since the self-absorption of neutrons within the fuel is not significant. In fact, the neutron calculations did not include any neutron absorptions within the fuel or any of the RTG materials. Consequently, the shape of the neutron isoflux contours is determined by the geometry of the fuel distribution.
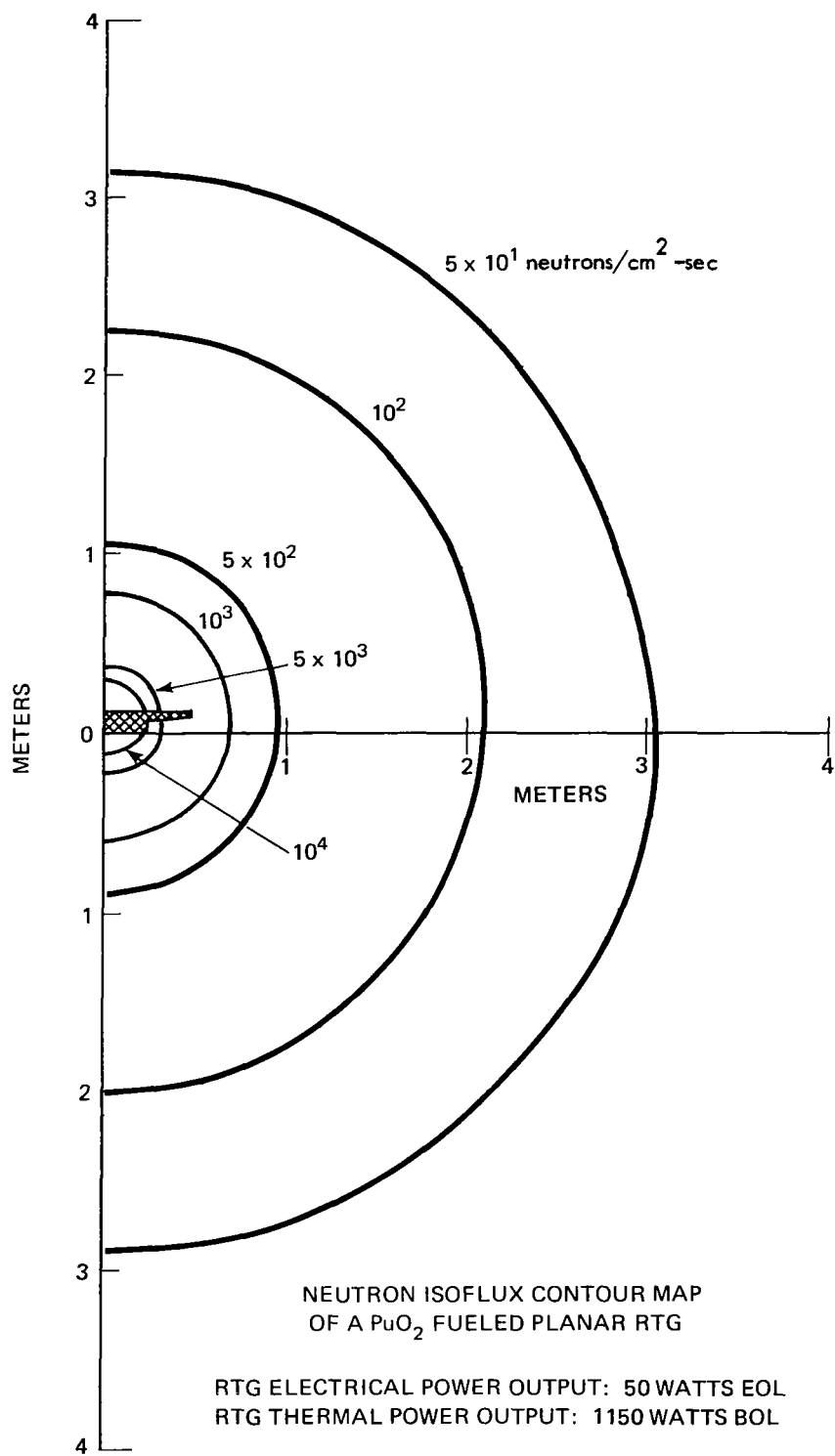
147

Figure II-7. Neutron Isoflux Contours for a 50-watt(e) RTG

Within the figure:

5×10^1 gammas/cm^2 -sec

10^2

5×10^2

10^3

5×10^3

10^4

METERS

METERS

GAMMA ISOFLUX CONTOUR MAP
OF A PuO$_2$ FUELED PLANAR RTG

RTG ELECTRICAL POWER OUTPUT: 50 WATTS EOL
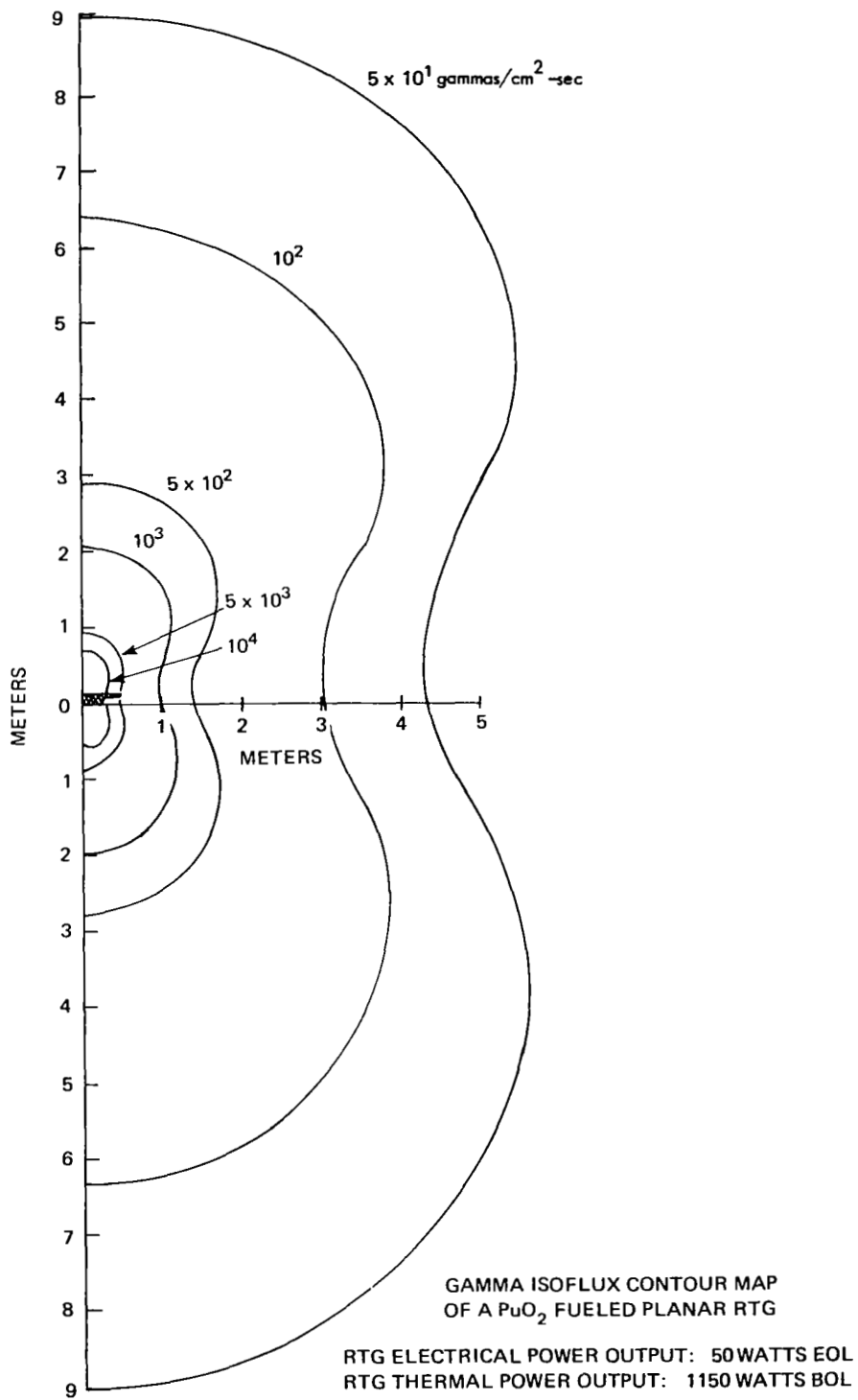RTG THERMAL POWER OUTPUT: 1150 WATTS BOL

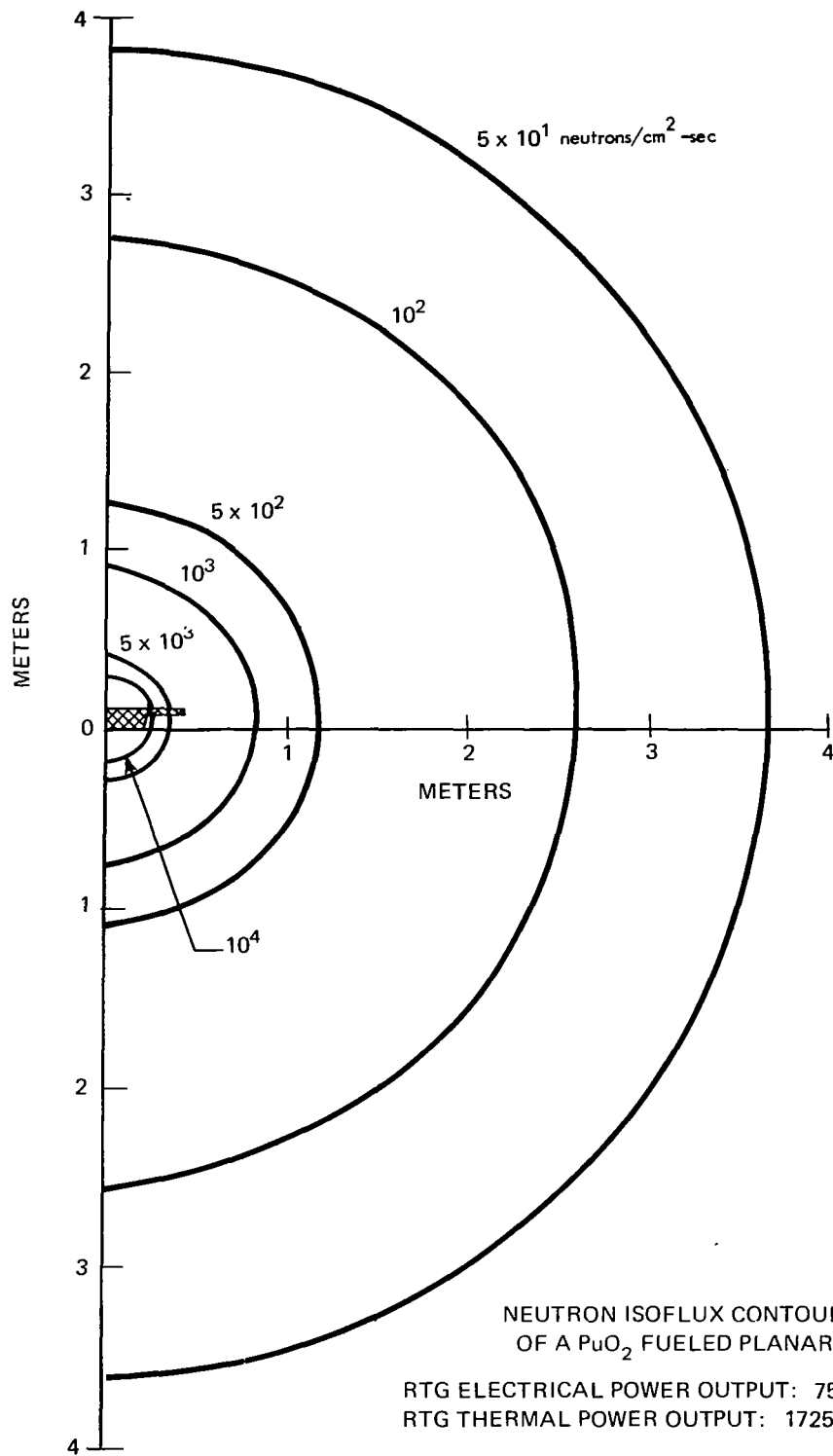Figure II-8. Gamma Isoflux Contours for a 50-watt(e) RTG

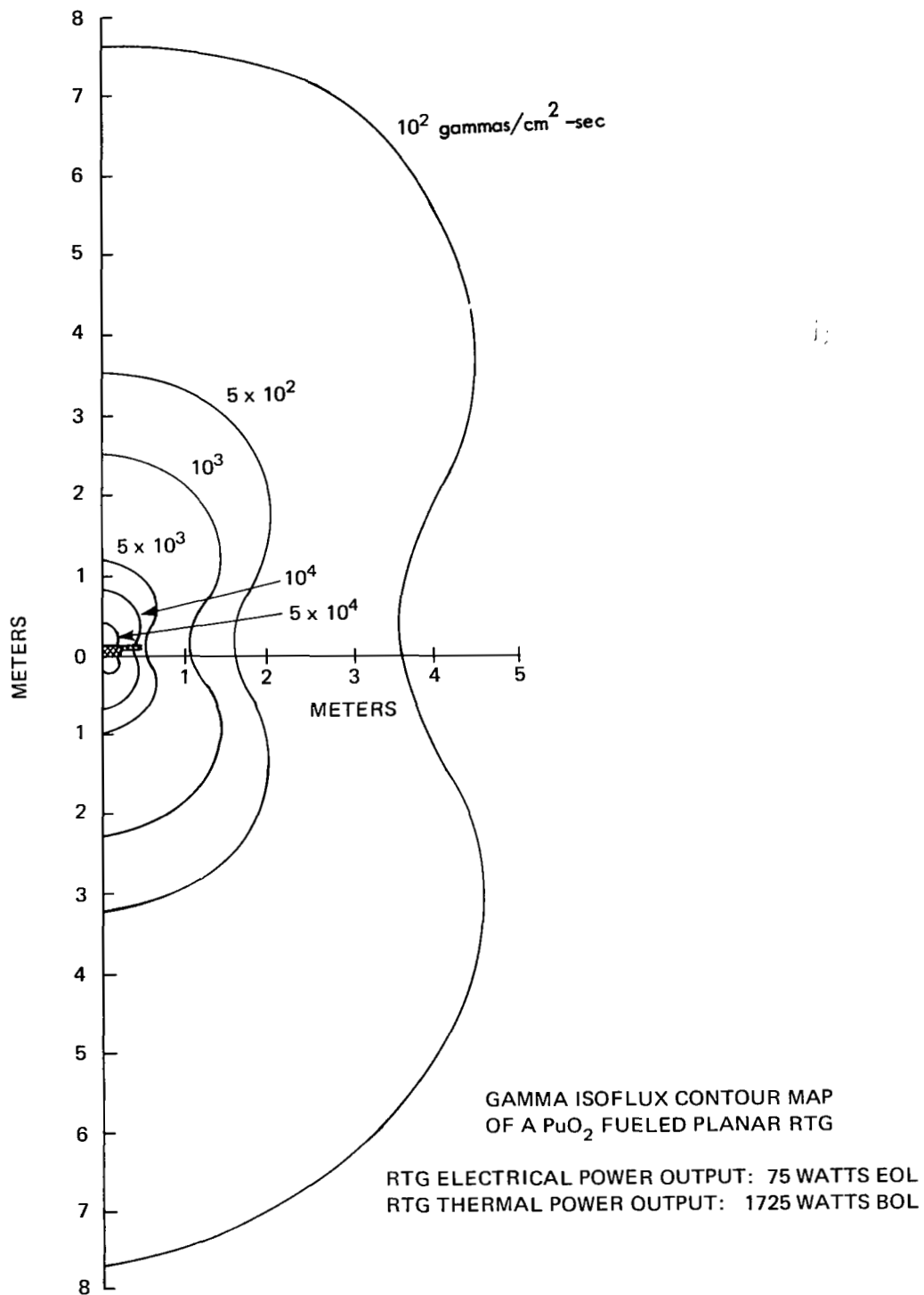Figure II-9. Neutron Isoflux Contours for a 75-watt(e) RTG
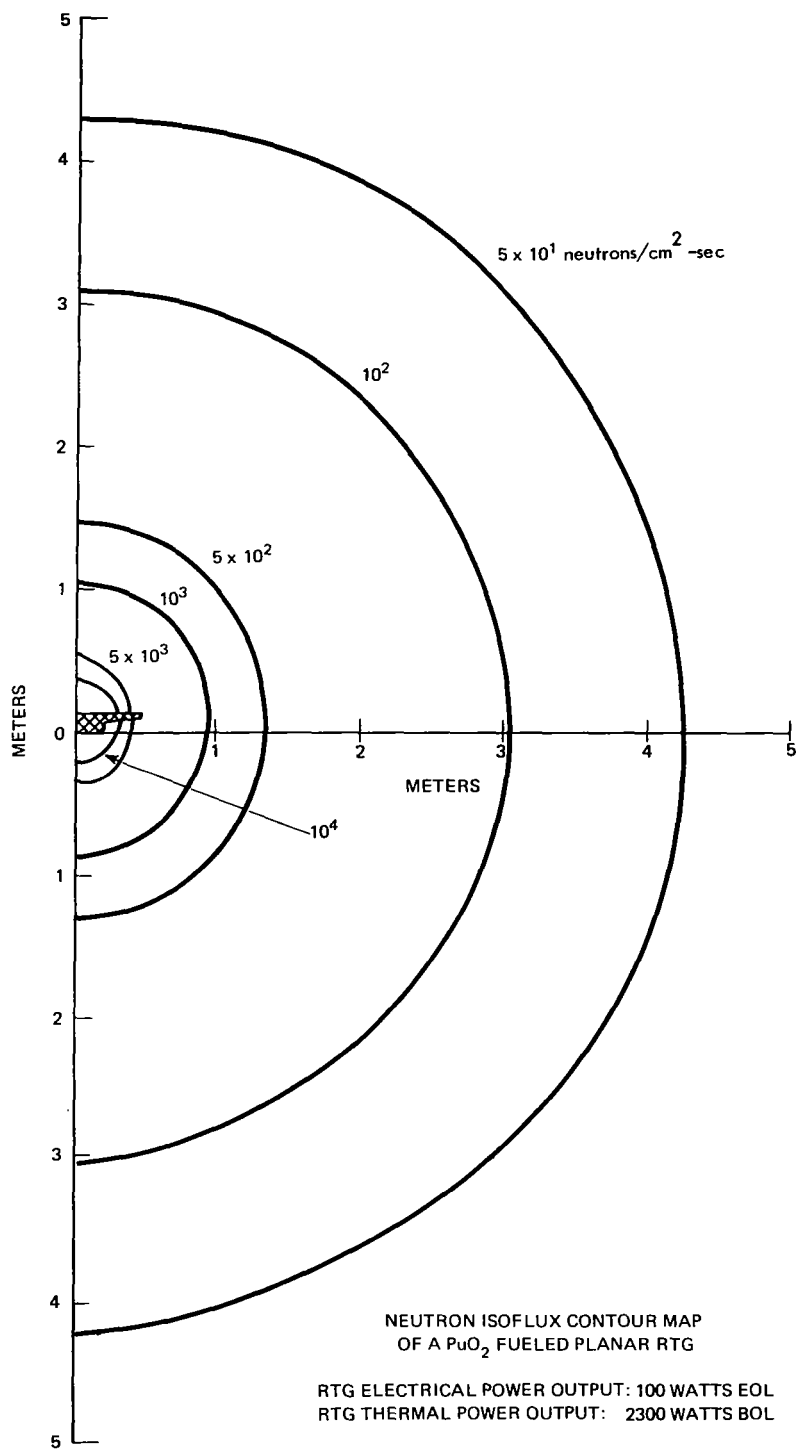
Figure II-10. Gamma Isoflux Contours for a 75-watt(e) RTG
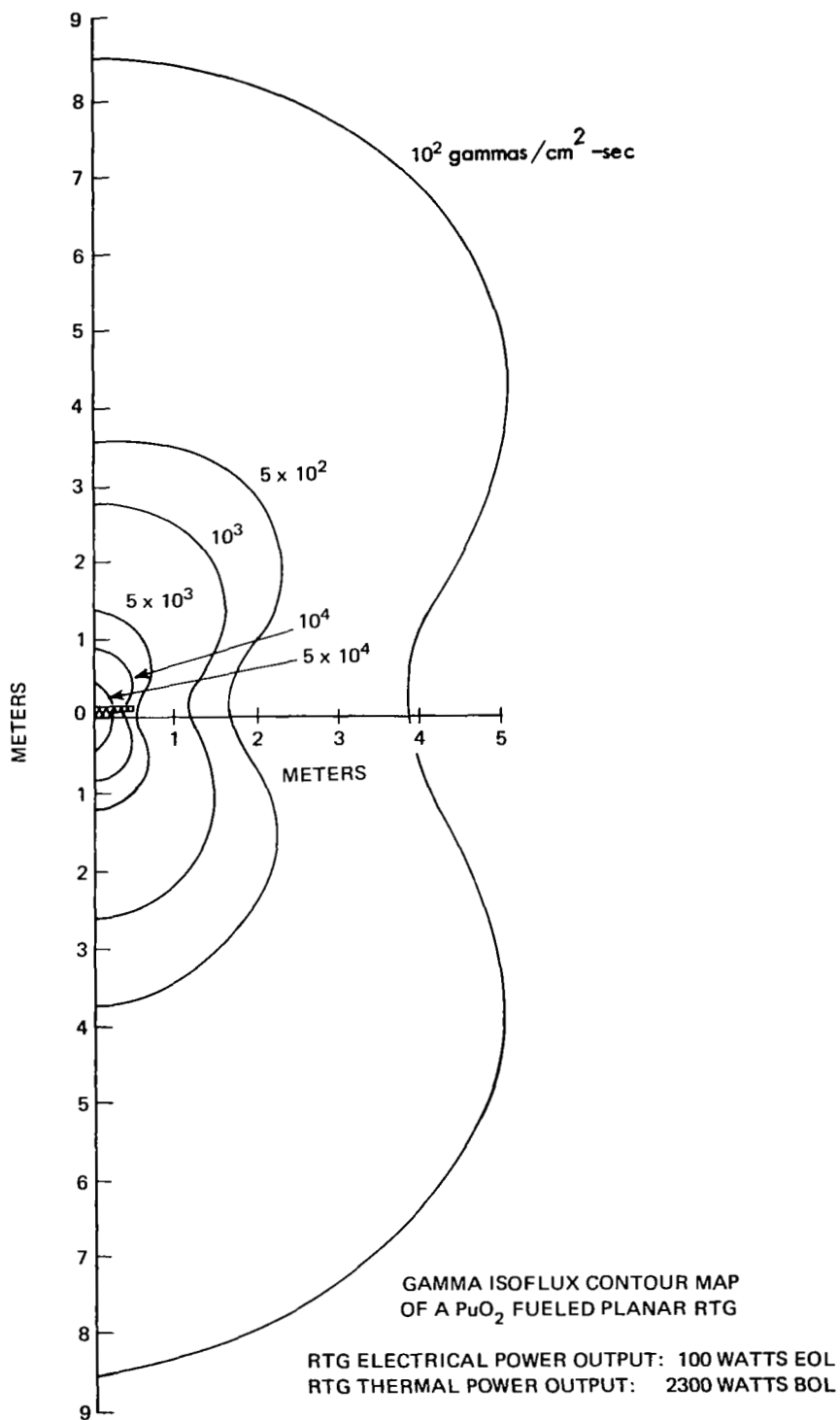
Figure II-11. Neutron Isoflux Contours for a 100-watt(e) RTG

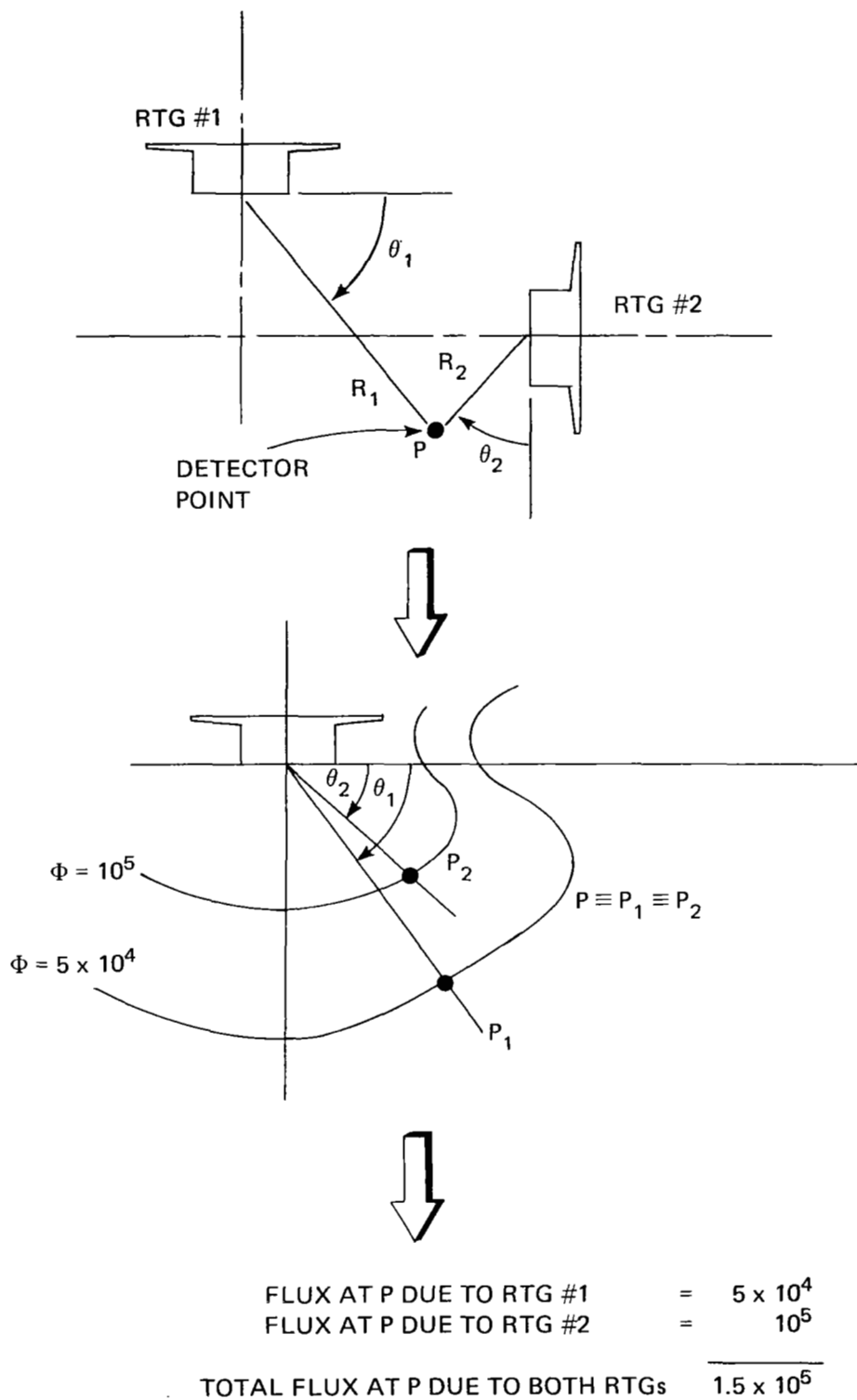Figure II-12. Gamma Isoflux Contours for a 100-watt(e) RTG

153

Figure II-13. Application of Isoflux Maps to Multiple RTG Configurations

FLUX AT P DUE TO RTG #1 $= 5 \times 10^4$
FLUX AT P DUE TO RTG #2 $= 10^5$

TOTAL FLUX AT P DUE TO BOTH RTGs $\quad 1.5 \times 10^5$

B. Effects of O^{18} Depletion

It has been estimated (Ref. 14) that about 90 percent of all the neutrons emitted by PuO_2 originate in (α, n) reactions involving the oxygen and some light element impurities. If the plutonium is compounded with naturally occurring oxygen, the resulting dioxide will contain several oxygen isotopes. Of these, O^{18} is the principal contributor to (α, n) reactions. Experimental measurements (Ref. 11) have shown that the total neutron emission rate varies linearly with the O^{18} content in PuO_2, and so it is possible to establish a simple relationship between the two variables. This can be done with a simple multiplicative constant that can be used directly in conjunction with the neutron isoflux maps.

An approximate relationship between the neutron emission rate and the content of O^{18} can be written in the form

$$N(x) = kx + c,$$

where

$$x = \text{percent content of } O^{18},$$

$$N(x) = PuO_2 \text{ neutron emission rate with x percent of } O^{18}, \text{ and}$$

$$k, c = \text{empirical constants based on the best available upper (natural } O^{18}$$
$$\text{content in } PuO_2) \text{ and lower (} Pu^{238} \text{ metal) neutron emission rates.}$$

The best available value of the neutron emission rate for PuO_2 with natural oxygen (0.201 percent O^{18}) is 2×10^4 neutrons/sec-g Pu^{238} (Ref. 1). The corresponding lowest value is about 3.7×10^3 neutrons/sec-g Pu^{238}. With this information, it is possible to define an emission reduction factor in the form

$$R(x) = \frac{N(x)}{N(0.201)} = \frac{kx + c}{2 \times 10^4} = (4.07x + 0.185).$$

To find the neutron emission rate for PuO_2 with x percent of O^{18}, it is only necessary to multiply 2×10^4 neutrons/sec-g Pu^{238} by the reduction factor $R(x)$. Since the neutron flux magnitudes are proportional to the PuO_2 neutron emission rate, then it follows that the same reduction factor can be applied to the isoflux maps. Any neutron flux magnitude obtained directly from the isoflux maps represents a maximum value. The effect of O^{18} depletion

can be assessed easily by using the reduction factor R(x) for a selected O^{18} content. In brief, we have

$$\begin{pmatrix} \text{Neutron flux from} \\ \text{PuO}_2 \text{ with x percent} \\ O^{18} \end{pmatrix} = R(x) \begin{pmatrix} \text{Neutron flux from} \\ \text{PuO}_2 \text{ with natural} \\ \text{content of } O^{18} \end{pmatrix}$$

C. Nuclear Fuel Data

The calculated RTG radiation fields are based on the PuO_2 gamma and neutron emission rates listed in Table II-5. The gamma emission spectrum represents a synthesis of data from References 14 and 15. Reference 15 contains a finely resolved PuO_2 gamma spectrum below 1 MeV. However, it does not have quantitative data above 1 MeV. High energy data were taken from Reference 14 and combined with those of Reference 15 to form a composite PuO_2 gamma spectrum.

As indicated in Reference 14, the gamma emission rates at higher energies (1 to 3 MeV) vary significantly with time. In order to be conservative, the spectrum with the highest emission rates (corresponding to 5-year-old PuO₂) was selected.

The PuO_2-microsphere neutron emission rate listed in Table II-5 represents the product of the "best-value" of the specific neutron emission rate (2×10^4 neutrons/sec-g Pu^{238}, Ref. 15) and the specific power (0.4 watts/g PuO_2, Ref. 15). The emission rate is based on PuO_2 with the natural O^{18} content (0.20 percent).

D. Method of Analysis

The RTG radiation fields were obtained with the ISOQAD shielding code. A multizone nuclear mockup of the planar RTG was generated separately for each power level [50 watts(e), 75 watts(e), and 100 watts(e)]. The nuclear mockup, together with other nuclear and geometric RTG data, was used as ISOQAD program input information. The program's output consisted of gamma and neutron fluxes as a function of distance and orientation with respect to the RTG. A graphical technique was used to reduce the output data to a set of gamma and neutron isoflux contours for each RTG power level.

Figure II-14 shows the zones used in the nuclear mockup of each RTG. Due to the relative thinness of the RTG components and the absence of hydrogenous

Table II-5

Gamma and Neutron Emission Rates For PuO$_2$ Microspheres

GAMMAS	
Energy (MeV)	Emission Rate (gammas/watt-sec)
0.0435	4.25×10^8
0.0998	1.01×10^8
0.1531	1.12×10^7
0.203	4.47×10^4
0.776	5.59×10^5
0.810	2.24×10^5
1.5	2.475×10^4
2.5	3.0×10^5
4.0	3.25×10^2
6.0	5.5×10^1
NEUTRONS	
Energy (MeV)	Emission Rate* (neutrons/watt-sec)
0-12	5×10^4

*Based on a specific emmission rate of 2×10^4 neutrons/sec-g Pu^{238} and a specific power of 0.4 watts/g PuO$_2$

materials, it was possible to neglect neutron attenuation within the RTG. Consequently, the zones were selected on the basis of distinct material regions pertinent to gamma-ray attenuation. To avoid unreasonably long computation times, approximations were introduced in some of the zone descriptions. For example, the thermoelectrics were represented as a single zone. Instead of having a separate zone for each thermoelement, the entire thermoelectric assembly (i.e.,
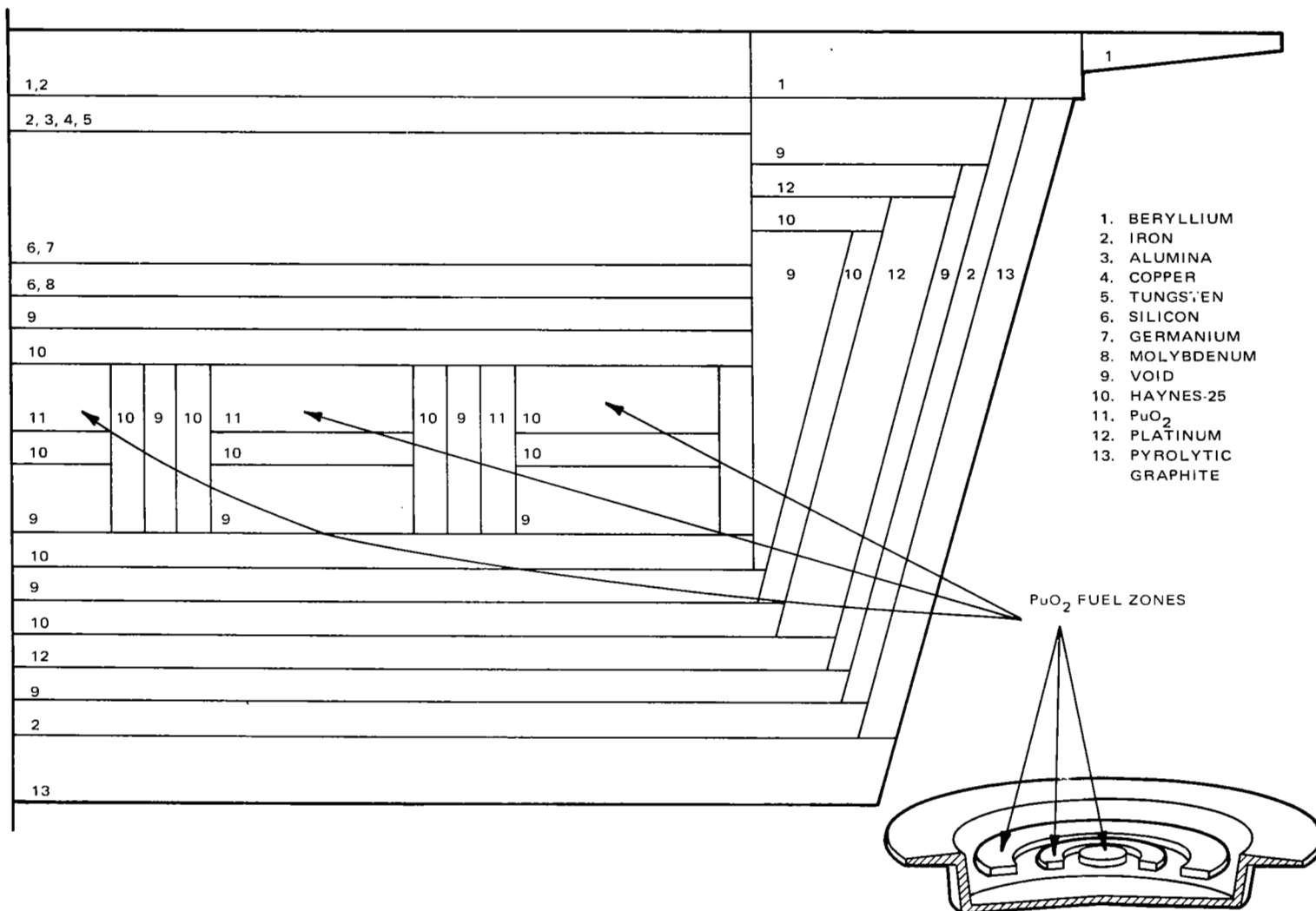
1,2

2, 3, 4, 5

6, 7

6, 8

9

10

11   10   9   10   11   10   9   11   10

10   10   10

9   9   9

10

9

10

12

9

2

13

1

9

12

10

9   10   12   9   2   13

1. BERYLLIUM
2. IRON
3. ALUMINA
4. COPPER
5. TUNGSTEN
6. SILICON
7. GERMANIUM
8. MOLYBDENUM
9. VOID
10. HAYNES-25
11. PuO_2
12. PLATINUM
13. PYROLYTIC
    GRAPHITE

PuO_2 FUEL ZONES

Figure II-14. Nuclear Mockup of a PuO_2 Fueled Planar RTG

thermoelements, hot shoes, cold shoes, hot straps, etc.) was described by a single equivalent material. The equivalent material is a result of a mixing process performed by ISOQAD. The program is supplied with a volume fraction for each element within the volumetric confines of the thermoelectric assembly. It uses them to "reconstitute" a single material with equivalent radiation attenuation properties.

A similar smearing process was applied to the PuO_2 fuel capsules. As shown in Figure II-14 three fuel zones were defined. The 19-capsule configuration was approximated by a central capsule, an intermediate ring of six capsules, and an outer ring of 12 capsules. The cross sections of the capsule wall and the PuO_2 fuel are rectangular. A circular cross section of the spherical capsule, when revolved about the RTG axis of symmetry, would generate toroidal surfaces. Toroidal geometry cannot be described with the current version of the ISOQAD program.

Figure II-15 illustrates the distribution of detector points with respect to a planar RTG. The gamma and neutron fluxes were calculated with ISOQAD at each detector point. The transition from the radiation fluxes at each detector point to isoflux contours was achieved by a cross-plotting technique. A graphical plot of flux versus distance was done along each line of detectors (see Figure II-16). A typical plot is shown in Figure II-16 for gamma radiation along a 40° detector line. Selection of a particular flux magnitude, e.g., 10^4 photons/cm^2-sec, yields a distance, as indicated in Figure II-16. The same flux magnitude generates other distances with respect to flux versus distance plots for 0°, 10°, 20°, 30°, etc. In effect, a unique distance is associated with each angle for a given flux magnitude. This information, when plotted in polar coordinates, is transformed into an isoflux contour, as shown in Figure II-17.
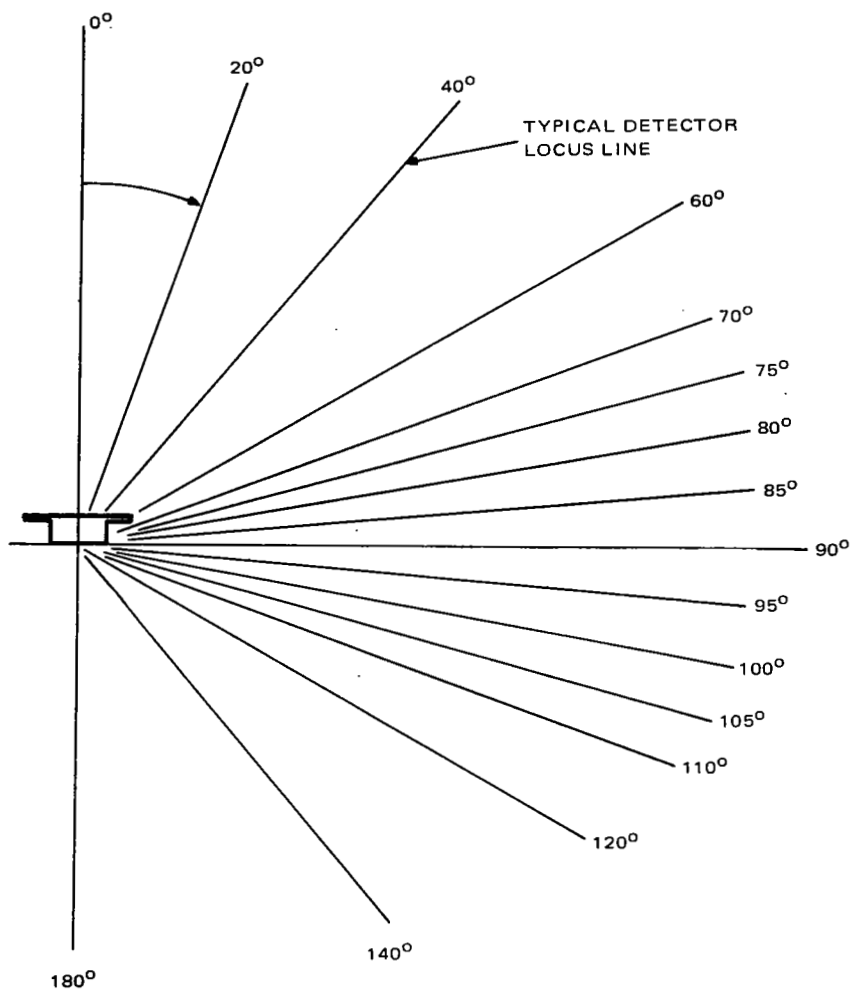
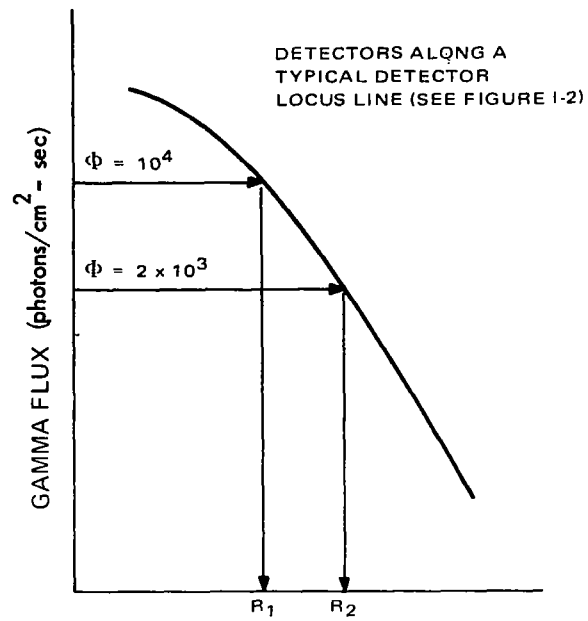Figure II-15. Detector Distribution With Respect to the Planar RTG

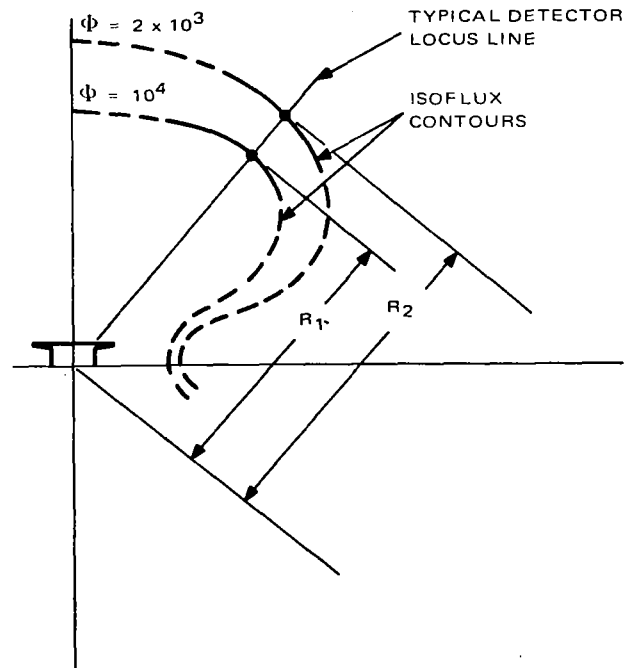Figure 11-16. Gamma Flux vs. Distance From RTG Along a Typical Detector Locus Line

Figure 11-17. Method of Construction of the Isoflux Contours

161

V. Conclusions and Recommendations

A. Effect of O^{18} Depletion on Neutron Shield Weight

As discussed in Section IIIB, total O^{18} depletion should produce about a sixfold reduction in the PuO_2 neutron emission rate. For a given neutron shield configuration, the O^{18} depletion can be translated into a decrease in shield thickness. The neutron shield thickness curves presented in "Task IV Weight Minimization " can be utilized for that purpose. For example, suppose the ratio of the shielded to bare neutron flux at a selected location with respect to a planar RTG is 5×10^{-3}. Then, according to Figure 20, Infinite Area Shield, 37.4 cm of lithium hydride are required. Total O^{18} depletion would reduce the bare neutron flux by about a factor of 6, so that the ratio of shielded to bare neutron flux would increase to 30×10^{-3}. Reference to Figure 20, Infinite Area Shield, shows that the lithium hydride thickness would be reduced to 26.5 cm. On a weight per unit area basis, the neutron shield weight reduction would amount to about 0.13 lb/in^2.

In practice, however, according to the best available data for $Pu^{238}O_2$ and Pu^{238} metal, the actual neutron emission reduction by total O^{18} depletion in large batch quantities is only about threefold. Thus, the shield weight savings in the above example would be somewhat less than 0.13 lb/in^2.

B. Safety Aspects of PuO_2 Cermets

Intensified development work in the area of improved Pu^{238} fuel forms is recommended. The use of a chemically and thermally stable, non-degradable fuel form in the NEW MOONS generator would provide a safety backup which would significantly simplify the safety assessment and virtually ensure a safe system under all conceivable accident situations.

C. Accuracy of Planar RTG Radiation Field Data

The accuracy of the radiation isoflux contours presented in this report is subject to analytic approximations inherent in the ISOQAD shielding code and, to some degree, because of fuel data variation from one "fuel batch" to the next. The isoflux data are useful in establishing preliminary radiation intensities and radiation shielding estimates. This is especially true when evaluating the possible

two-RTG configurations with respect to the spacecraft, as discussed in Section IVA.

Precise information on the shielding requirements, in view of the extremely low permissible radiation flux levels at the sensors, can be obtained only with experimental measurements and more rigorous analytic methods with respect to an RTG-spacecraft flight unit. A proposed experimental program is outlined in "Task IV-Test Program to Verify RTG Shielding Requirements." More accurate analytic tools, such as the Monte Carlo Transport code SOBER, can be applied to an RTG-spacecraft system. The code would permit an evaluation of additional radiation considerations, such as scattered radiation, secondary radiation emission, and precise spectral data with respect to gammas and neutrons.

APPENDIX II REFERENCES

1. "Plutonium-238 and Polonium-210 Data Sheets," MLM-1441, Mound Laboratory, Miamisburg, Ohio, September 29, 1967.

2. Jones, L. V., et al., "Preparation and Properties of Plutonium-Bearing Oxide Particulates," I&EC Prod. Res. Dev., 3:78, 1964.

3. Chikalla, T. D., McNeilly, C. E., and Skavdahl, R. E., "The Plutonium-Oxygen System," J. Nucl. Mater., 12:131, 1964.

4. Grison, E., Lord, W. B. H., and Fowler, R. D., (eds.), Plutonium 1960, London: Cleaver-Hume Press, Ltd., 1960.

5. Sandenaw, T. A., "Heat Capacity of Plutonium Dioxide below 325°K," J. Nucl. Mater., 10:165, 1963.

6. Mound Laboratory unpublished data (see Reference 1).

7. Chikalla, T. D., "The Liquidus for the System UO_2-PuO_2," HW-69832, General Electric Co., Handford Atomic Products Operation, Richland, Washington, June 1961.

8. Paprocki, S. J., et al., "The Chemical Reactivity of PuO_2 with Reactor Materials," BMI-1580, Battelle Memorial Institute, Columbus, Ohio, 1964.

9. Holley, C. E., et al., "Thermodynamics and Phase Relationships for Plutonium Oxide," Proceedings of the Second United Nations Informational Conference on the Peaceful Uses of Atomic Energy, Vol. 6, p. 701, United Nations, Geneva, 1958.

10. Battelle Memorial Institute unpublished data (see Reference 8).

11. Rutherford, W. M., Huffman, G. N., and Coffey, D. L., "Preparation and Neutron Counting of ^{238}PuO$_2$ Depleted in ^{18}O," Nucl. Appl., 3:366-71, 1967.

12. Gilman, W. S., "Review of the Dissolution of PuO$_2$," MLM-1264, Mound Laboratory, Miamisburg, Ohio, 1965.

13. Serdiukova, I. A., Khabakhpashev, A. G., and Tsenter, E. M., "Investigation of the (α, n) Reaction on Oxygen," Bull. Acad. Sci. USSR Phys., 21:1017, 1957.

14. Stoddard, D. H. and Albenesius, E. L., "Radiation Properties of Pu-238 Produced for Isotopic Power Generators," DP-984, Atomic Energy Commission, Savannah River Laboratory, July 1965.

15. "Data Sheets: Plutonium-238 Fuels," Mound Laboratory, Miamisburg, Ohio, July 1, 1967.

APPENDIX III

TYPICAL DESIGN CRITERIA ON PREDICTED DEGRADATION
FOR SEMICONDUCTORS UNDER SPACE RADIATION

165

Table III-1

Typical Radiation Specification for TIROS M Mission

(Taken From: RCA-Astro Electronics Division, Drawing No. 1960811 Rev. 3)

Manu-facturer*	Transistor Type	Operating I_c (mA)	Assumed Initial Beta	Location with Average Exposure		Most Exposed Location	
				Final Beta	I_{CBO} Change	Final Beta	I_{CBO} Change
	2N718A NPNS	0.5	30 70 100	25 48 61	0.1μA	20 32 37	0.2μA
		5.0	40 80 120	36 66 .92		31 51 65	
	2N722 PNPS	0.5	20 40 60	16 25 32	0.2μA	13 19 23	0.5μA
		5.0	30 60 90	25 43 57		22 34 41	
	2N869A PNPS	0.5	30 55 85	27 46 65	0.2μA	25 39 52	0.5μA
		5.0	40 80 120	38 73 105		36 67 93	
	2N916 NPNS	0.5	35 70 150	28 48 76	0.1μA	23 34 46	0.2μA
		5.0	50 100 200	45 82 140	.	40 67 100	

TIROS M Mission: 6 Months, 750 mi (nautical), $82°$ Orbit

Doses For Most Exposed Location: 1×10^5 rads: 1×10^{13} DENI

Dose For Location With Average Exposure: 2×10^4 rads: 5×10^{12} DENI
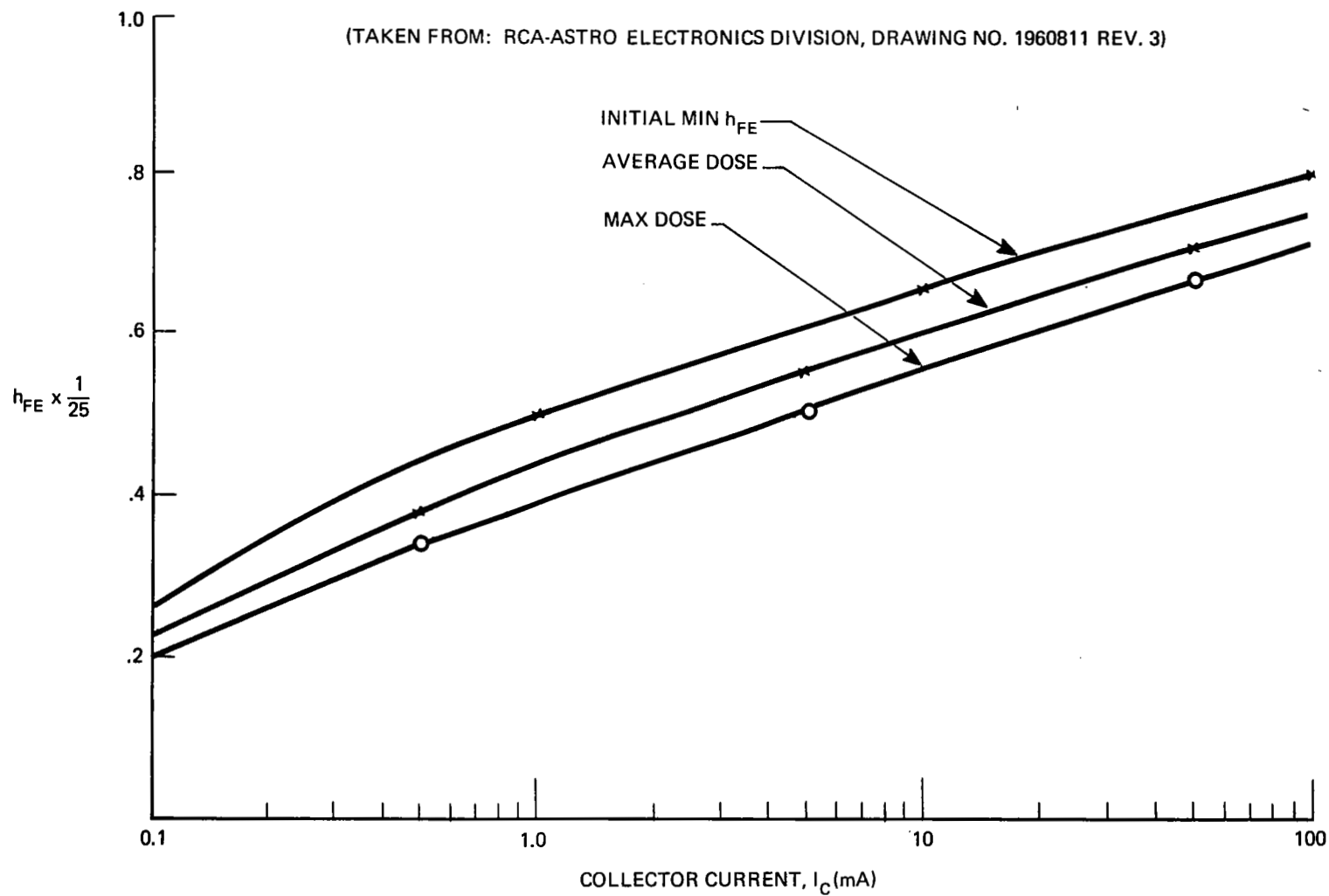
*Manufacturer's name deleted.

Figure III-1. Typical Specification for the Effect of Radiation on Gain in the TIROS M Environment
Transistor Types 2N722 and 2N1132 (Taken From RCA-Astro Electronics Division, Drawing No. 1960811 Rev. 3)